UCRL-TR-208672

A Non-Electrostatic Surface Complexation Approach to Modeling Radionuclide Migration at the Nevada Test Site: II. Aluminosilicates

Mavrik Zavarin and Carol J. Bruton

June 6, 2004

U.S. Department of Energy

Lawrence Livermore National Laboratory

DISCLAIMER

This work was performed under the auspices of the U.S. Department of Energy by the University of California, Lawrence Livermore National Laboratory under Contract No. W-7405-Eng-48.

A Non-Electrostatic Surface Complexation Approach to Modeling Radionuclide Migration at the Nevada Test Site
II. Aluminosilicates

Mavrik Zavarin and Carol J. Bruton
Lawrence Livermore National Laboratory
Livermore, California

Prepared for the Underground Test Area Project
U.S. Department of Energy
National Nuclear Security Administration
Nevada Site Office

Final Report
June 6, 2004

TABLE OF CONTENTS

LIST OF FIGURES

LIST OF TABLES

SUMMARY

Reliable quantitative prediction of contaminant transport in subsurface environments is critical to evaluating the risks associated with radionuclide migration. As part of the Underground Test Area (UGTA) program, radionuclide transport away from selected underground nuclear tests conducted in the saturated zone at the Nevada Test Site (NTS) is being examined. In the near-field environment, reactive transport simulations must account for changes in water chemistry and mineralogy as a function of time and their effect on radionuclide migration. Unlike the K_d approach, surface complexation reactions, in conjunction with ion exchange and precipitation, can be used to describe radionuclide reactive transport as a function of changing environmental conditions. They provide a more robust basis for describing radionuclide retardation in geochemically dynamic environments. In a companion report (Zavarin and Bruton, 2004), a database of radionuclide surface complexation reactions for calcite and iron oxide minerals was developed. In this report, a second set of reactions is developed: surface complexation (SC) and ion exchange (IE) to aluminosilicate minerals. The most simplified surface complexation model, the one-site non-electrostatic model (NEM), and the Vanselow IE model were used to fit a large number of published sorption data and a reaction constant database was developed. Surface complexation of Am(III), Eu(III), Np(V), Pu(IV), Pu(V), and U(VI) to aluminum oxide, silica, and aluminosilicate minerals was modeled using a generalized approach in which surface complexation to aluminosilicate >SiOH or >AlOH reactive sites was considered equivalent to the reactivity of aluminum oxide and silica reactive sites. Ion exchange was allowed to be mineral-dependent.

The generalized NEM approach, in conjunction with Vanselow IE, was able to fit most published sorption data well. Fitting results indicate that surface complexation will dominate over ion exchange at pH >7 for the rare earth and actinide ions examined here. Ion exchange is effectively suppressed due to aqueous speciation at high pH which tends to result in neutral or negatively charged aqueous species that are less likely to undergo ion exchange. The resulting set of average NEM and Vanselow IE constants provides a consistent set of constants for use in reactive transport simulations. The average NEM and Vanselow IE constants were used to predict single-mineral K_ds under conditions similar to K_d measurements reported by the Yucca Mountain site characterization program. In most cases, predicted K_ds were consistent with measured K_ds. In some cases, differences could be explained by surface area, mineralogy, or redox state.

The NEM and Vanselow IE constants described here are an attempt to arrive at a consistent simplified database of reaction constants to be used in reactive transport simulations in chemically and mineralogically heterogeneous environments. The accuracy of these reaction constants is limited by the quality and quantity of available sorption data and the limitations of the NEM and Vanselow IE approach used. The reactivity and accessibility of natural minerals is complicated and cannot be assumed to behave ideally. Thus, the validity of the NEM and Vanselow IE constants must always be examined for the sediment of interest. For example, Triay et al. (1997) suggested that the weak sorption of Np(V) on tuff containing small amounts of hematite may indicate

that the iron oxide mineral is passivated. Thus, the reactive surface area of hematite in these samples may be lower than expected. On the other hand, a limited comparison of NEM and Vanselow IE constants determined here and K_ds reported by Wolfsberg (1978) for alluvium from Frenchman Flat, NTS, suggests that the reaction constants and reactive surface areas developed here would provide a conservative estimate of radionuclide retardation in Frenchman Flat alluvium.

1 INTRODUCTION

In modeling radionuclide migration in the environment, distribution coefficients (K_d) are often used to model sorption. K_ds are typically reported as the ratio of total sorbed concentration (mol/g) to total aqueous concentration (mol/mL). Although the K_d approach can adequately describe the sorptive behavior of a particular sediment at a particular pH and solution composition, many factors that affect radionuclide sorption in geochemically dynamic environments cannot be accounted for. Surface complexation (SC) and ion exchange (IE) reactions provide a more mechanistic approach to modeling sorption and can account for the effect of changing environmental conditions on sorption. The following report is a synthesis of work conducted to describe radionuclide migration in the complex dynamic geochemical environment located near underground nuclear tests conducted at the Nevada Test Site (NTS). In a companion report (Zavarin and Bruton, 2004), a database describing radionuclide interaction with iron oxide and calcite minerals was developed. Sorption to iron oxide and calcite minerals was modeled using the most simplified surface complexation model, the one-site non-electrostatic model (NEM). Here, a model for radionuclide interaction with aluminosilicate minerals is developed. Unlike iron oxide minerals that sorb radionuclides via surface complexation, aluminosilicate minerals (particularly clays) may sorb radionuclides through surface complexation and/or ion exchange reactions. In this report, radionuclide sorption to aluminosilicate minerals is modeled using the NEM in conjunction with the Vanselow IE model. Surface complexation is modeled using a generalized approach in which surface complexation to aluminosilicate >SiOH or >AlOH reactive sites is considered equivalent to the reactivity of aluminum oxide and silica reactive sites. Ion exchange is allowed to be mineral-dependent. The approach used to describe surface complexation reactions (i.e., the NEM approach) was detailed in the companion report (Zavarin and Bruton, 2004) and will not be repeated here. The approach used to describe ion exchange reactions follows.

The permanent charge on some clay minerals is the result of non-charge-balanced ion substitution. For example, substituting Al^{3+} for Si^{4+} in a clay will result in a permanent negative charge. A permanent negative charge is typically balanced by cations in solution that are attracted to the mineral surface. For example, the aluminosilicate montmorillonite may have a permanent negative charge of ~800 meq/kg. In soils, the majority of the clay permanent charge is balanced by the major cations in the waters (Na^+, K^+, Ca^{2+}, and Mg^{2+}). When other cations such as Am^{3+} or Sr^{2+} are present, they may also become associated with the negative aluminosilicate surface via ion exchange. The distribution of cations at aluminosilicate surfaces as a result of permanent charge can be described by ion exchange reactions of the following form:

$$Na\text{-}X + Cs^+ \Leftrightarrow Cs\text{-}X + Na^+ \qquad (1)$$

with an associated equilibrium constant :

$$K = \frac{(Cs - X)\left(Na^{+}\right)}{(Na - X)\left(Cs^{+}\right)} \qquad (2)$$

where "X" designates a surface association and the four terms in parentheses are the activities of the respective species. For homovalent exchange such as the reaction shown in Equation 1, the activity of surface-associated species is often assumed to be defined by the relative concentration of each species ($\frac{[Cs - X]}{[Cs - X] + [Na - X]}$ and $\frac{[Na - X]}{[Cs - X] + [Na - X]}$). Because the denominators for Cs-X and Na-X activity are identical, the activity ratio of surface species can be simplified to the total mol ratio of Cs and Na associated with the mineral surface. The activity of species in solution are determined from species concentration and solution ionic strength activity corrections. The constant, K, describes the relative activity of the various species at equilibrium.

For heterovalent ion exchange, the equilibrium reaction is complicated by the fact that the two exchanging ions balance different amounts of charge on the surface. Heterovalent ion exchange reactions can be written in several forms. By the Vanselow convention (used in this report), the heterovalent exchange reaction is written in a form that relates to the relative mol concentration of surface species instead of relative equivalent concentrations. In this case, an ion exchange reaction is written as:

$$\text{Na-X} + 0.5\text{Ca}^{2+} \Leftrightarrow 0.5\text{Ca-X}_2 + \text{Na}^{+} \qquad (3)$$

with an associated equilibrium constant of the form:

$$K = \frac{\left(Ca - X_2\right)^{0.5}\left(Na^{+}\right)}{(Na - X)\left(Ca^{2+}\right)^{0.5}} \qquad (4)$$

The two terms in the above equation that relate to surface species activity are determined by:

$$\left(\frac{[Ca - X_2]}{([Ca - X_2] + [Na - X])}\right)^{0.5} \text{ and } \left(\frac{[Na - X]}{([Ca - X_2] + [Na - X])}\right) \qquad (5)$$

where the terms in the brackets relate to mol concentrations. By the Vanselow convention, the activity of the surface species cannot be simplified to equivalent concentrations or mol concentrations of the two surface species because the denominator cannot be canceled out.

A special case of the Vanselow convention is when only a trace quantity of one exchanging species is likely to be associated with the mineral surface. For example, if

one assumes that only a trace quantity of Na will be associated with the surface, the above Vanselow equation can be simplified to:

$$K = \frac{(Ca - X_2)^{0.5}\left(Na^{+}\right)}{(Na - X)\left(Ca^{2+}\right)^{0.5}} = \frac{\left(\frac{[Ca - X_2]}{[Ca - X_2] + [Na - X]}\right)^{0.5}\left(Na^{+}\right)}{\left(\frac{[Na - X]}{[Ca - X_2] + [Na - X]}\right)\left(Ca^{2+}\right)^{0.5}} \tag{6}$$

$$\cdots = \frac{\left(\frac{[Ca - X_2]}{[Ca - X_2]}\right)^{0.5}\left(Na^{+}\right)}{\left(\frac{[Na - X]}{[Ca - X_2]}\right)\left(Ca^{2+}\right)^{0.5}} = \frac{[Ca - X_2]\left(Na^{+}\right)}{[Na - X]\left(Ca^{2+}\right)^{0.5}}$$

2 NON-ELECTROSTATIC MODEL DATABASE CONSTRUCTION

Modeling the interaction of radionuclides with aluminosilicates was accomplished by fitting published sorption data to a non-electrostatic surface complexation model (NEM) in conjunction with the Vanselow IE model when appropriate.[1] Unlike other surface complexation models, the NEM (Kurbatov et al., 1951) assumes that surface electrical charge does not affect equilibrium surface complexation. The electrostatic models typically contain one or more parameters that account for surface charge effects. While the NEM approach does not account for charging effects, several investigators have used this model approach to describe sorption reactions (Bradbury and Baeyens, 1997; Davis et al., 1998; Zachara et al., 1994). Davis et al. (1998) argued that the NEM approach may be the most appropriate for complex environmental applications since the surface charging behavior of non-ideal natural mineral phases is not well known. A detailed description of surface complexation modeling and the NEM can be found in the companion report (Zavarin and Bruton, 2004). The Vanselow IE model was adopted here to take advantage of several previously compiled ion exchange reaction data sets (Fletcher and Sposito, 1989; Viani and Bruton, 1992; Viani and Bruton, 1996). Also, Viani and Bruton (1992) showed that model predictions of Sr and Cs sorption (using Vanselow ion exchange) to tuff from Yucca Mountain, NV, were in agreement with experimental data.

Fitting NEM and Vanselow IE reactions to radionuclide sorption data was accomplished with the fitting program FITEQL (Herbelin and Westall, 1994). Data were typically retrieved from published sorption data using the Datathief 1.0.8 program (Huysen and van der Laan, 1992). While fitting the data, ionic strength, pH, and aqueous complexation were taken into account while electrostatic effects were ignored. The effect of ionic strength on ion activity was accounted for by the Davies equation.[2] Aqueous complexation constants were based on the GEMBOCHS thermodynamic database version data.com.V8.R6 (Johnson and Lundeen, 1997) with revisions as noted in Pawloski et al. (2001). A summary of these aqueous complexation constants is reported in Appendix A.

Several authors have recently shown that sorption of radionuclides on aluminosilicate minerals can be related to surface complexation on alumina and silica surfaces since surface functional groups are comparable (McKinley et al., 1995; Turner et al., 1996). In the following sections, this generalized aluminosilicate NEM model is used to fit published radionuclide-aluminosilicate sorption data. Although the assumption that all >AlOH or >SiOH surface reactive sites are equivalent irrespective of the mineral substrate can only be defended in a very qualitative manner, the results presented below

---

[1] Selection criteria for radionuclides were based on abundance, half-life, toxicity to human and environmental health, potential mobility at NTS, and availability of adequate data (Tompson et al., 1999).

[2] The Davies activity correction equation is considered valid only to ionic strengths of 0.1. As a result, model fits to sorption experiments performed at higher ion strength will contain systematic errors; we address these errors in the discussion of data fits (Section 3).

indicate that the relationships do hold true in many cases. Nevertheless, caution must be exercised when attempting to extrapolate generalized >AlOH and >SiOH NEM constants to aluminosilicate minerals for which data is not available. The equivalent reactivity of various aluminosilicate minerals should only be used as a validation effort for available data and extrapolation should only be attempted in a hypothetical manner.

In order to retain the most simplified approach to describing the reactive sites on aluminosilicate minerals, several simplifying assumption were made. These assumptions were held constant for all sorption data fits so as to produce a consistent set of NEM reactions. A single type of >SiOH and/or >AlOH reactive site was used to fit each data set. For all minerals, a site density of 2.31 sites/nm^2 was used. Dzomback and Morel (1990) used this site density for surface complexation modeling of hydrous ferric oxide surfaces. Turner (1995) also used this site density for a variety of minerals to minimize the number of fitting parameters and arrive at a uniform set of surface complexation reactions; this same approach is taken here.

The acidity constants used for >AlOH and >SiOH surface reactive sites were taken from SiO_2 and α-Al_2O_3 diffuse layer model fits reported by Turner (1995). In the companion report (Zavarin and Bruton, 2004), the DLM acidity constants for hydrous ferric oxide were used to model radionuclide sorption to iron oxides. Depending on the SC model, surface acidity Log K constants can vary drastically. The diffuse layer model acidity constants were chosen for convenience. If acidity constants were varied during data fitting along with radionuclide surface complexation constants, less variability in Log K constants might be achieved. However, the limited data for most radionuclide–mineral sorption reactions do not merit additional fitting parameters in our NEM model.

McKinley et al. (1995) determined from transmission electron microscopy (TEM) measurements that Swy-1 montmorillonite broken edge sites (those that account for >SiOH and >AlOH sites) account for ~30% of the measured BET surface area (assuming 2.31 sites/nm^2). Turner et al. (1996) reported similar values from particle size and crystallographic data but chemical methods resulted in much higher site concentrations. Several authors have used a surface complexation reactive site density equivalent to 10% of total BET surface area to model montmorillonite sorption results (Bertetti et al., 1998; Pabalan et al., 1998; Turner et al., 1998). Their site density was based on potentiometric titration results of Wanner et al. (1994). Bertetti et al. (1998) used the same reduced effective surface area to account for reduced Np(V) sorption to clinoptilolite relative to quartz and α-alumina. In the following aluminosilicate fits to sorption data, 10% of BET surface area was used for all montmorillonite, illite, and clinoptilolite data fits. For all sorption fits, the pKa's for >SiOH and >AlOH sites were also held constant. This minimized the number of fitting parameters and resulted in a consistent set of surface complexation reactions.

For each radionuclide–mineral pair, NEM and/or Vanselow IE reaction constants are reported based on average fits to all available sorption data sets.[3] However, fits to certain data sets were omitted from the database average when the quality of sorption data was questionable. In other cases, NEM constants that yielded the most conservative estimate of sorption were included in the database to ensure conservative estimates of radionuclide transport. The process of data rejection is rather subjective. Nevertheless, justification for data rejection is reported in the following section. A discussion of the average NEM and Vanselow IE constants is presented in Section 4.

[3] We define a data set as one or more batch sorption experiments performed while varying a single parameter such as pH or sorber concentration and fit simultaneously using the SC approach. In the literature, when the pH is varied, the data set is often called a "sorption envelope"; when the sorber concentration is varied, the data set is called a "sorption isotherm."

3 SORPTION DATA FITTING RESULTS

3.1 Am(III) on Aluminum Oxide

Several references to Am(III) sorption to aluminum oxides were examined (Allard et al., 1989; Allard et al., 1982; Moulin et al., 1992; Righetto et al., 1991; Righetto et al., 1988). The sorption experiments include both α-Al_2O_3 and γ-Al_2O_3. To retain the most simplified fitting approach, the behavior of the >AlOH surface sites was assumed to be identical for all aluminum oxide minerals.

Righetto et al. (1988) measured the sorption of Am(III) to γ-Al_2O_3 at very low surface loads (<0.1%); data and predicted sorption using the average NEM constant (Table 2) are plotted in Figures 1 to 3. An additional sorption data set by the same author but in a separate publication (Righetto et al., 1991) is shown in Figure 4. Data fits are reported in Table 1. Most of the data is fit quite well with only one surface species (>$AlOAm^{2+}$). The effect of ionic strength is also accounted for (e.g. Figure 2). In Figure 3, Am(III) sorption at high carbonate alkalinity is shown. These samples were prepared in a solution that initially contained 0.05 mol/L inorganic carbonate but solution degassing was not controlled.[4] Assuming 0.05 mol/L inorganic carbonate in solution, the fit using the NEM constant from Table 2 is quite poor. It results in 2-15% Am(III) sorbed instead of 90-100% as the experimental data would suggest. The fit severely underestimates the sorptive capacity of γ-Al_2O_3. Because the carbonate alkalinity was not strictly controlled, this underestimation may or may not be the result of CO_2(g) degassing. For example, if it is assumed that the solutions degassed and reached equilibrium with atmospheric CO_2(g), the formation of aqueous Am-carbonate complexes would be reduced. This, in turn, would increase Am sorption to the γ-alumina surface (Figure 3). This effect can be seen in Table 1 where surface complexation constant fits to individual sorption data sets are reported. The discrepancy points to one of the major deficiencies in sorption data collected from the literature: in many cases, carbonate alkalinity will be a primary factor in controlling radionuclide sorption but its concentration is rarely controlled rigorously.

[4] Details regarding experimental methods were lacking in this reference.

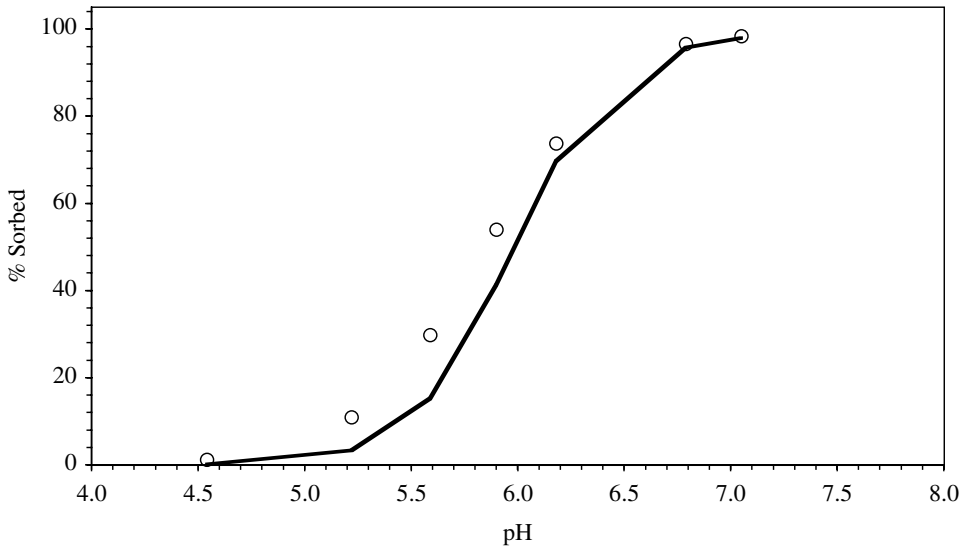

Figure 1. Sorption of 5×10^{-10} mol/L Am(III) on colloidal alumina. Solid lines represent model prediction using NEM constants from Table 2. I = 0.1; 10 ppm Al_2O_3; 130 m^2/g Al_2O_3; open to air; data from Righetto et al. (1988).

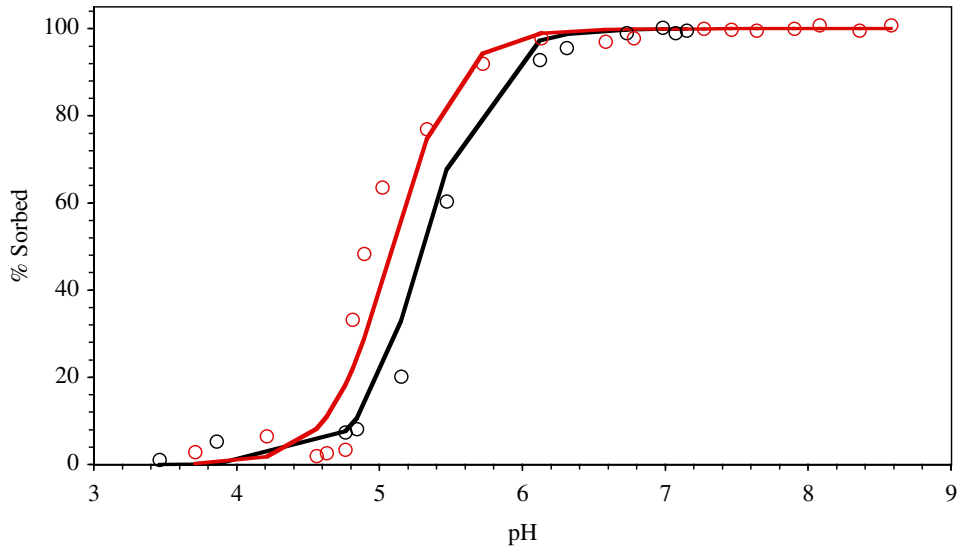

Figure 2. Sorption of 5×10^{-10} mol/L Am(III) on colloidal alumina in 0.1 (black) and 0.01 (red) mol/L $NaClO_4$. Solid lines represent model prediction using NEM constants from Table 2. 200 ppm Al_2O_3; 130 m^2/g Al_2O_3; open to air; data from Righetto et al. (1988).

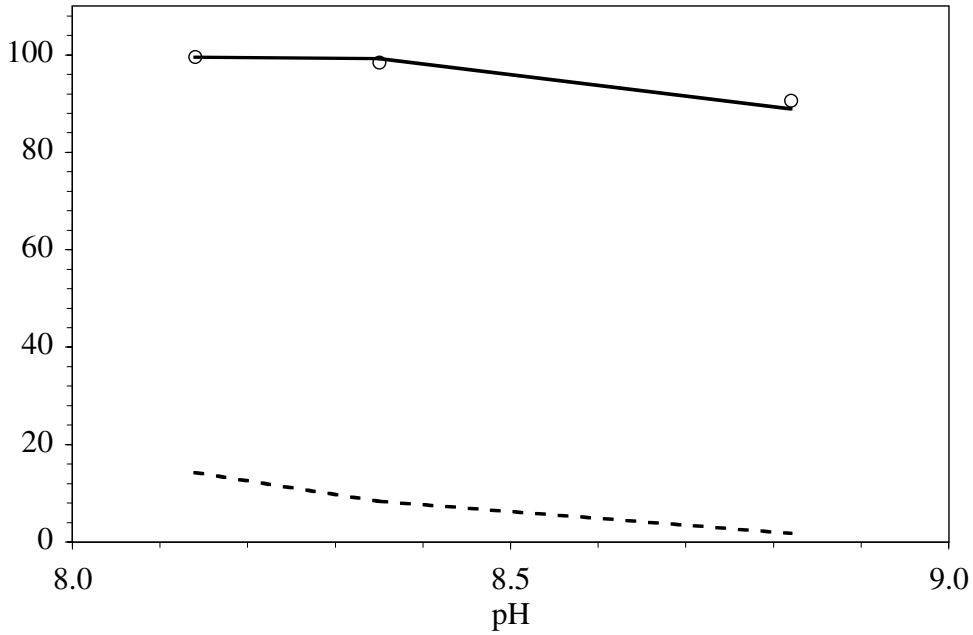

Figure 3. Sorption of 5×10^{-10} mol/L Am(III) on colloidal alumina in 0.05 mol/L HCO_3^-. Model prediction using NEM constants from Table 2 with no loss of HCO_3^- (dashed line) and equilibrium with atmospheric CO_2 (solid line). 0.1 mol/L $NaClO_4$; 10 ppm Al_2O_3; 130 m^2/g Al_2O_3; data from Righetto et al. (1988).

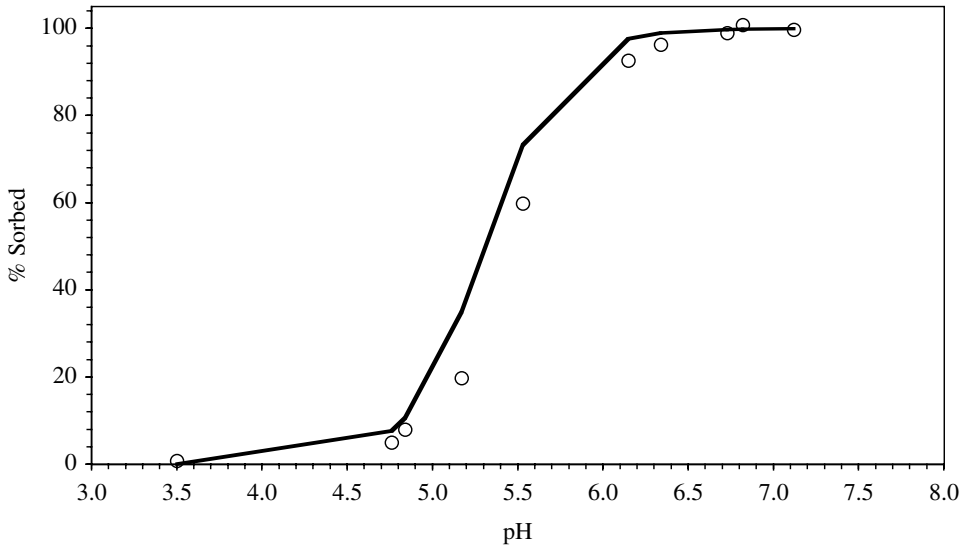

Figure 4. Sorption of 5×10^{-10} mol/L Am(III) on γ–Al_2O_3. Solid lines represent model prediction using NEM constants from Table 2. I = 0.1; 200 ppm Al_2O_3; 130 m^2/g Al_2O_3; open to air; data from Righetto et al. (1991).

Table 1. List of all aluminosilicate sorption data sets and their surface complexation and ion exchange reaction fits.

Sorption Type	Element Conc.	Sorption Sites	Ionic Strength	pCO_2[a]	Species	log K	Comments	Refs.
	--------	mol/l	--------					
Am(III) on γ-Al_2O_3	5E-10	5E-6	0.1	5E-5†	$>AlOAm^{2+}$	2.79	pH curve	1
	5E-10	1E-4	0.01	5E-5	$>AlOAm^{2+}$	2.44	pH curve	1
	5E-10	1E-4	0.1	5E-5	$>AlOAm^{2+}$	2.32	pH curve	1
	5E-10	5E-6	0.1	0.05	$>AlOAm^{2+}$	5.21‡‡	pH curve	1
				3.5	$>AlOAm^{2+}$	2.56*	pH curve	1
	5E-10	1E-4	0.1	5E-5	$>AlOAm^{2+}$	2.25	pH curve	2
Am(III) on Al_2O_3	2.9E-7	4.6-6.4E-7	0.01	5E-5	$>AlOAm^{2+}$	6.52	pH curve	3
	2.3E-9	4.6-6.4E-7	0.01	5E-5	$>AlOAm^{2+}$	5.91	pH curve	3
	1E-8	5.8-3.9E-7	0.01	5E-5	$>AlOAm^{2+}$	3.95	pH curve	4
	1E-8	5.8-3.9E-7	0.1	5E-5	$>AlOAm^{2+}$	4.10	pH curve	4
Am(III) on α-Al_2O_3	1E-8	2.69E-6	0.1	5E-5	$>AlOAm^{2+}$	2.41	pH curve	5
						2.92‡	pH curve	5
	1E-8	2.69E-6	0.01	5E-5	$>AlOAm^{2+}$	2.20	pH curve	5
Am(III) on SiO_2	5E-10	8.05E-4¶	0.1	5E-5	$>SiOAm^{2+}$	-1.94	pH curve	2
					$>SiOAm(OH)_2$	-17.2		
	1E-8	2.88E-6	0.1	5E-5	$>SiOAm^{2+}$	0.66	pH curve	5
					$>SiOAm(OH)_2$	-13.34		
	1E-8	2.88E-6	0.01	5E-5	$>SiOAm^{2+}$	0.66	pH curve	5
					$>SiOAm(OH)_2$	-14.82		
	2.3E-9	9.66-6.94E-7	0.01	5E-5	$>SiOAm^{2+}$	0.79	pH curve	3
					$>SiOAm(OH)_2$	-14.34		
Am(III) on smectite/	1E-8	1.15E-4(Al,Si)	3.0	5E-5	$Am^{3+} \Rightarrow 3Na^+$	2.54	low pH	6
kaolinite clay§		3.45E-3(IE)	1.0	5E-5	$Am^{3+} \Rightarrow 3Na^+$	3.14	fit	6
			0.1	5E-5	$Am^{3+} \Rightarrow 3Na^+$	1.77	~1.0 visual	6
			0.01	5E-5	$Am^{3+} \Rightarrow 3Na^+$	-0.79	fit	6
Eu(III) on Al_2O_3	1E-8	4.6E-3¶	0.01	5E-5	$>AlOEu^{2+}$	1.86	pH curve	7
	1E-8	4.6E-3¶	0.1	5E-5	$>AlOEu^{2+}$	2.11	pH curve	7
	1E-8	4.6E-3¶	0.5	5E-5	$>AlOEu^{2+}$	2.89	pH curve	7
	7E-9	>4.6E-7	0.01	5E-5	$>AlOEu^{2+}$	4.47	pH curve	8
	7E-9	>4.6E-7	0.1	5E-5	$>AlOEu^{2+}$	4.59	pH curve	8
Eu(III) on SiO_2	1E-8	4.3E-6	0.01	5E-5	$>SiOEu^{2+}$	-1.13	pH curve	9
					$>SiOEu(OH)_2$	-14.20		
	1E-9	3.2E-5	0.05	5E-5	$>SiOEu^{2+}$	-0.12	pH curve	10
					$>SiOEu(OH)_2$	-14.05		
	7E-9	>6.9E-7	0.01	5E-5	$>SiOEu^{2+}$	0.98	pH curve	8
					$>SiOEu(OH)_2$	-13.16		
			0.1	5E-5	$>SiOEu^{2+}$	2.37	pH curve	8
					$>SiOEu(OH)_2$	-13.16		

Table 1. Continued.

Sorption Type	Element Conc.	Sorption Sites	Ionic Strength	pCO_2	Species	log K	Comments	Refs.
	--------	mol/l	--------					
Eu(III) on illite	1E-8	2.7E-5(Al,Si)	0.02	3.5	$Eu^{3+} \Rightarrow 3Na^{+}$	0.99	pH curve	11
		7.1E-5(IE)	0.1	3.5	$Eu^{3+} \Rightarrow 3Na^{+}$	2.62	pH curve	11
			0.2	3.5	$Eu^{3+} \Rightarrow 3Na^{+}$	3.06	pH curve	11
			0.5	3.5	$Eu^{3+} \Rightarrow 3Na^{+}$	3.75	pH curve	11
Np(V) on colloidal alumina	1E-14	9.97E-5	0.1	3.5	$>AlONpO_2$	-2.31	pH curve	1
					$>AlONpO_3H^-$	-13.59		
	1E-14	9.97E-5	0.1	0.05M	$>AlONpO_2$	-2.18	pH curve	1
					$>AlONpO_3H^-$	-10.19		
	1E-14	9.97E-5	0.1	3.5	$>AlONpO_2$	-2.18	pH curve	2
					$>AlONpO_3H^-$	-13.65		
	6E-6	6.71E-4	0.1	3.5	$>AlONpO_2$	-2.49	pH curve	12
					$>AlONpO_3H^-$	-13.62		
Np(V) on α-Al_2O_3	6E-6	9.59E-6	0.1	3.5	$>AlONpO_2$	-4.36	pH curve	12
					$>AlONpO_3H^-$	-14.21		
	1E-6	3.53E-6	0.01	none	$>AlONpO_2$	-4.78	pH curve	13
					$>AlONpO_3H^-$	-14.27		
	1E-6	3.53E-6	0.01	none	$>AlONpO_2$	-4.86	pH curve	13
					$>AlONpO_3H^-$	-14.29		
	1.9E-7	4.6-6.4E-7	0.01	5E-5	$>AlONpO_2$	-2.52	pH curve	3
					$>AlONpO_3H^-$	-12.84		
	1.9E-9	4.6-6.4E-7	0.01	5E-5	$>AlONpO_2$	-2.74	pH curve	3
					$>AlONpO_3H^-$	-12.44		
Np(V) on SiO_2	1E-14	8.05E-4	0.1	3.5	$>SiONpO_2$	-5.31	pH curve	2
					$>SiONpO_3H^-$	-12.90		
	1E-7	4.6E-6	0.1	3.5	$>SiONpO_2$	-3.59	pH curve	13
					$>SiONpO_3H^-$	-11.77		
	1E-7	9.2E-6	0.1	3.5	$>SiONpO_2$	-3.74	pH curve	13
					$>SiONpO_3H^-$	-11.59		
	1E-6	4.6E-6	0.1	3.5	$>SiONpO_2$	-3.90	pH curve	13
					$>SiONpO_3H^-$	-12.06		
	1E-6	4.6E-6	0.1	none	$>SiONpO_2$	-3.82	pH curve	13
					$>SiONpO_3H^-$	-12.03		
	1E-6	7.67E-6	0.1	none	$>SiONpO_2$	-3.56	pH curve	13
					$>SiONpO_3H^-$	-12.29		
Np(V) on clinoptilolite	1E-6	2.33E-6 (Al), 1.32E-5 (Si)	0.1 0.1	3.5 none			average fit	13
	1E-6	4.65E-6 (Al), 2.64E-5 (Si)	0.01 0.01	3.5 none				
Np(V) on montmorillonite	9.25E-7 9.13E-7	7.66E-5 (Al,Si) 7.59E-5 (Al,Si)	0.1 0.1	3.5 none			average fit	14

Table 1. Continued.

Sorption Type	Element Conc.	Sorption Sites	Ionic Strength	pCO_2	Species	log K	Comments	Refs.
	--------	mol/l	--------					
Pu on alumina	2E-10	9.97E-5	0.1	3.5	$>AlOPuO_2$	-2.33	Pu(V)?	2
					$>AlOPu(OH)_2^+$	3.39	Pu(IV)?	2
					$>AlOPu(OH)_4^-$	-11.79		
	6E-8	6.44-4.64E-7	0.01	3.5	$>AlOPu(OH)_2^+$	7.44	Pu(IV)?	3
					$>AlOPu(OH)_4^-$	-11.21		
	6E-10	6.44-4.64E-7	0.01	3.5	$>AlOPu(OH)_2^+$	7.42	Pu(IV)?	3
					$>AlOPu(OH)_4^-$	-11.51		
	6E-8	6.44-4.64E-7	0.01	3.5	$>AlOPu(OH)_2^+$	3.63	Pu(IV)?	3
					$>AlOPu(OH)_4^-$	-6.49		
Pu on silica gel	1E-14	1.68E-2	0.7	3.5	$>AlOPuO_2$	-6.24	Pu(V)?	15
					$>AlOPuO_3H^-$	-14.46		
	1E-11	1.68E-2	0.1	3.5	$>AlOPuO_2$	-6.62	Pu(V)?	15
					$>AlOPuO_3H^-$	-15.14		
Pu(IV) on montmorillonite	1E-14	3.8E-6 (Al,Si)	0.7	3.5	$>AlOPu(OH)_2^+$	5.85	Pu(IV)	15
					$>AlOPu(OH)_4^-$	-11.93		
					$>SiOPu(OH)_2^+$	3.30		
	1E-14	3.8E-6 (Al,Si)	0.7	3.5	$>AlOPu(OH)_2^+$	6.63	30day	15
					$>AlOPu(OH)_4^-$	-11.93	Pu(V)	
					$>SiOPu(OH)_2^+$	2.62		
	1E-14	3.8E-6 (Al,Si)	0.7	3.5	$>AlOPu(OH)_2^+$	5.76	37 day	15
					$>AlOPu(OH)_4^-$	-11.93	Pu(V)	
					$>SiOPu(OH)_2^+$	2.19		
	1E-11	3.8E-6 (Al,Si)	0.1	3.5	$>AlOPu(OH)_2^+$	5.54	5 day	15
					$>AlOPu(OH)_4^-$	-11.93	Pu(V)	
					$>SiOPu(OH)_2^+$	1.18		
Pu(V) on montmorillonite	1E-14	3.8E-6 (Al,Si)	0.7	3.5	$>SiOPuO_2$	-6.43	1 hour	15
					$>SiOPuO_3H^-$	-14.80	sorption	
					$>AlOPuO_2$	-4.09		
	1E-11	3.8E-6 (Al,Si)	0.1	3.5	$>SiOPuO_2$	-6.43	1 hour	15
					$>SiOPuO_3H^-$	-14.80	sorption	
					$>AlOPuO_2$	-2.09		
U(VI) on $Al(OH)_3$	8.5E-6	2.36E-4	0.001	none	$>AlOUO_2^+$	3.26	pH curve	16
	8.5E-6	2.42E-4	0.1	none	$>AlOUO_2^+$	2.91	pH curve	16
	8.5E-6	2.36E-5	0.1	none	$>AlOUO_2^+$	3.14	pH curve	16
U(VI) on α-Al_2O_3	4.84E-7	2.46E-6	0.1	3.5	$>AlOUO_2^+$	3.20	pH curve	17
U(VI) on Al_2O_3	2.1E-7	4.6 to 6.4E-7	0.01	5E-5	$>AlOUO_2^+$	5.25	pH curve	3

Table 1. Continued.

Sorption Type	Element Conc. -------- mol/l --------	Sorption Sites	Ionic Strength	pCO_2	Species	log K	Comments	Refs.
U(VI) on SiO_2	1E-6	1.23E-4	0.005	3.5	$>SiOUO_3H$	-5.35	pH curve	18
					$>SiOUO_3^-$	-11.23		
	1E-6	1.23E-4	0.01	3.5	$>SiOUO_3H$	-5.33	pH curve	18
					$>SiOUO_3^-$	-11.18		
	1E-6	1.23E-4	0.1	3.5	$>SiOUO_3H$	-5.61	pH curve	18
					$>SiOUO_3^-$	-10.47		
	1E-6	1.23E-4	0.1	3.5	$>SiOUO_3H$	-5.37	pH curve	18
					$>SiOUO_3^-$	-11.18		
	1E-6	1.23E-4	0.1	3.5	$>SiOUO_3H$	-5.21	pH curve	18
					$>SiOUO_3^-$	-11.48		
	2.1E-6	6.71E-3¶[	?	.001M	$>SiOUO_3H$	-6.3	pH curve	19
					$>SiOUO_3^-$	-14.0		
	2.1E-6	6.71E-3¶[	?	5E-5	$>SiOUO_3H$	-5.46	pH curve	19
					$>SiOUO_3^-$	-11.39		
	8.5E-6	9.13E-6	0.1	none	$>SiOUO_3H$	-5.2	pH curve	16
					$>SiOUO_3^-$	-11.39		
	8.5E-6	9.13E-5	0.1	none	$>SiOUO_3H$	-5.05	pH curve	16
					$>SiOUO_3^-$	-11.64		
	8.5E-6	1.05E-4	0.1	none	$>SiOUO_3H$	-5.15	pH curve	16
					$>SiOUO_3^-$	-11.02		
	1E-6	1.92E-4	?	5E-5	$>SiOUO_3H$	-4.22	pH curve	20
					$>SiOUO_3^-$	-11.39		
	2.06E-7	5.76E-6	0.1	3.5	$>SiOUO_3H$	-4.86	pH curve	17
					$>SiOUO_3^-$	-12.03		
	2.0E-8	2.3E-6	0.1	3.5	$>SiOUO_3H$	-4.52	pH curve	17
					$>SiOUO_3^-$	-11.5		
	2.15E-6	5.76E-6	0.1	3.5	$>SiOUO_3H$	-5.36	pH curve	17
					$>SiOUO_3^-$	-12.35		
	2.1E-7	6.9 to 9.7E-7	0.01	5E-5	$>SiOUO_3H$	-4.48	pH curve	3
					$>SiOUO_3^-$	-11.06		

Table 1. Continued.

Sorption Type	Element Conc.	Sorption Sites	Ionic Strength	pCO_2	Species	log K	Comments	Refs.
	--------	mol/l	--------					
U(VI) on montmorillonite	var.	9E-4 (I.E.)	0.002	5E-5	$UO_2^{2+} \Rightarrow Ca^{2+}$	-0.25	isotherm	21
					$UO_2^{2+} \Rightarrow 2Na^{+}$	-0.08	extrapol.	22
	8.5E-6	2.85E-5 (Al,Si)	0.001Na	none			average	16
		5.22E-4 (I.E.)	0.01Na	none			fit	
			0.1Na	none				
			0.005Ca	none				
			0.05Ca	none				
	8.4E-6	2.97E-6 (Al,Si)	0.001Na	none				23
		4.37E-4 (I.E.)	0.01Na	none				
			0.1Na	none				
	2.45E-7	5.95E-5 (Al,Si)	0.1	3.5			average	17
	2.06E-7	5.03E-6 (Al,Si)	0.1	3.5			fit	
	2.1E-7	5.2E-7 (Al,Si)	0.1	3.5				
U(VI) on clinoptilolite	2.17E-7	1.2E-6 (Al) 6.7E-6 (Si)	0.1	3.5			average fit	17
	2.22E-6	1.2E-6 (Al) 6.9E-6 (Si)	0.1	3.5				
	1.9E-8	1.2E-6 (Al) 6.7E-6 (Si)	0.1	3.5				
	2.17E-7	1.2E-6 (Al) 6.8E-6 (Si)	1.0	3.5				
	2.1E-7	1.2E5 (Al) 6.7E-5 (Si)	0.1	3.5				
	2.1E-7	1.4E-6 (Al) 8E-6 (Si)	0.1	2.0				

* log K fit assuming that the 0.05M HCO_3^- came to equilibrium with atmospheric CO_2(g) partial pressure.

† 5×10^{-5} mol/L HCO_3^- used instead of constant pCO_2 because previous experiments have shown that solution are unlikely to be at equilibrium with atmospheric CO_2(g) at high pH unless they are done so rigorously.

‡ Fit completed by determining best fit with aqueous concentration data instead of sorbed concentration.

§ Fit to sorption data was compared with average silanol and aluminol surface complexation constants determined from individual alumina and silica experiments (i.e. no fitting). Ion exchange constant was a qualitative fit because insufficient data was available to fit ion exchange reaction properly.

¶ Surface area taken from Turner (1991)

[a] pCO_2 is reported here because is has been shown to greatly affect both the sorption of various radionuclides. Its treatment during data fitting (assuming equilibrium with atmospheric CO_2(g), assuming an approximate molar concentration, assuming its absence, etc.) will have a great effect on the resulting fitted Log K constant. Since the state of solutions with respect to CO_2 is not always stated explicitly in published data, we specify in this table how CO_2 is treated during data fitting based on the information available in the publication.

REFERENCES: 1. (Righetto et al., 1988); 2. (Righetto et al., 1991); 3. (Allard et al., 1982); 4. (Allard et al., 1989); 5. (Moulin et al., 1992); 6. (Stammose and Dolo, 1990); 7. (Shiao et al., 1981); 8. (Norden et al., 1994); 9. (Ledin et al., 1994); 10. (Fairhurst et al., 1995); 11. (Wang et al., 1998); 12. (Nakayama and Sakamoto, 1991); 13. (Bertetti et al., 1998); 14. (Turner et al., 1998); 15. (Sanchez, 1983); 16. (Turner et al., 1996); 17. (Pabalan et al., 1998); 18. (Waite et al., 1992); 19. (Lieser et al., 1992); 20. (Dent et al., 1992); 21. (Tsunashima et al., 1981); 22. (Fletcher and Sposito, 1989); 23. (McKinley et al., 1995).

Two sets of sorption data by Allard et al. (1989; 1982) were fit. However, surface areas were not reported; only a range of particle size was reported based on the sieved size fraction (see Table 1 and Figures 5 and 6). We estimated the mineral surface area by assuming cubic particles with an average particle size equivalent to the average sieved particle size. However, surface areas calculated assuming ideal cubic particles are generally much lower than true surface areas. It should, therefore, not be surprising that the fitted Log K is significantly greater than the Log K fit to the more quantitative data of Righetto et al. (1991; 1988). In addition, Allard et al. (1982) indicated that sorption experiments did not include an accounting of radionuclide loss to container walls. For highly sorbing elements such as Am(III), this may result in much higher observed sorption than expected. This may also account for the unusually broad sorption edge in their results (Figures 5 and 6). Due to the questionable data quality, these data fits were not used in calculating the average Log K reported in Table 2. Nevertheless, the data and model prediction using the average NEM constant are in approximate agreement. High surface loading, poor surface area calculation, and lack of background Am(III) loss measurements all contributed to the poor agreement between this data and that of Righetto et al. (1991; 1988).

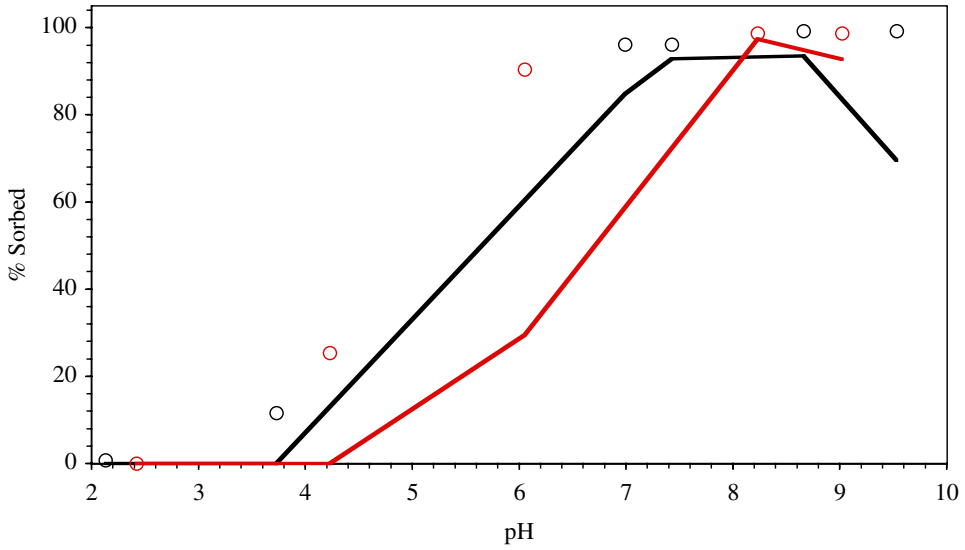

Figure 5. Sorption of 2.9×10^{-7} (black) and 2.3×10^{-9} (red) mol/L Am(III) on Al_2O_3. Solid lines represent model prediction using NEM constants from Table 2. I = 0.1; 100 mL/g Al_2O_3; 0.09-0.125 mm particle diameter; open to air; data from Allard et al. (Allard et al., 1982).

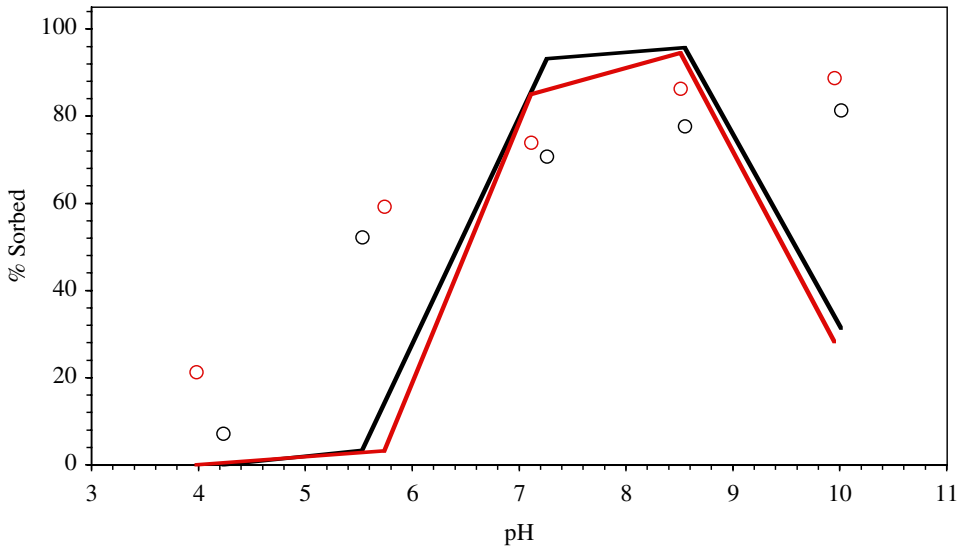

Figure 6. Sorption of 9.97×10^{-9} mol/L Am(III) on α–Al_2O_3. I = 0.01 (black) and I = 0.1 (red)). Solid lines represent model prediction using NEM constants from Table 2. 100 mL/g Al_2O_3; 0.1-0.15 mm particle diameter; open to air; data from Allard et al. (1989).

Moulin et al. (1992) measured the sorption of Am(III) to α-Al_2O_3 at two ionic strengths (Figures 7 and 8). Fits based on the average NEM constant are good and the single surface species (>$AlOAm^{2+}$) is able to fit the data well. For the data set shown in Figure 8, fits were accomplished using aqueous and sorbed Am(III) data. As reported in Table 1, using the aqueous or sorbed data results in slightly different fitted NEM constants. The fit to the aqueous and sorbed data results in Log K constants of 2.92 and 2.41, respectively. This difference can be related to the estimation of error in the data sets. For example, in this data set, nearly all Am(III) is sorbed (>90%) above pH 7.5. If it is assumed that the error in these values is near 5%, sorption at high pH is nearly constant. If the data is examined from the standpoint of aqueous Am(III) and a 5% error is attributed to the data, the concentration of Am(III) in solution varies by an order of magnitude above pH 7.5 and exhibits statistically significant variation. Because sorption data in the literature is generally plotted as percent sorbed versus pH, information related to aqueous radionuclide concentration in samples that sorb >99% of the particular radionuclide cannot be easily extracted from a plot. When data is reported as K_d versus pH, subtle changes in aqueous radionuclide concentration are better presented and radionuclide concentrations are presented more precisely. This is because the K_d constant emphasizes changes in the aqueous concentration instead of sorbed concentration.

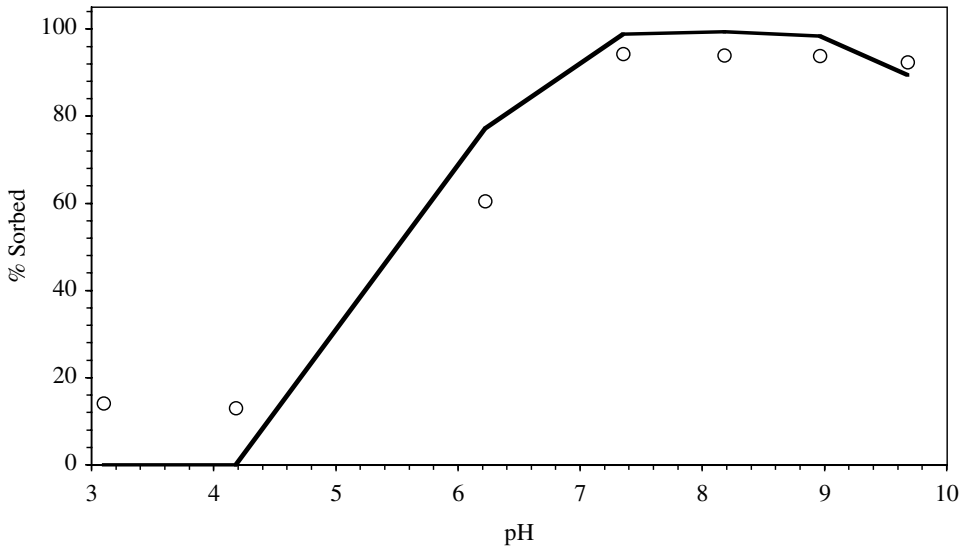

Figure 7. Sorption of 10^{-8} mol/L Am(III) on α–Al_2O_3. Solid lines represent model prediction using NEM constants from Table 2. I = 0.01; 100 mL/g Al_2O_3; 0.07 m^2/g Al_2O_3; open to air; data from Moulin et al. (1992).

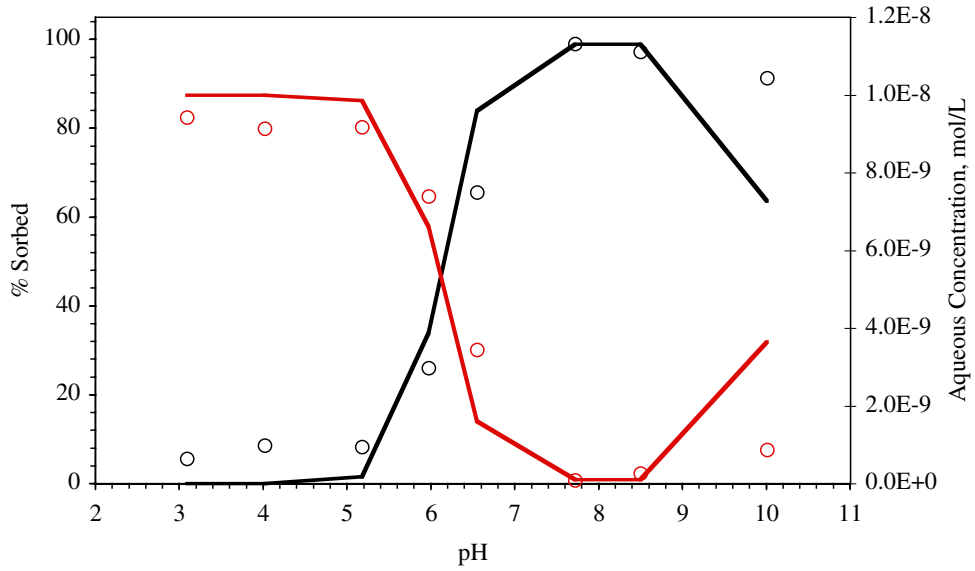

Figure 8. Sorption of 10^{-8} mol/L Am(III) on α–Al_2O_3. Solid lines represent model prediction using NEM constants from Table 2. (red represents data and fit to aqueous Am(III) concentration shown on right axis). I = 0.1; 100 mL/g Al_2O_3; 0.07 m^2/g Al_2O_3; open to air; data from Moulin et al. (1992).

Table 1 lists the best fit NEM constants for all Am(III)-alumina sorption data sets examined. Based on the data of Moulin et al. (1992) and Righetto et al. (1988; 1991), the average Log K constant for the $>AlOAm^{2+}$ surface species on alumina surfaces is 2.49 ± 0.26. If all data fitting results were averaged, the Log K constant would be 3.51 ± 1.5. The former average constant yields a more conservative estimate of sorption with a much smaller uncertainty; it is reported in our database (Table 2).

3.2 Am(III) on Silica

Several authors examined the sorption of Am(III) on silica surfaces (Allard et al., 1982; Moulin et al., 1992; Righetto et al., 1991). Righetto et al. (1991) examined the sorption of Am(III) on hydrous silica at very low surface loads. The surface area of the hydrous silica was not determined. Fitting was accomplished using the silica surface area reported by Turner (1995) (175 m^2/g). Figure 9 is a plot of this data and the best fit model using two surface species ($>SiOAm^{2+}$ and $>SiOAm(OH)_2$). A single surface species did not adequately fit the data. The fit to the data of Righetto et al. (1991) is significantly different from the fit to data of Allard et al. (1982) and Moulin et al. (1992). It is possible that the surface area used during the fit was unreasonably high, resulting in low fitted NEM constants (Table 1). Righetto et al. (1991) reported that their precipitated silica, when examined by electron microscopy, was composed of 1 μm polydispersed aggregates. If Am(III) sorbed only to the outer surface of these aggregates, the surface area of the precipitated silica would be nearly two orders of magnitude lower than reported by Turner (1995) (175 versus 2 m^2/g). When the data in Figure 9 was fit using average NEM constants but varrying surface area, 0.4 m^2/g was needed to achieve a good fit. It is, therefore, possible that the poor agreement between the data of Righetto et al. (1991) and others is a result of poor surface area estimation. Fits to the data of Righetto et al. (1991) were not used to calculate the average NEM constants (i.e. Table 2).

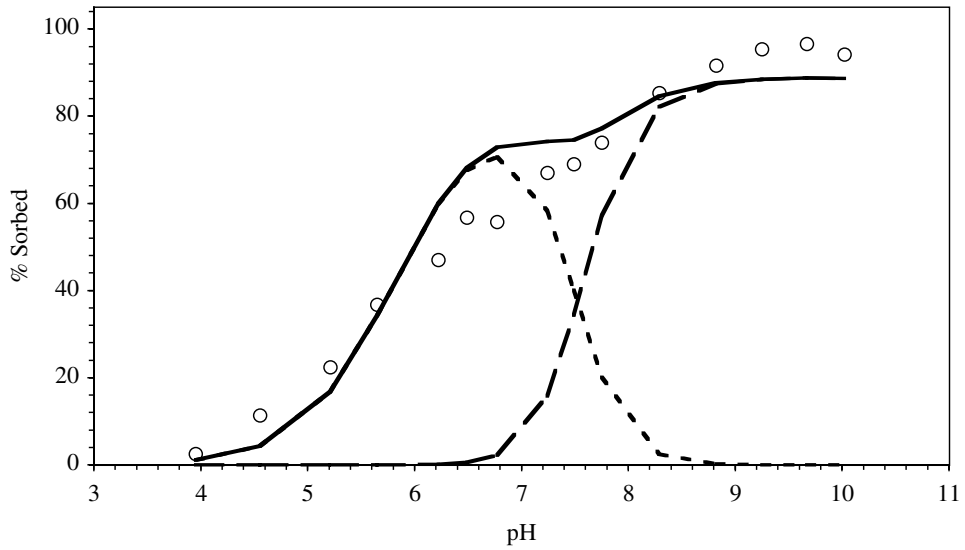

Figure 9. Sorption of 5×10^{-10} mol/L Am(III) on silica. Solid line represents data fit using best fit NEM constants. I = 0.1; 1200 ppm SiO_2; 175 m^2/g from Turner et al. (1995); open to air; data from Righetto et al. (1991).

Moulin et al. (1992) examined the interaction of silica with Am(III) at two ionic strengths. As shown in Figure 10, the average NEM constants were able to match the two data sets well. The data of Allard et al. (1982) is consistent with this data set as well (Figure 11). Allard et al. (1982) only reported a particle diameter range for the silica solids. For data fitting purposes, the surface area was estimated by assuming cubic particles with an average sieved particle diameter. The problem with extrapolating surface area from particle diameter was discussed in the previous section. Surprisingly, the average NEM constants are able to match the sorption data of Allard et al. (1982) quite well. Average Log K constants (excluding fit to Righetto et al., 1991) for $>SiOAm^{2+}$ and $>SiOAm(OH)_2$ surface species on silica are 0.7 ± 0.1 and -14.2 ± 0.8, respectively.

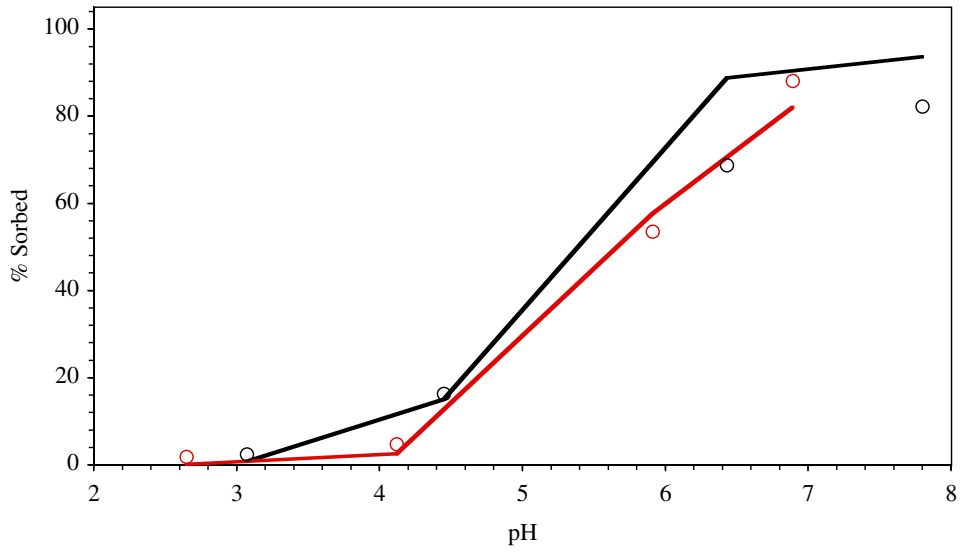

Figure 10. Sorption of 10^{-8} mol/L Am(III) on SiO_2. I = 0.01 (black) and I = 0.1 (red). Solid lines represent model prediction using NEM constants from Table 2. 100 mL/g SiO_2; 0.075 m^2/g SiO_2; open to air; data from Moulin et al. (1992).

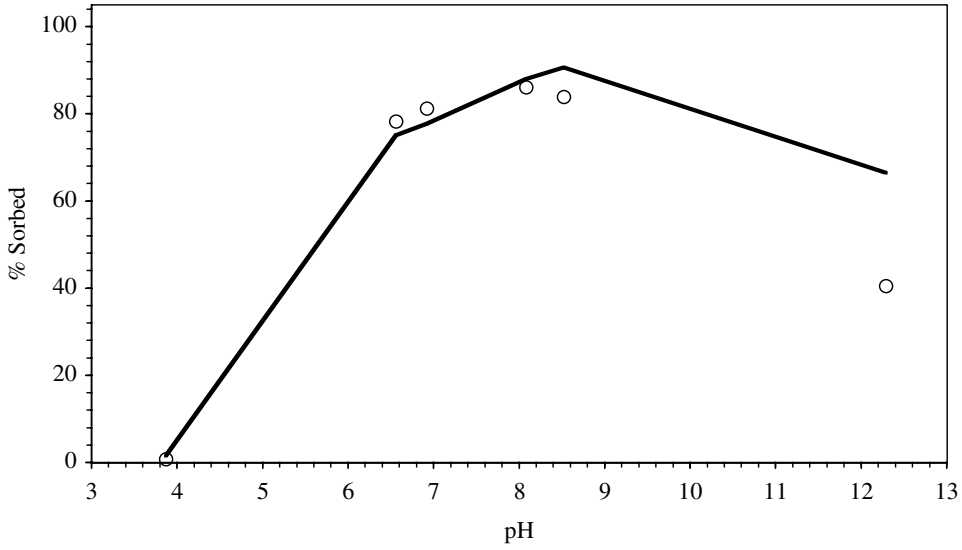

Figure 11. Sorption of 2.3×10^{-9} mol/L Am(III) on SiO_2. Solid lines represent data fits using NEM constants from Table 2. I = 0.01; 100 mL/g SiO_2; 0.09-0.125 mm particle diameter; open to air; data from Allard et al. (1982).

3.3 Am(III) on Aluminosilicates

Stammose and Dolo (1990) examined the sorption of Am(III) on a natural clay material as a function of pH and ionic strength. Before the sorption experiments were run, the clayey sediment was treated with de-ionized water, sodium dithionite/citrate, and acetic acid to remove gypsum, iron oxide, and calcite, respectively. The final clay product consisted of a mixed kaolinite-smectite clay with 0.69 meq/g cation exchange capacity and 120 m^2/g surface area. We fit the sorption data was fit using the average NEM constants determined for aluminum oxide and silica minerals (Table 2). It was assumed that 10% of the BET surface area was composed of edge >SiOH and >AlOH sites and that the ratio of >SiOH to >AlOH surface sites was 1:1. Chemical analysis indicated that the sample was composed largely of a Na-exchangeable clay. Therefore, ion exchange was assumed to occur between Na^+ and Am^{3+} at the permanently charged surface sites. Ion exchange data was fit using the simplified Vanselow IE reaction (Equation 6) appropriate for Am^{3+} sorption at low surface loads.

Data fits are shown in Figures 12 to 14. Because the sorption data set was small and involved both surface complexation and ion exchange reactions, a quantitative constant for ion exchange of $Am^{3+} \rightarrow Na^+$ could not be determined. Instead, a qualitative constant of 1.0 was determined from a visual data fit. Figure 12 presents sorption data at low ionic strength (I = 0.01). At pH >7, surface complexation begins to dominate over ion exchange even at this low ionic strength. Thus, reactive transport at neutral to high pH will be controlled by surface complexation reactions even when permanently charged sites are accessible. At higher ionic strengths, the dominance of surface complexation over ion exchange only increases such that, at I = 1, ion exchange does not seem to contribute significantly to sorption at any pH (Figure 13). The good fit between sorption data and average NEM constants indicates that extrapolation of >AlOH and >SiOH surface site reactivities from aluminum oxide and silica sorption experiments results in a good fit to this mixed clay system. Figure 14 is a plot of Am(III) sorption to clay at I = 3. The poor data fit is a result of inadequate ionic strength correction in the FITEQL fitting routine and not a poor sorption data fit. The fitting routine uses the Davies equation to determine species activity ($\log(\text{activity}) = -z^2 0.509\left(\frac{\sqrt{I}}{1+\sqrt{I}} - 0.3I\right)$ where z is ion charge and I is ionic strength). As the ionic strength increases above I = 0.1, the Davies equation first underestimates the activity of species in solution but later overestimates activity severely, particularly for high z ions. Thus, the poor sorption fit results from a limitation in the fitting routine.

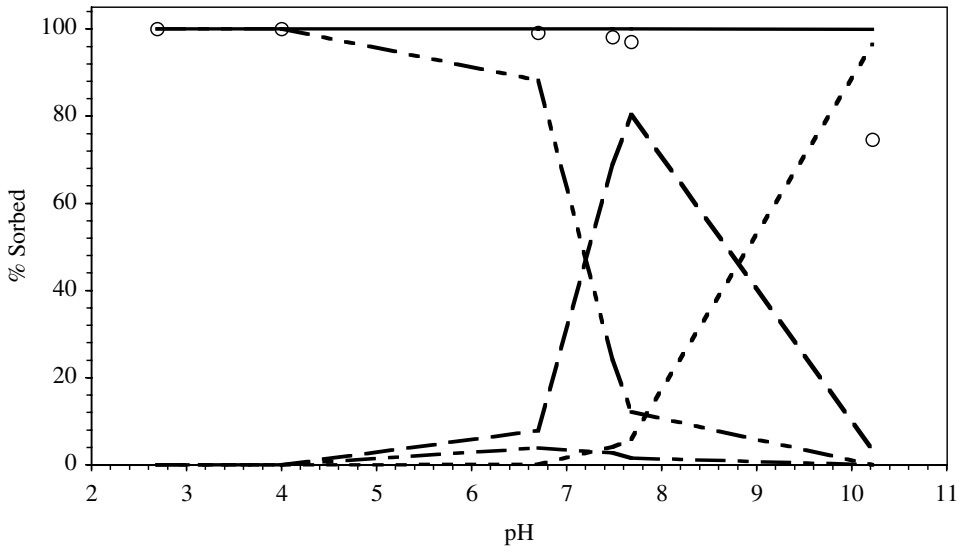

Figure 12. Sorption of 10^{-8} mol/L Am(III) on mixed kaolinite/smectite clay. Solid lines represent model prediction using NEM constants from Table 2. I = 0.01; 200 mL/g clay; 120 m^2/g clay; 0.69 meq/g; open to air; dashed lines represent contribution of individual IE and SC reactions; data from Stammose and Dolo (1990).

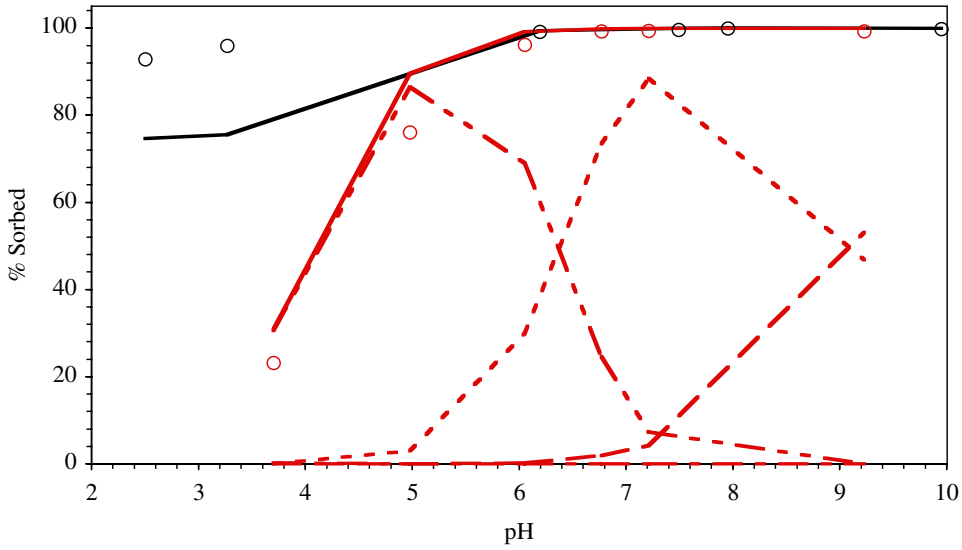

Figure 13. Sorption of 10^{-8} mol/L Am(III) on kaolinite/smectite clay. I = 0.1 (black) and I = 1 (red). Solid lines represent data fits using average NEM and Vanselow IE constants. 200 mL/g clay; 120 m^2/g; 0.69 meq/g; open to air; dashed lines represent contribution of individual IE and SC reactions for I = 1 data set; data from Stammose and Dolo (1990).

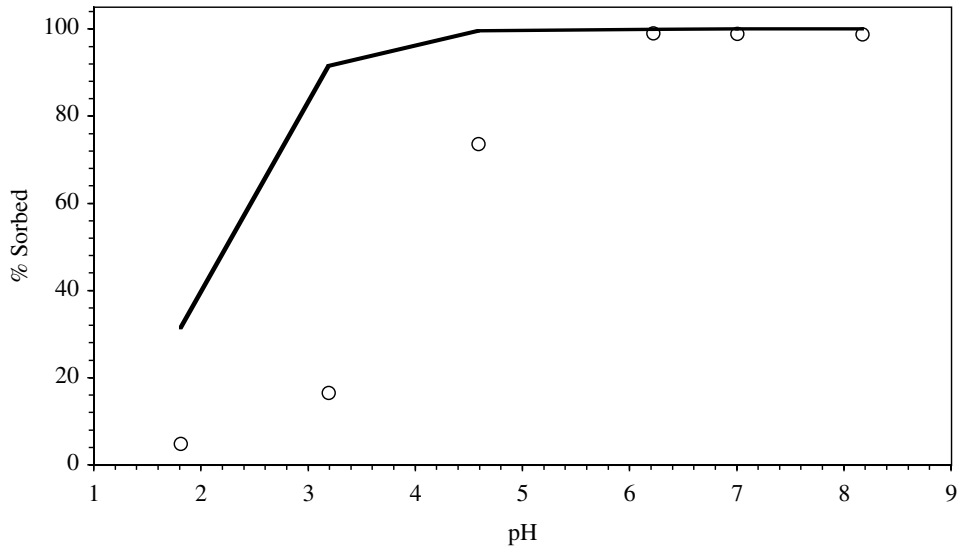

Figure 14. Sorption of 10^{-8} mol/L Am(III) on kaolinite/smectite clay. Solid lines represent model prediction using NEM constants from Table 2. I = 3; 200 mL/g clay; 120 m^2/g; 0.69 meq/g; open to air; data from Stammose and Dolo (1990).

3.4 Eu(III) on Aluminum Oxide

Two references that report sorption of Eu(III) on aluminum oxide surfaces were examined. Shiao et al. (1981) measured Eu(III) sorption to freshly precipitated Al_2O_3 as a function of pH and ionic strength. The surface area of the precipitated material was not measured; the value reported by Turner (1995) was used to fit data. Data was presented in K_d form and >90% of the Eu(III) sorbed over the entire pH range. Thus, a better fit could be accomplished by fitting the changes in aqueous Eu(III) as a function of pH instead of percent sorbed. Figures 15 to 17 present the data and fits. The fit was satisfactory at all pH and ionic strength using a single surface species. Best fits to the data are listed in Table 1. Norden et al. (1994) also measured the sorption of Eu(III) on Al_2O_3. Unfortunately, surface area was not measured in their samples as well. Particle size was defined only as ≤63 µm in diameter. Estimating the surface area using 63 µm cubic particle diameter, fitted NEM constants are much greater than for Shiao et al. (1981). Using the average Log K constant of Shiao et al. (1981) and a particle diameter of 63 µm, the model significantly underestimates sorption (Figure 18). Since the particle size of Al_2O_3 in the sorption experiments was 63µm or less, it is likely that sorption would be underestimated using exclusively 63 µm as particle size. The average Log K for $>AlOEu^{2+}$ (using data of Shiao et al. (1981) only) is 2.29±0.45 (Table 2). The value is very near that of Am(III) of Al_2O_3, consistent with the observation that these two elements behave in a similar manner.

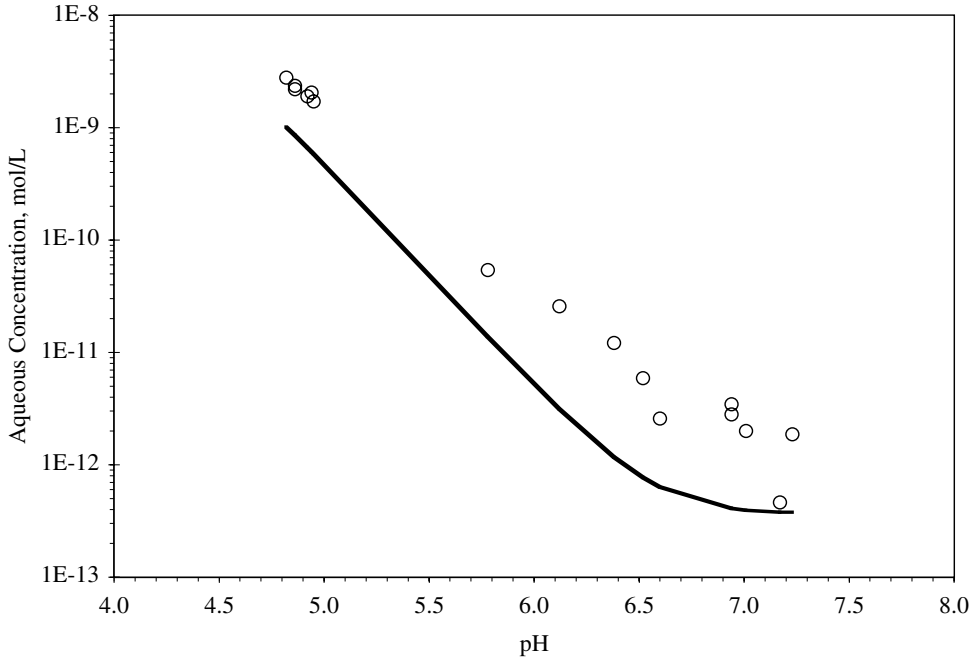

Figure 15. Sorption of 10^{-8} mol/L Eu(III) on Al_2O_3. Solid lines represent model prediction using NEM constants from Table 2. I = 0.01; 10 g/L Al_2O_3; 4.6×10^{-3} mol/L sorption sites estimated from Turner et al. (1995); open to air; data from Shiao et al. (1981).

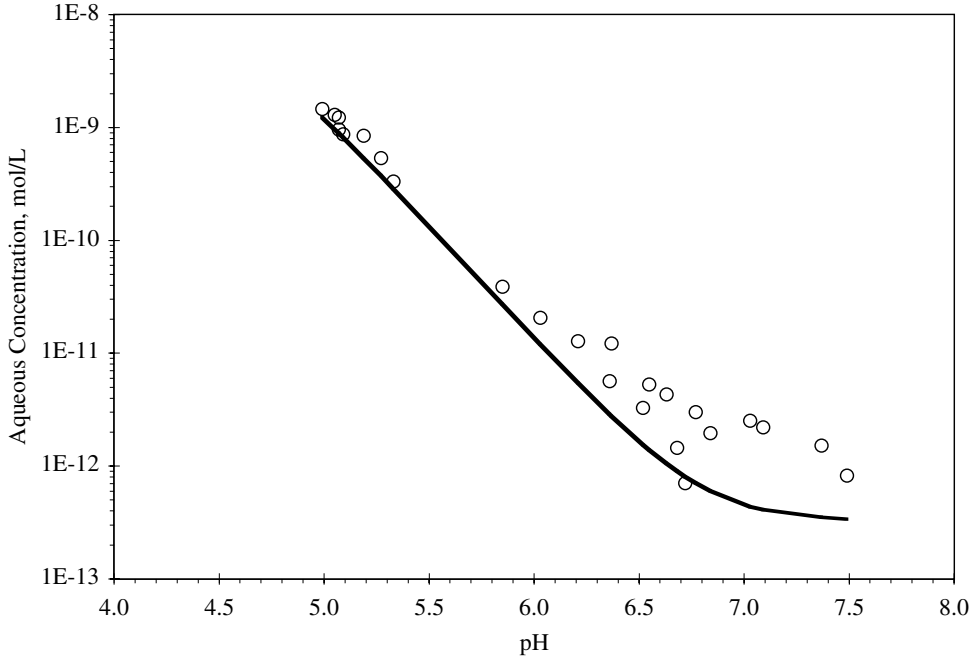

Figure 16. Sorption of 10^{-8} mol/L Eu(III) on Al_2O_3. Solid lines represent model prediction using NEM constants from Table 2. I = 0.1; 10 g/L Al_2O_3; 4.6×10^{-3} mol/L sorption sites estimated from Turner et al. (1995); open to air; data from Shiao et al. (1981).

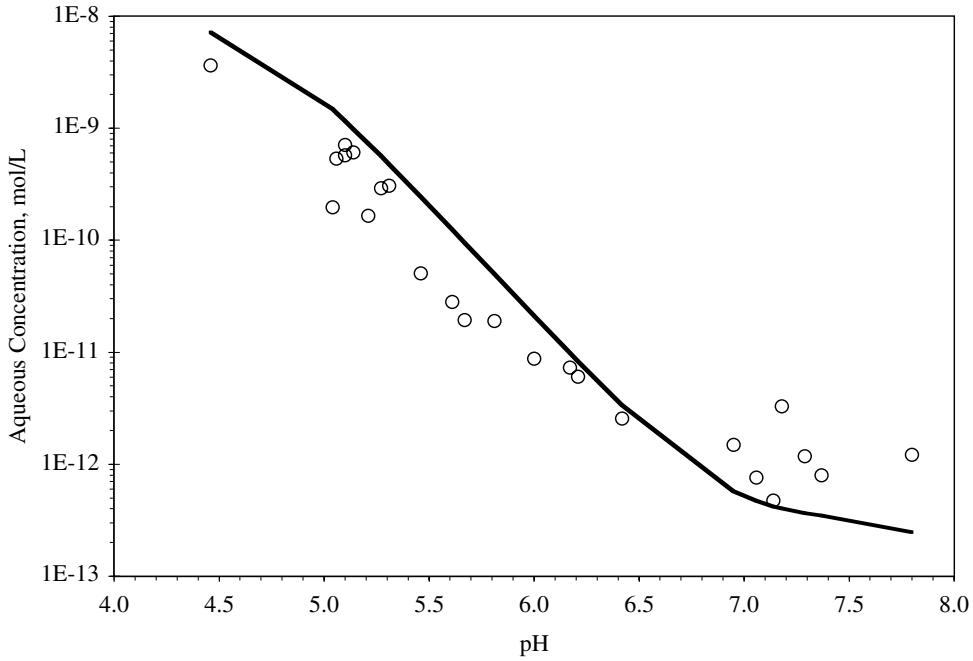

Figure 17. Sorption of 10^{-8} mol/L Eu(III) on Al_2O_3. Solid line represents data fit using average NEM constant. I = 0.5; 10 g/L Al_2O_3; 4.6×10^{-3} mol/L sorption sites estimated from Turner et al. (1995); open to air; data from Shiao et al. (1981).

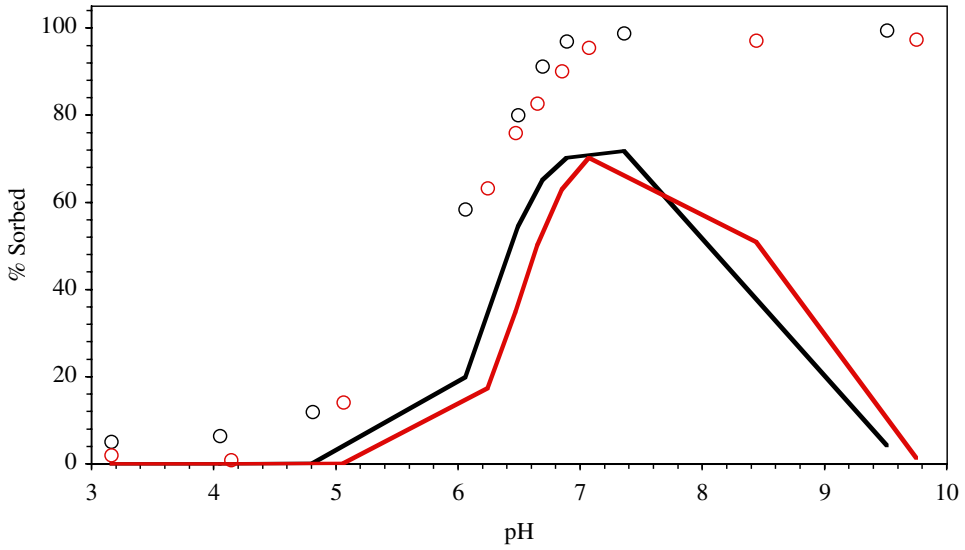

Figure 18. Sorption of 7×10^{-9} mol/L Eu(III) on α-Al_2O_3 at I = 0.01 (black) and I = 0.1 (red). Solid lines represent model prediction using NEM constants from Table 2. 5 g/L Al_2O_3; <0.063 mm particle size fraction; open to air; data from Norden et al. (1994).

3.5 Eu(III) on Silica

Eu(III) sorption to silica was investigated by several authors (Fairhurst et al., 1995; Ledin et al., 1994; Norden et al., 1994). Data fits are shown in Figures 19 to 21 and fitted NEM constants are listed in Table 1. NEM constant fits to data of Fairhurst et al. (1995) and Ledin et al. (1994) are in agreement. As discussed in the previous section, Norden et al. (1994) did not report surface area measurements. Surface area was estimated from the maximum particle size that was listed (mineral sample was sieved to ≤63mm particle size). The fitted NEM constants for this data set are, therefore, expected to be significantly greater than for the other references. This result is consistent with that of Eu(III) on aluminum oxide, as discussed in the previous section. Average Log K constants for Eu(III) on SiO_2 (excluding data of Norden et al., 1994) are -0.63 and -14.13 for $>SiOEu^{2+}$ and $>SiOEu(OH)_2$, respectively (Table 2). Standard deviations could not be measured because only two sorption data sets were used in the average. The difference in the two data sets for the two species are 1.0 and 0.15, respectively.

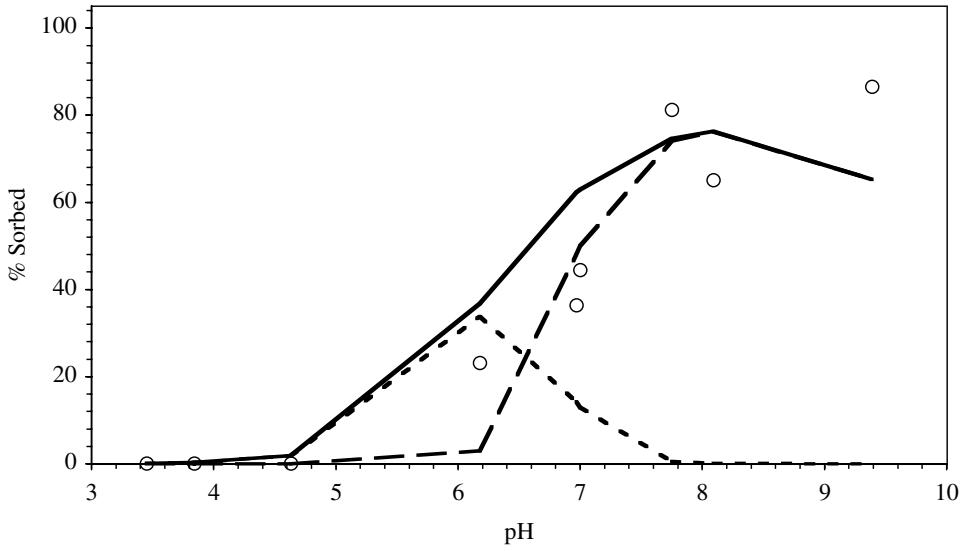

Figure 19. Sorption of 10^{-8} mol/L Eu(III) on SiO_2. Solid lines represent model prediction using NEM constants from Table 2. Dashed lines indicate individual contribution of surface species. I = 0.01; 70 mg/L SiO_2; 16 m^2/g SiO_2; open to air; data from Ledin et al. (1994).

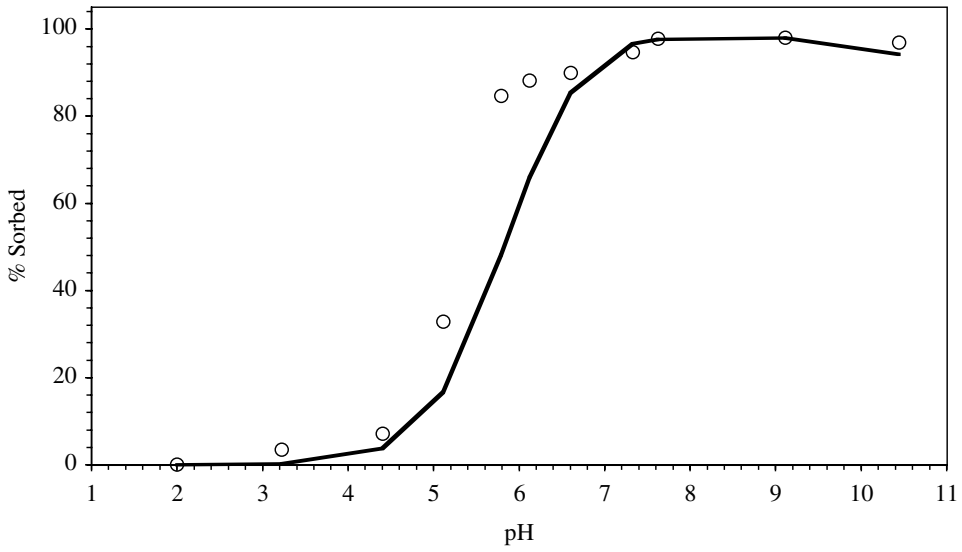

Figure 20. Sorption of 10^{-9} mol/L Eu(III) on SiO_2. Solid lines represent model prediction using NEM constants from Table 2. I = 0.05; 22.7 g/L SiO_2; 0.37 m^2/g SiO_2; open to air; data from Fairhurst et al. (1995).

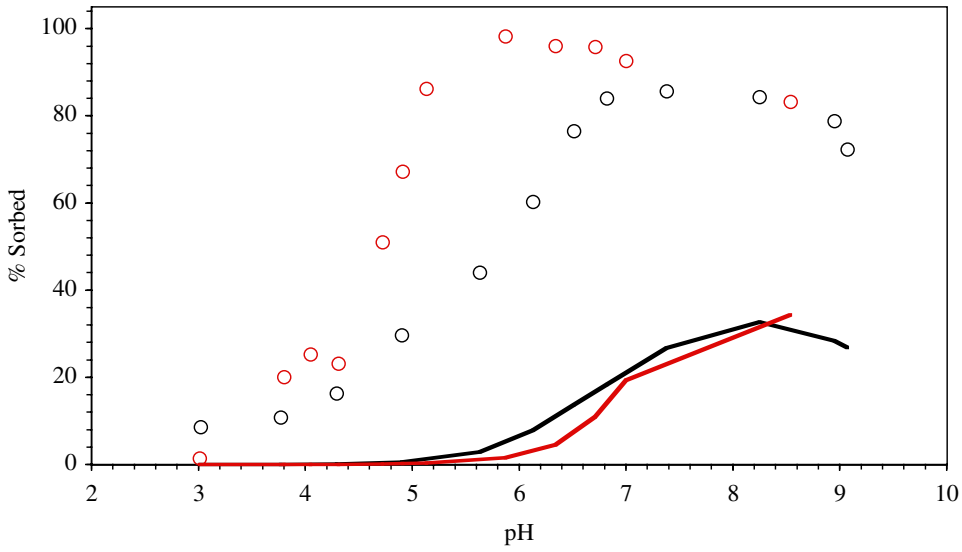

Figure 21. Sorption of 7×10^{-9} mol/L Eu(III) on SiO_2 at I = 0.01 (black) and I = 0.1 (red). Solid lines represent model prediction using NEM constants from Table 2. 5 g/L SiO_2; <63mm particle size; open to air; data from Norden et al. (1994).

3.6 Eu(III) on Aluminosilicates

Two references to Eu(III) sorption to aluminosilicates were examined (Kornilovich et al., 1997; Wang et al., 1998). Kornilovich et al. (1997) examined the interaction of Eu(III) with natural montmorillonite and kaolinite. Because surface area measurements were not determined and Eu(III) concentrations were high enough (10^{-4} mol/L) to possibly induce precipitation, these data were not evaluated. Sorption of Eu(III) to Silver Hill illite was investigated by Wang et al. (1998). Sorption was measured as a function of ionic strength and pH. The concentration of surface complexation and ion exchange sites was taken directly from the reference. The concentration of surface complexation sites reported in the reference is nearly equal to the surface site concentration predicted using the BET surface area and assuming 2.31sites/nm^2. For illite, the fraction of BET surface area related to edge sites is likely to be much greater than the 10% used for smectite calculations. Wang et al. (1998) attempted to fit the sorption data using ion exchange and surface complexation reactions and found that the best fit ion exchange constant varied with ionic strength. They hypothesized that the high Na concentration in the experiments may have led to non-ideal ion exchange behavior. The non-ideal behavior of ion exchange was also observed here. As reported in Table 1, Vanselow IE Log K constants varied from 0.33 to 1.25 with increasing ionic strength. Typically, ion exchange on illite is modeled using 3 site types with varying sorption affinities. It is likely that the different affinity of Eu(III) for the three site types can account for the non-ideal ion exchange observation. Surface complexation was based on aluminum oxide and silica average NEM constants (Table 2). Results are shown in Figure 22. Above pH ~6, surface complexation begins to dominate over ion exchange as the primary mode of sorption. The result is not unlike that of Am(III) sorption to smectite, as shown earlier. In fact, NEM and Vanselow IE constants for Am(III) and Eu(III) are nearly the same. This similar behavior is expected given their similar valence and speciation behavior.

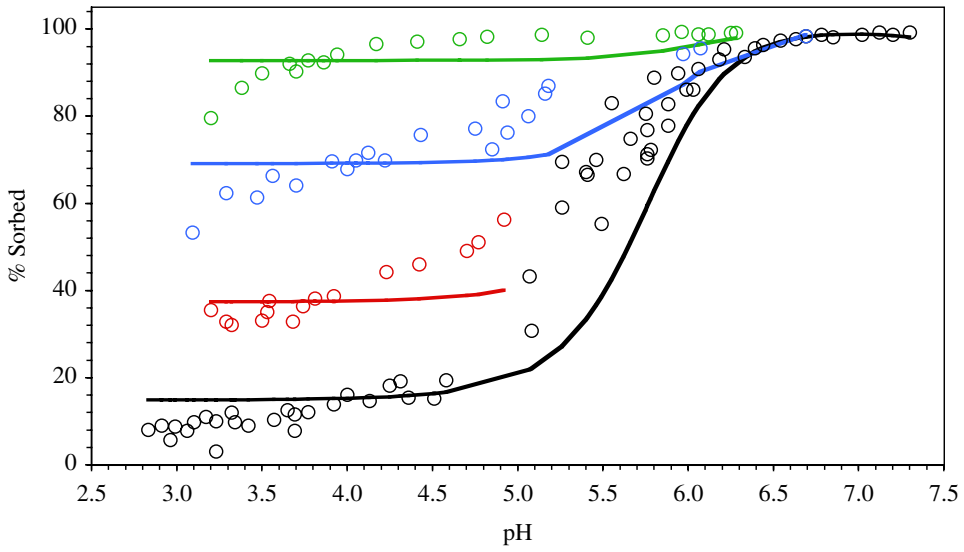

Figure 22. Sorption of 10^{-8} mol/L Eu(III) on illite. I = 0.5 (black), I = 0.2 (red), I = 0.1 (blue), and I = 0.02 (green). Solid lines represent model prediction using NEM surface complexation constants from Table 2 and best fit IE constants. 1 g/L illite; 5.7×10^{-5} mol/g illite edge sites; 1:1 Si:Al site ratio; CEC = 71meq/kg illite; open to air; data from Wang et al. (1998).

3.7 Np(V) on Aluminum Oxide

Several authors have examined the interaction of Np(V) with aluminum oxide minerals (Allard et al., 1982; Bertetti et al., 1998; Nakayama and Sakamoto, 1991; Righetto et al., 1991; Righetto et al., 1988). Sorption experiments were performed on both colloidal and larger particle size Al_2O_3. Sorption experiments performed on colloidal material resulted in very low surface loads. During fitting, it was found that fitted NEM constants determined for colloidal and larger particle sorption experiments differed significantly. Np(V) sorbed more strongly to colloidal aluminum oxide even when surface area differences were accounted for. This difference may be the result of recrystallization of colloidal material or the presence of multiple reactive site types. Regardless of the underlying mechanisms, average NEM Log K constants were calculated for high and low surface area sorbing materials separately. Fitted NEM constants for each data set are listed in Table 1. Average NEM database constants (Table 2) were based on the low surface area aluminum oxide minerals.

Model results using average fitted NEM constants for colloidal aluminum oxide experiments are shown in Figures 23 to 26. For nearly all colloidal aluminum oxide sorption data, best fit Log K constants are quite similar resulting in a good match between the average Log K constants model results and data. The average values are -2.37 ± 0.55 and -13.62 for $>AlONpO_2$ and $>AlONpO_3H^-$, respectively. A standard deviation for the $>AlONpO_3H^-$ NEM constant could not be determined because it is an average of two values; its effect on sorption is significant only at very high pH where data are limited.

Figure 24 shows the data and fit to sorption experiments conducted in 0.05 mol/L $NaHCO_3$. In this case, the data fit is poor. As discussed for the Am(III) sorption data presented earlier (Righetto et al., 1988), control of carbonate alkalinity in solution may not have been adequate to control degassing. Thus, the poor fit is not necessarily the result of missing or inappropriate NEM constants. The underestimated sorption at high pH may be indicative of additional ternary surface complexes but the limited data are not sufficient to justify additional NEM reactions.

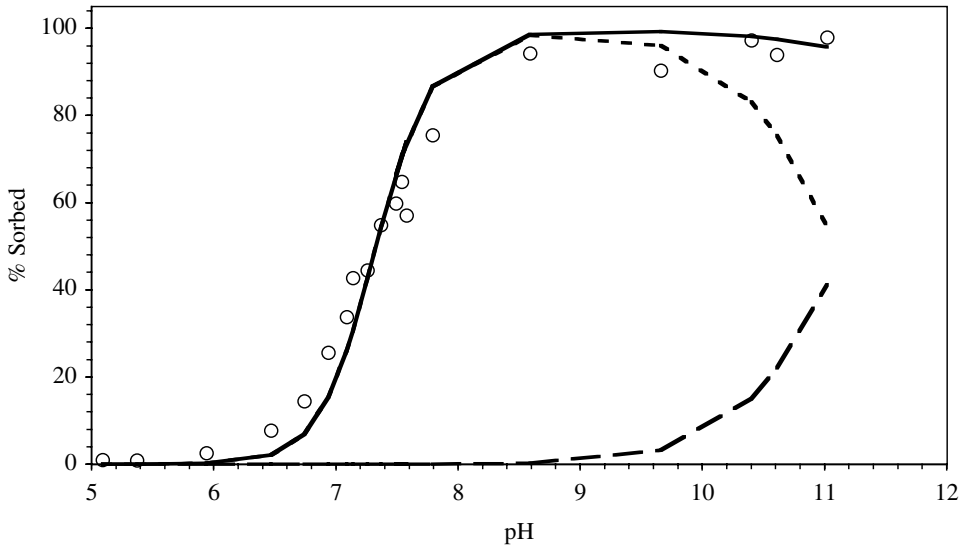

Figure 23. Sorption of 10^{-14} mol/L Np(V) on colloidal alumina. Solid lines represent data fits using average colloidal alumina NEM constants. Dashed lines represent contribution of individual surface species to sorption. I = 0.1; 200 ppm Al_2O_3; 130 m^2/g Al_2O_3; open to air; data from Righetto et al. (1988).

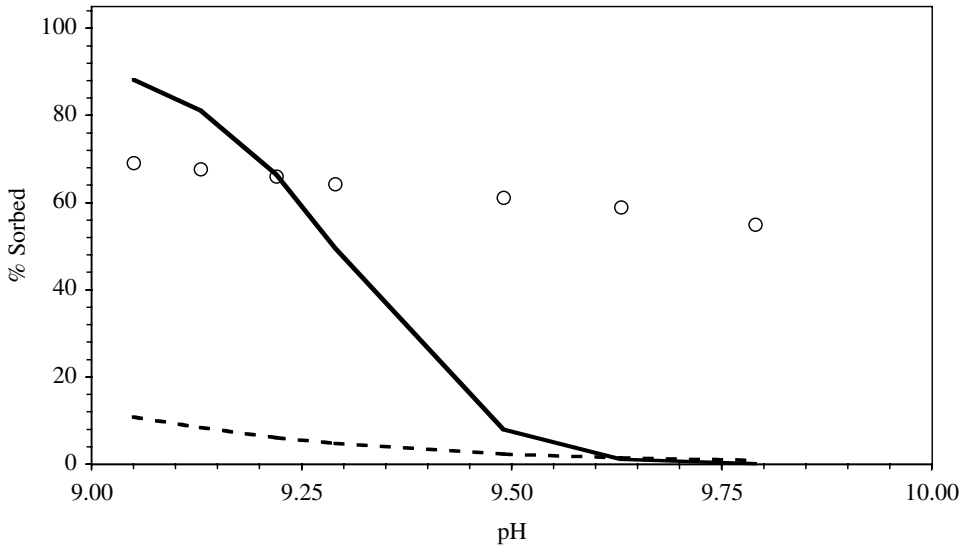

Figure 24. Sorption of 10^{-14} mol/L Np(V) on colloidal alumina. Solid lines represent data fits using average colloidal alumina NEM constants. 0.05 mol/L HCO_3^- (solid line) and atmospheric CO_2 (dashed line); I = 0.1; 200 ppm Al_2O_3; 130 m^2/g Al_2O_3; open to air; data from Righetto et al. (1988).

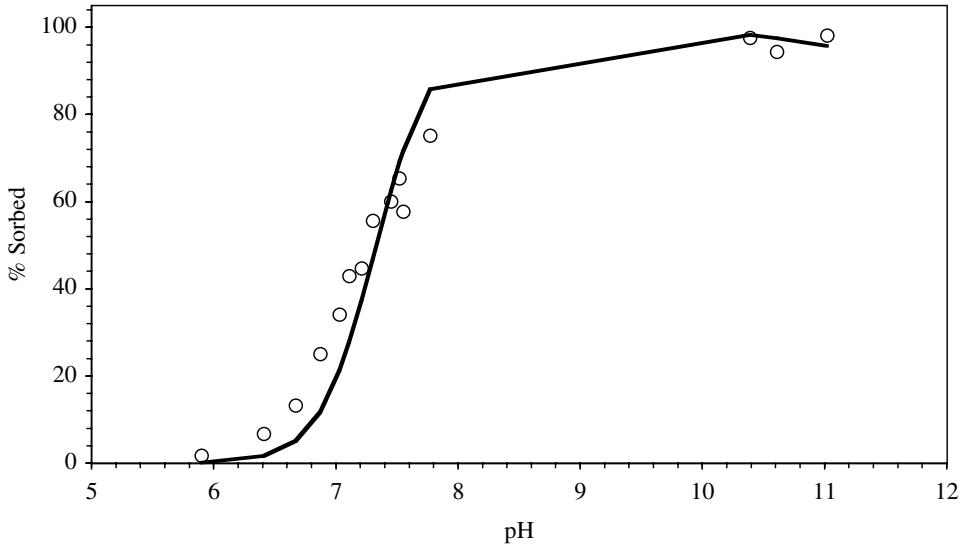

Figure 25. Sorption of 10^{-14} mol/L Np(V) on colloidal alumina. Solid line represents data fit using average colloidal alumina NEM constants. I = 0.1; 200 ppm Al_2O_3; 130 m^2/g Al_2O_3; open to air; data from Righetto et al. (1991).

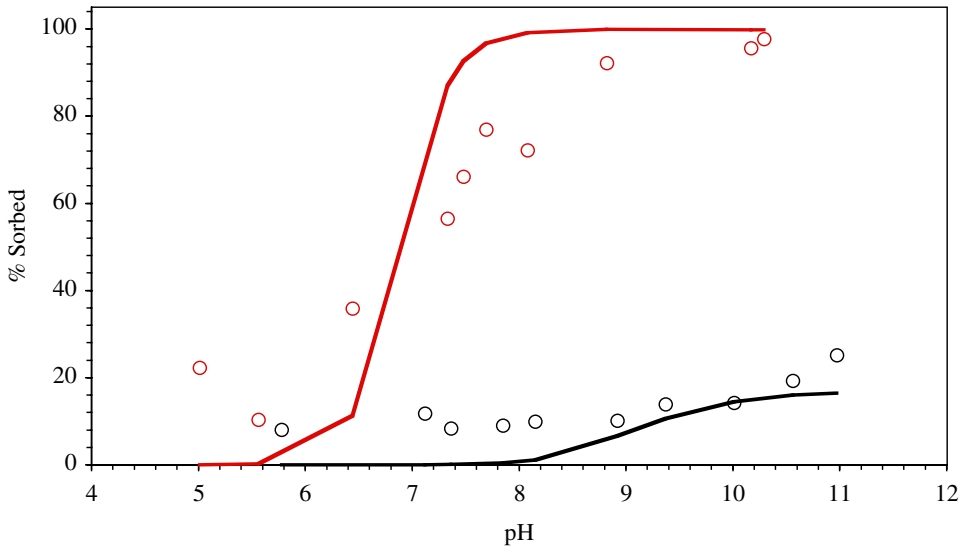

Figure 26. Sorption of 6×10^{-6} mol/L Np(V) on colloidal alumina (175 m^2/g) (red) and low surface area α-alumina (2.5 m^2/g) (black). Solid lines represent data fits using average colloidal alumina and α-alumina NEM constants. I = 0.1; 1 g/L Al_2O_3; open to air; data from Nakayama and Sakamoto (1991).

Several authors examined the sorption of Np(V) on aluminum oxide material of low surface area and relatively high surface loads (Allard et al., 1982; Bertetti et al., 1998; Nakayama and Sakamoto, 1991). The best fit NEM constants to data of Nakayama and Sakamoto (1991) and Bertetti et al. (1998) (Table 1 and Figures 26 and 27) are in good agreement. The best fit NEM constant to data of Allard et al. (1982) (Table 1 and Figure 28) is significantly higher. The best fit NEM constants for Am(III) sorption data of Allard et al. (1989; 1982) were also higher than for other published data. Since surface areas for these experiments were estimated from sieving results, it is likely that surface area estimates were too low, resulting in unusually high NEM constants. Ignoring the data of Allard et al. (1982), the average Log K constants for low surface area aluminum oxide data were estimated to be -4.67 ± 0.27 and -14.26 ± 0.04 for $>AlONpO_2$ and $>AlONpO_3H^-$, respectively.

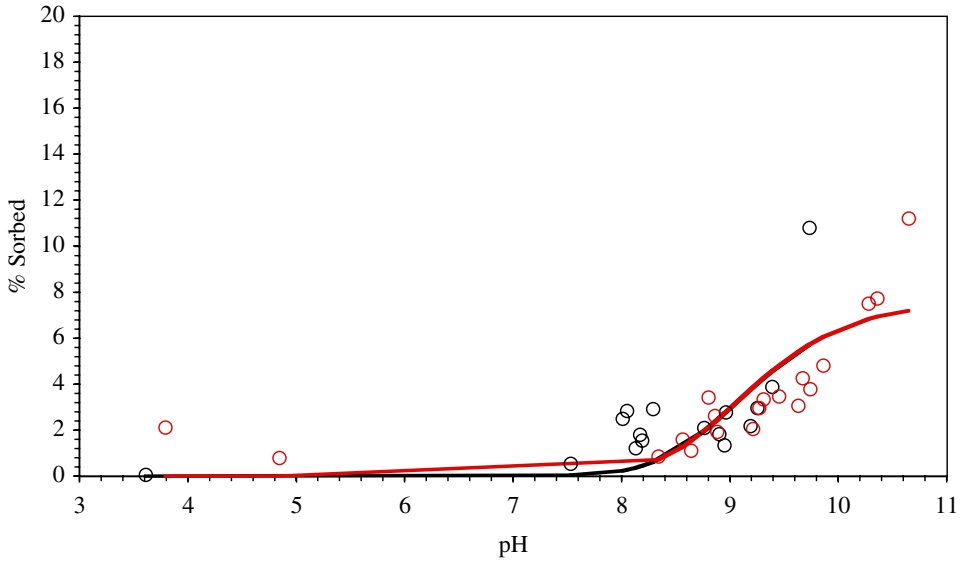

Figure 27. Sorption of 10^{-6} mol/L Np(V) on low surface area α-Al_2O_3 (two data sets). Solid lines represent data fits using average low surface area α-Al_2O_3 NEM constants. I = 0.01; 4 g/L Al_2O_3; 0.23 m^2/g Al_2O_3; in the absence of CO_2; data from Bertetti et al. (1998).

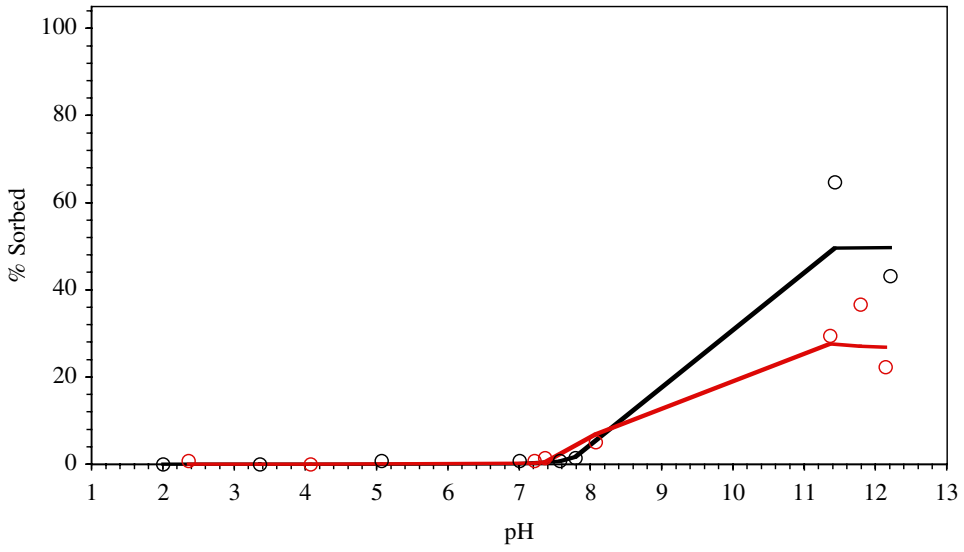

Figure 28. Sorption of 1.9×10^{-7} (red) and 1.9×10^{-9} (black) mol/L Np(V) on alumina. Solid lines represent data fits using <u>best fit</u> NEM constants. I = 0.01; 0.2 g in 20mL; 0.09-0.125 mm particle diameter; open to air; data from Allard et al. (1982).

The difference in NEM constants for the low surface area and high surface area aluminum oxide minerals is indicative of possible multiple-site binding on the aluminum oxide surface similar to iron oxides. However, the available data is rather limited. The lower NEM constants (high surface load) are more conservative with respect to radionuclide transport. These NEM constants also fit aluminosilicate sorption data (Section 4.9) suggesting that they may be more appropriate. They are, therefore, reported in Table 2. Nevertheless, colloidal aluminum oxide sorption data suggest that Np(V) may sorb to aluminum oxides significantly more strongly at very low surface loads.

3.8 Np(V) on Silica

Np(V) sorption to silica was examined by Righetto et al. (1991) and Bertetti et al. (1998) (Figures 29 to 31). The fitted NEM constants for the data of Righetto et al. (1991) are significantly lower than fitted NEM constants for the data of Bertetti et al. (1998) (Table 1). For the data of Righetto et al. (1991), an overestimated colloidal silica surface area could account for the low fitted NEM constant. This same conclusion was made with respect to fitted Am(III) NEM constants for the data reported by these same authors (see Am(III) discussion above). The multiple data sets of Bertetti et al. (1998) all resulted in similar fitted NEM constants (Table 1). The average Log K constants using these data fits are –3.72±0.15 and –12.16 for $>SiONpO_2$ and $>SiONpO_3H^-$, respectively. An error estimate could not be performed for $>SiONpO_3H^-$ because this surface species contributed to sorption only when CO_2 was absent from solutions. Only two data sets were reported by Bertetti et al (1998) at low $CO_2(g)$.

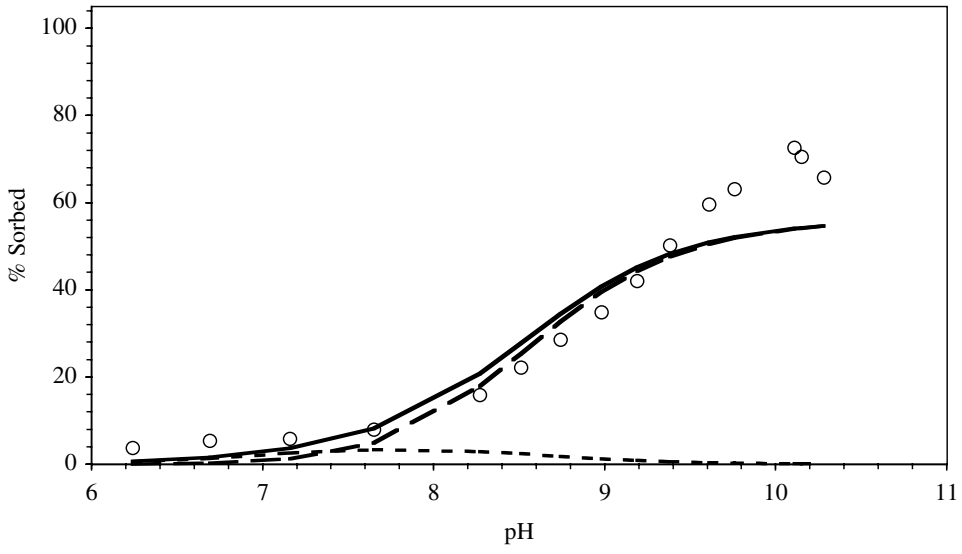

Figure 29. Sorption of 10^{-14} mol/L Np(V) on colloidal silica. Solid lines represent data fits using best fit NEM constants. Dashed lines represent contribution of individual surface species. I = 0.1; 1200 ppm SiO_2; 175 m^2/g SiO_2 from Turner (1995); open to air; data from Righetto et al. (1991).

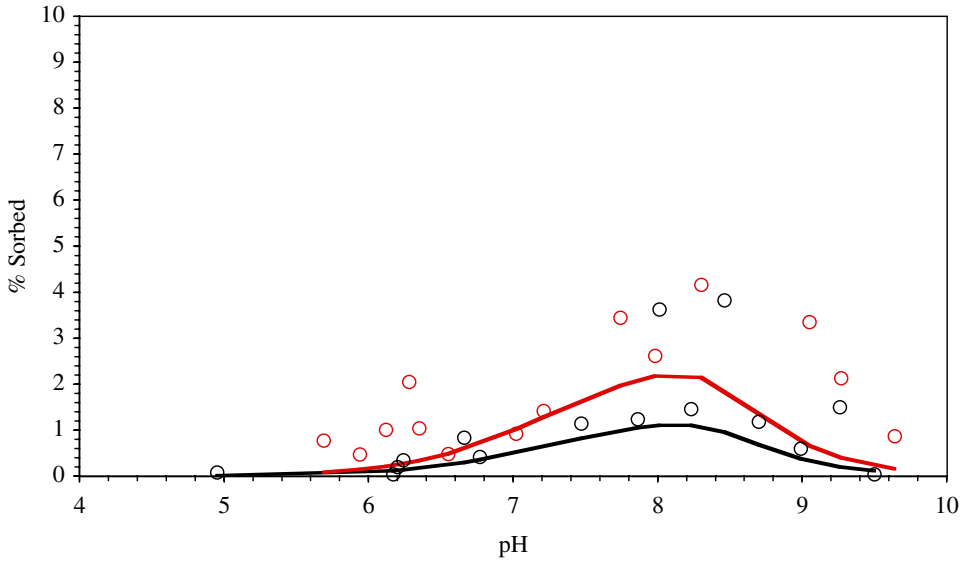

Figure 30. Sorption of 10^{-7} mol/L Np(V) to 40 g/L (black) and 80 g/L (red) on SiO_2. Solid lines represent model prediction using NEM constants from Table 2. I = 0.1; 0.03 m^2/g SiO_2; open to air; data from Bertetti et al. (1998).

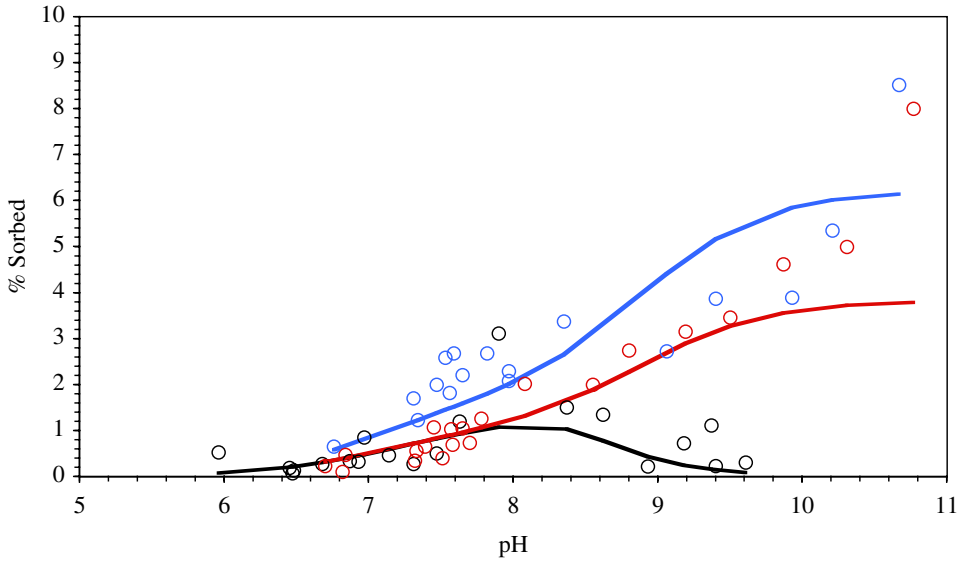

Figure 31. Sorption of 10^{-6} mol/L Np(V) on 40 g/L SiO_2 in air (black), 40 g/L SiO_2 w/o CO_2 (red), and 4 g/L fine grained SiO_2 w/o CO_2 (blue). Solid lines represent model prediction using NEM constants from Table 2. I = 0.1; 0.03 m^2/g SiO_2; 0.5 m^2/g fine grained SiO_2; data from Bertetti et al. (1998).

3.9 Np(V) on Aluminosilicates

Several authors have examined the interaction of Np(V) with aluminosilicates (Bertetti et al., 1998; Bertetti et al., 1995; Turner et al., 1998). Turner et al. (1998) hypothesized that Np(V) sorption to montmorillonite could be described by surface complexation to >AlOH and >SiOH sites at the edges of this layered clay mineral. Here, model results using average NEM constants determined for aluminum oxide and silica sorption experiments (Sections 3.7 and 3.8) are compared to montmorillonite sorption data. Following the suggestion of Turner et al. (1998), it was estimated that 10% of the BET surface area comprised reactive edge sites. Turner et al. (1998) used an Al/Si reactive site ratio of 0.83:1; in our case, we used a ratio of 1:1. Data fits are shown in Figure 32. No adjustment of NEM constants was performed. Because two sets of NEM constants were calculated for aluminum oxides (colloidal and low surface area), fits to montmorillonite data were examined with both sets of values. Only the low surface area aluminum oxide constants fit montmorillonite data well even though surface loads on montmorillonite were relatively low. At I = 0.1, sorption at low pH was minor; indicating that ion exchange of Np(V) on montmorillonite was not significant under these experimental conditions. At lower ionic strength, ion exchange may become significant though little data is available. Aksoyoglu et al. (1991) examined sorption of Np(V) on natural smectite clay at pH 1.5 and 7.6; they found that sorption was nearly pH-independent under their experimental conditions. This would indicate that ion exchange may only control sorption of Np(V) to montmorillonite at low ionic strength and at neutral to acid pH.

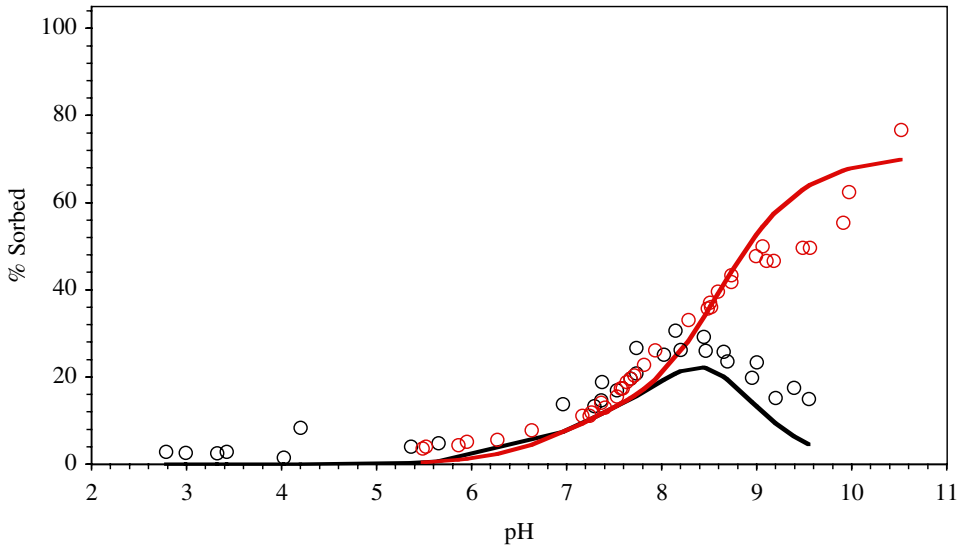

Figure 32. Sorption of ~9×10^{-7} mol/L Np(V) on montmorillonite in air (black) and w/o CO_2 (red). Solid lines represent model prediction using NEM constants from Table 2. I = 0.1; ~4 g/L montmorillonite; 97 m^2/g; 10% edge sites; 1:1 Si:Al site ratio; data from Turner et al. (1998).

Sorption of Np(V) to clinoptilolite was evaluated in the same manner as for montmorillonite. Again, reactive surface sites were estimated to comprise 10% of the BET surface area. This new site density was determined from comparisons made by Bertetti et al. (1998) that showed clinoptilolite sorption to be equivalent to that of montmorillonite (on a surface area basis). The Al:Si reactive site ratio was estimated by the molar ratio of these elements in clinoptilolite. Pabalan (1994) measured the concentration of Al and Si in the clinoptilolite used in the experiments of Bertetti et al. (1998). The Al:Si ratio was found to be approximately 15:85, typical of clinoptilolites in general. This ratio was used to estimate the concentration of >AlOH and >SiOH reactive sites on the clinoptilolite surface. Results are presented in Figure 33. As in the case of Np(V) on montmorillonite, ion exchange under these experimental conditions was not significant, though a small amount of sorption at low pH was evident.

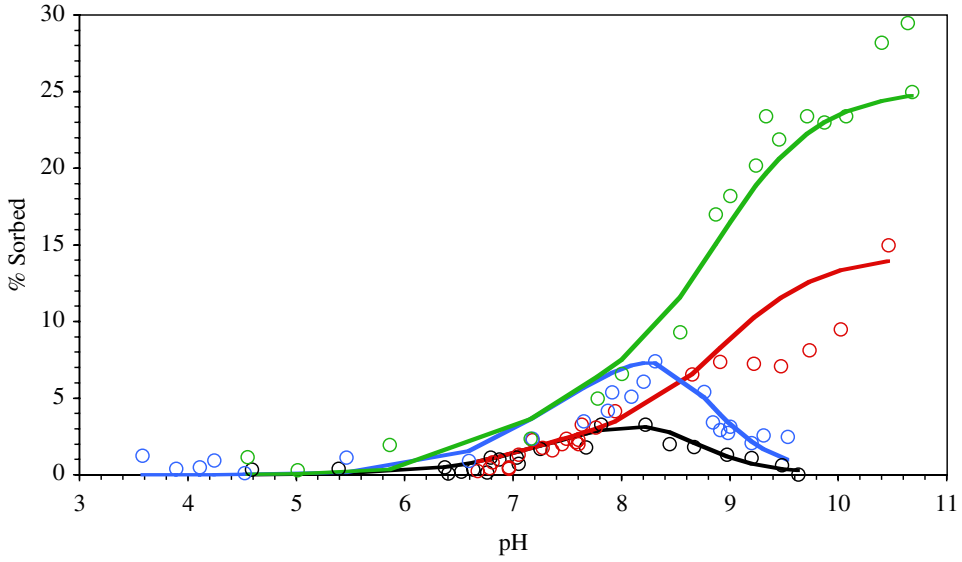

Figure 33. Sorption of 10^{-6} mol/L Np(V) on clinoptilolite with 4 g/L, I = 0.1, in air (black), 4 g/l, I = 0.1, w/o CO_2 (red), 8 g/L, I = 0.01, in air (blue), and 8 g/L, I = 0.01, w/o CO_2 (green). Solid lines represent model prediction using NEM constants from Table 2. 10.1 m^2/g clinoptilolite; 10% reactive edge sites; 15:85 Al:Si site ratio; data from Bertetti et al. (1998).

3.10 Pu on Aluminum Oxide

Pu sorption experiments are difficult to perform and model because Pu sorption is sensitive to oxidation state which is difficult to control. The reduction of Pu(V) to Pu(IV) during sorption to iron oxide surfaces was documented by Sanchez et al. (1985). Sanchez (1983) also found this reduction to occur on silica and montmorillonite surfaces. Newton et al. (1986) found that reduction of Pu(V) and Pu(VI) to Pu(IV) may also occur in the absence of any minerals. They hypothesized that the processes involved in reduction were: 1) disproportionation of Pu(V) to Pu(IV) and Pu(VI) and 2) alpha-particle induced reduction of Pu(VI) to Pu(V). Whatever the mechanism, it is likely that Pu may be reduced during

sorption reactions with aluminum oxide minerals. Sorption data must, therefore, be critically evaluated with respect to possible redox changes over the course of experiments.

Righetto et al. (1991) sorbed Pu to γ-alumina with an equilibration time of 7 days. The oxidation state of Pu was not measured during experiments. The data could be fit equally well by assuming either Pu(IV) or Pu(V) in solution. Fitted NEM constants and comparison of model to data are reported in Table 1 and Figure 34, respectively. Assuming that the alumina surface may enhance Pu(V) reduction (as in the case of iron oxide), some Pu is likely to have been in the +4 state during the sorption experiment. The Pu oxidation state would need to be known to estimate NEM constants from these data. These data, therefore, were not be used to calculate average NEM constants.

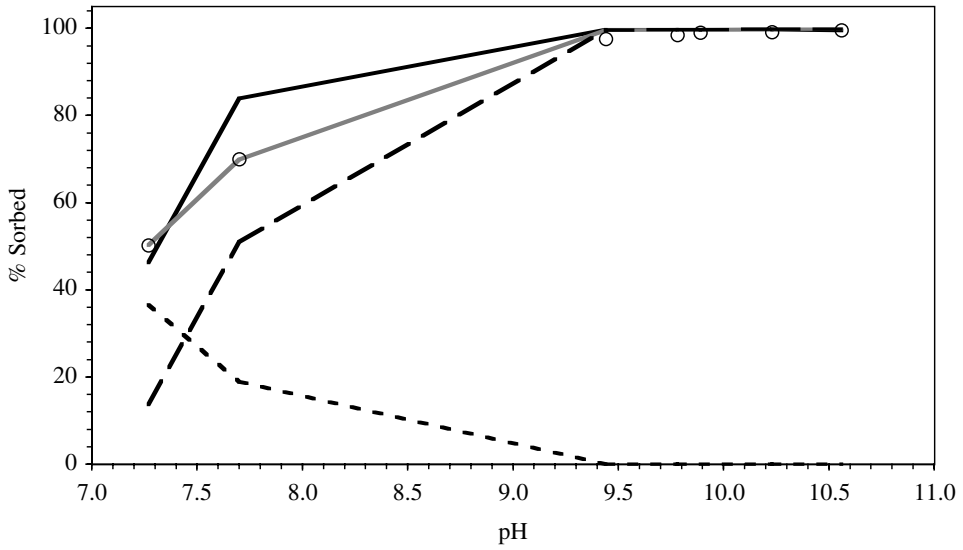

Figure 34. Sorption of 2×10^{-10} mol/L Pu on γ-Al_2O_3. Oxidation state of Pu is unknown. Solid lines represent data best fits with Pu(V) surface species (>$AlOPuO_2$) (black line) and with Pu(IV) surface species (>$AlOPu(OH)_2^+$ and >$AlOPu(OH)_4$) (gray line). Dashed line indicates contribution of two Pu(IV) species to sorption. I = 0.1; 200 ppm Al_2O_3; 130 m^2/g Al_2O_3; open to air; data from Righetto et al. (1991).

Allard et al. (1982) examined the sorption behavior of Pu on alumina in the same manner as Righetto et al. (1991). Sorption time in this case was 6 days and no oxidation state measurements were made. Nevertheless, some information can be gleaned from these data. Sorption data for several ions, including Am(III), Th(IV), and Np(V), and Pu was reported by Allard et al. (1982). Model fits to Am(III) and Np(V) data are discussed in earlier sections of this report. Th(IV) and Np(V) sorption data are shown in Figure 35 and 28, respectively. Th(IV) is expected to behave similar to Pu(IV) while Np(V) should behave as Pu(V). The data, therefore, suggests Pu(IV) will sorb strongly above pH 4 while Pu(V) will sorb only at high pH. Pu sorption data and model fits for Pu data are shown in Figure 36. Given the high sorption at low pH, it is likely that a majority of Pu

in these sorption samples was in the +4 state. Fitted NEM constants, assuming Pu(IV), are reported in Table 1. As discussed previously, NEM constants determined from the sorption data of Allard et al. (1982) are consistently high owing to poor surface area approximations. The Log K constants for Pu sorption to alumina are, therefore, likely to be 1 or 2 Log K units too high as well.

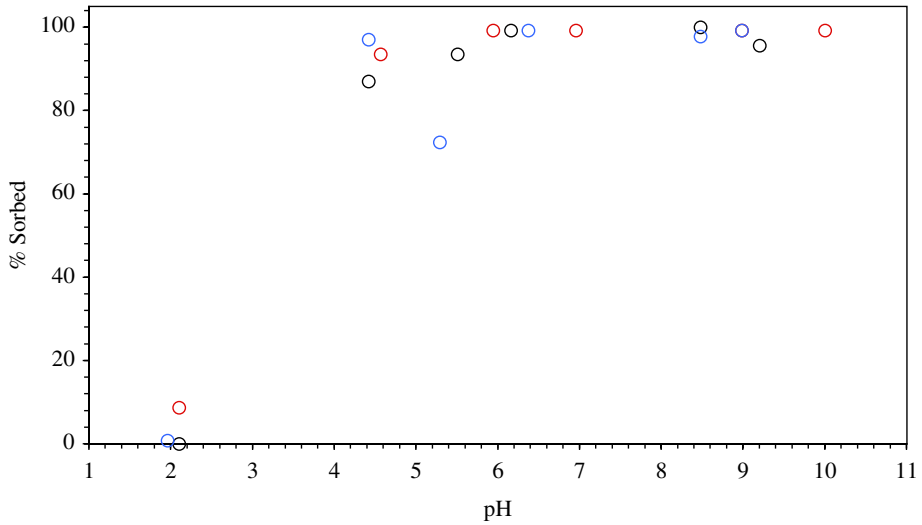

Figure 35. Sorption of 3×10^{-7} mol/L Th(IV) on alumina (black), 2.6×10^{-9} mol/L Th(IV) on alumina (red), and 2.6×10^{-9} mol/L Th(IV) on silica (blue). I = 0.01; 0.2 g in 20mL solution; 0.09-0.125mm particle size; open to air; data from Allard et al. (1982).

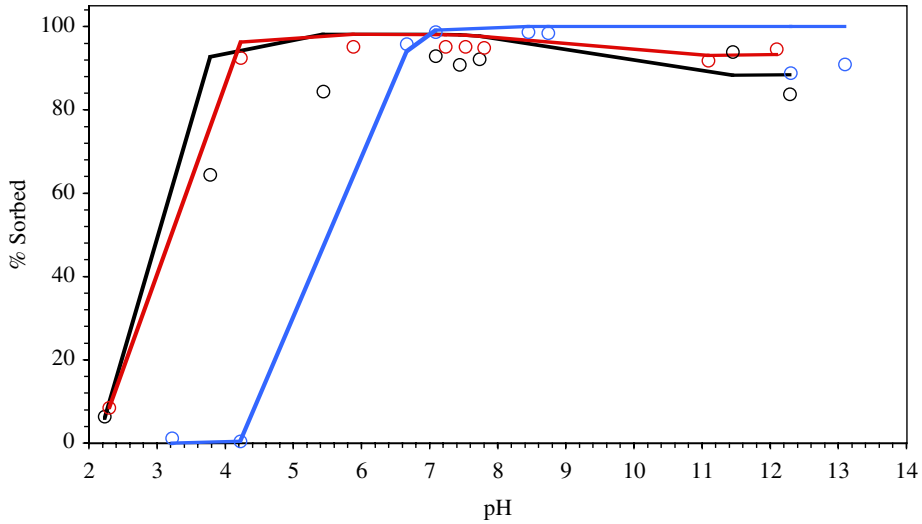

Figure 36. Sorption of 6×10^{-10} (black) and 6×10^{-8} (red and blue) mol/L Pu on Al_2O_3. Solid lines represent data fits using best fit NEM constants for Pu(IV). I = 0.01; 0.2 g in 20 mL solution; 0.09-0.125 mm particle diameter; N_2 atmosphere (black and red) and open to air (blue); data from Allard et al. (1982).

3.11 Pu on Silica

Sanchez (1983) examined the sorption of Pu(V) on colloidal silica. These experiments were performed to examine the oxidation state of Pu in aqueous solutions. An increase in K_d as a function of time, in addition to other experiments led to the conclusion that Pu(V) may begin to reduce to Pu(IV) in a matter of hours. Nevertheless, sorption measurements at short times could be used to model surface complexation of Pu(V) to silica surfaces. Data and fits using the average NEM constant are shown in Figure 37. As might be expected from Np(V) data, sorption of Pu(V) is significant only at high pH.
Fitted Log K constants are listed in Table 1. Average Log K constants for $>SiOPuO_2$ and $>SiOPuO_3H^-$ are –6.43 and –14.80, respectively (Table 2).

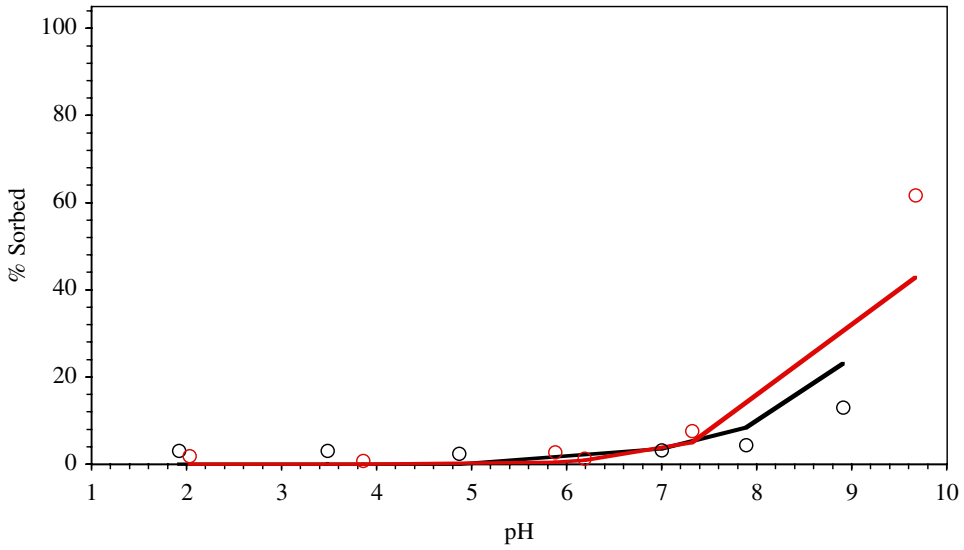

Figure 37. Sorption of 10^{-11} (I = 0.1) (black) and 10^{-14} (I = 0.7) (red) mol/L Pu(V) on colloidal silica. Solid lines represent model prediction using NEM constants from Table 2. 0.5 g silica in 20mL solution; 175 m^2/g silica from Turner et al. (1996); open to air; data from Sanchez (1983).

3.12 Pu on Aluminosilicates

Sanchez (1983) examined the sorption of trace Pu(IV) and Pu(V) on montmorillonite as a function of time and pH. All experiments were performed at high ionic strength (I = 0.1 or 0.7) to suppress ion exchange and highlight surface complexation at the edge sites of the clay. Reduction of Pu(V) to Pu(IV) was observed in these experiments. Pu(IV) sorption at 1 hour and 48 hours was equivalent while Pu(V) sorption changed significantly over several hours and continued to change during the experimental time period (up to 37 days). Oxidation-state-specific extraction of sorbed Pu indicated that the majority of Pu on the surface was in the +4 state. After 30 days of reaction, the sorption

curve for Pu(V) was nearly identical to that of Pu(IV). These data suggest that Pu(V) begins to reduce to Pu(IV) on the scale of hours. While the mechanism controlling the reduction was not determined, the results indicate that sorption of Pu(V) on montmorillonite can be evaluated only when reaction times are very short (~1 hour). Otherwise, the role of Pu(V) reduction needs to be taken into account.

Data and fits for Pu(IV) sorption to montmorillonite are shown in Figures 38 and 39. These sorption experiments were performed either by starting with Pu(IV) or using Pu(V) and evaluating sorption at long times (5 day, 30 day, and 37 day, as listed in Table 1). The surface area of montmorillonite was not reported; for data fits, surface area was assumed to be that of Turner et al. (1998). Edge site density and reactive sites were approximated as previously. Because Pu(IV) sorption to alumina or silica data was either not available or of poor quality, NEM constants were fit directly to montmorillonite data. Data fits to montmorillonite are in approximate agreement with the Pu-alumina sorption results of Allard et al. (1982). For example, fits to the data of Allard et al. (1982) result in Log K constants of 7.4 and -11.2 while fits to Pu(IV)-montmorillonite data of Sanchez (1983) result in average Log K constants of 5.85 and -11.93 for $>AlOPu(OH)_2^+$ and $>AlOPu(OH)_4^-$, respectively. The difference is most likely the result of inaccurate surface area estimates. The Log K constant for $>AlOPu(OH)_4^-$ was based only on the fit to the 30 day Pu(V) sorption data set because this surface species is significant only at high pH (other data sets did not include high pH, see Figure 39). The best fit $>SiOPu(OH)_2^+$ NEM constant varies significantly between the 4 montmorillonite sorption data sets of Sanchez (1983). This may result from incomplete Pu(V) reduction. For example, a fit to the 5 day Pu(V) sorption data set resulted in a Log K for $>SiOPu(OH)_2^+$ of 1.18, a fit to the 37 day Pu(V) sorption data set results in a Log K of 2.19 and a fit to the Pu(IV) sorption data set results in a Log K of 3.30. As a conservative estimate of Pu(IV) sorption to montmorillonite, the average NEM constants were calculated using all 4 sorption data sets. This resulted in Log K constants of 2.32±0.89, 5.95±0.47, and -11.93 for $>SiOPu(OH)_2^+$, $>AlOPu(OH)_2^+$, and $>AlOPu(OH)_4^-$, respectively (Table 2).

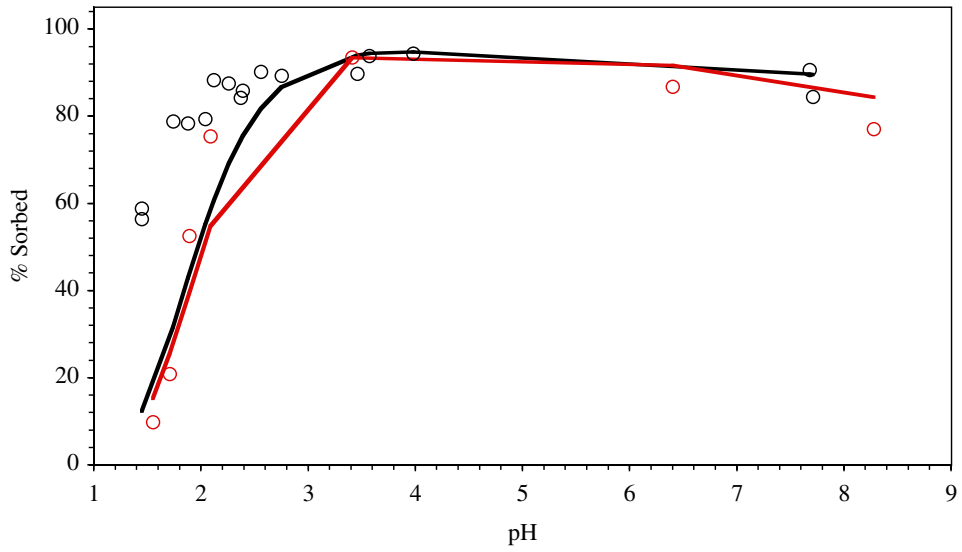

Figure 38. Sorption of 10^{-14} mol/L Pu(IV) (black) and 10^{-14} mol/L Pu(V) (37 day equilibration time) (red) on montmorillonite. Solid lines represent model prediction using NEM constants from Table 2. I = 0.7; 0.2 g/L montmorillonite; 100 m^2/g from Turner et al. (1996); 10% edge site density; 1:1 Si:Al site ratio; open to air; data from Sanchez (1983).

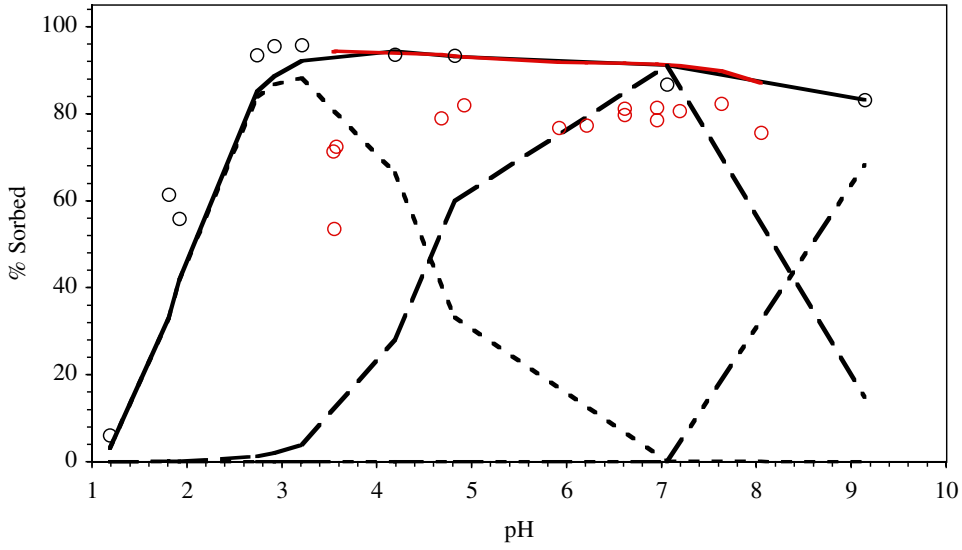

Figure 39. Sorption of 10^{-14} (I = 0.7, 30 day equilibration) (black) and 10^{-11} (I = 0.1, 5 day equilibration) (red) mol/L Pu(V) on montmorillonite. Solid lines represent model prediction using NEM constants from Table 2. Dashed lines indicate contribution of individual surface species. 0.2 g/L montmorillonite; 100 m^2/g montmorillonite from Turner et al. (1996); 10% edge site density; 1:1 Si:Al site ratio; open to air; data from Sanchez (1983).

Data and fits for Pu(V) sorption to montmorillonite are shown in Figure 40. This sorption data was collected at a reaction time of ≤1 hour to limit possible redox changes. It is, therefore, reasonable to assume that only a small fraction of Pu(V) had reduced during the reaction time. NEM constants to >SiOH sites on montmorillonite were based on fitted Log K constants determined from Pu(V) sorption experiments on colloidal silica. Since data for Pu(V) sorption on alumina surfaces was not available, NEM constants for Pu(V) sorption to >AlOH sites were fitted. The results are listed in Table 1. The fitted Log K constants for $>AlOPuO_2$ were -4.09 and -2.09 for the two sorption data sets. The large difference may be, in part due to some Pu(V) reduction effects. It is also a result of the rather small number of data points and small degree of sorption. The average Log K (-3.09) is reported in Table 2.

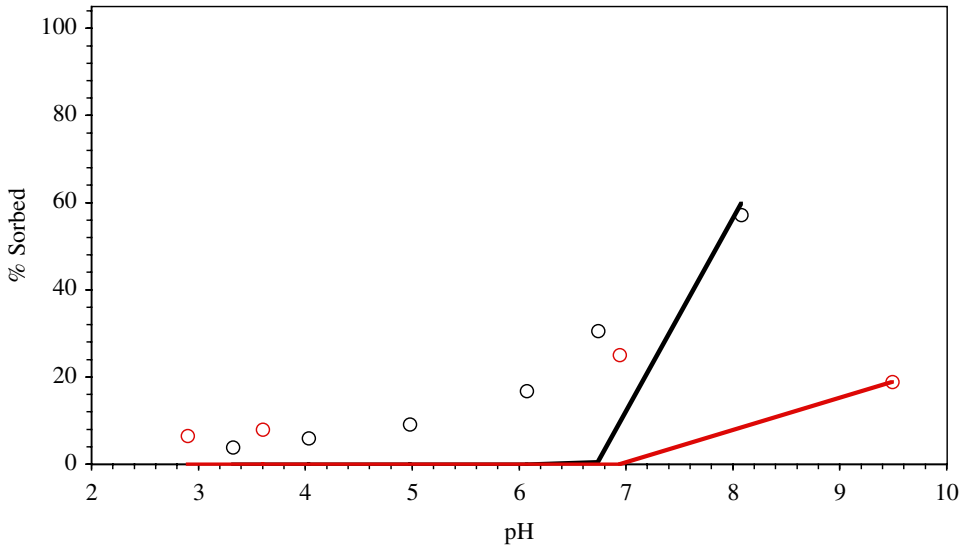

Figure 40. Sorption of 10^{-11} (I = 0.1) (black) and 10^{-14} (I = 0.7) (red) mol/L Pu(V) montmorillonite. Solid lines represent model prediction using NEM constants from Table 2. 1 hour equilibration; 0.2 g/L montmorillonite; 100 m^2/g montmorillonite from Turner et al. (1996); 10% edge site density; 1:1 Al:Si site ratio; open to air; data from Sanchez (1983).

3.13 U(VI) on Aluminum Oxide

Several authors have examined the sorption of U(VI) on aluminum oxide surfaces (Allard et al., 1982; McKinley et al., 1995; Pabalan et al., 1998; Turner et al., 1996). Turner et al. (1996) and McKinley et al. (1995) examined the sorption of U(VI) to gibbsite at surface loads of 4 to 40% in the absence of CO_2. Data and model results using average NEM constants are shown in Figure 41. McKinley et al. (1995) fit the sorption data to the triple layer electrostatic model with two surface species: $>AlOUO_2^+$ and $>AlO(UO_2)_3(OH)_5$. The selection of surface species was made from calculations establishing the dominance of UO_2^{2+} and $(UO_2)_3(OH)_5^+$ aqueous species at the

experimental conditions encountered during sorption. The use of the $>AlO(UO_2)_3(OH)_5$ surface species made it possible to explain the difference in sorption at high and low surface loads: At low loads, $>AlOUO_2^+$ dominated sorption and at high loads, $>AlO(UO_2)_3(OH)_5$ dominated. To retain the simplified NEM approach used for all other sorption data described above, the high-load surface species suggested by McKinley et al. (1995) was not used in our model. Consequently, our data fit at high pH (particularly for the high-load sorption samples) was poor. Because this tri-uranium surface species plays a significant role in U(VI) sorption only at very high surface loads, it is not likely to play an important role in environments with relatively low UO_2^{2+} concentrations in solution.

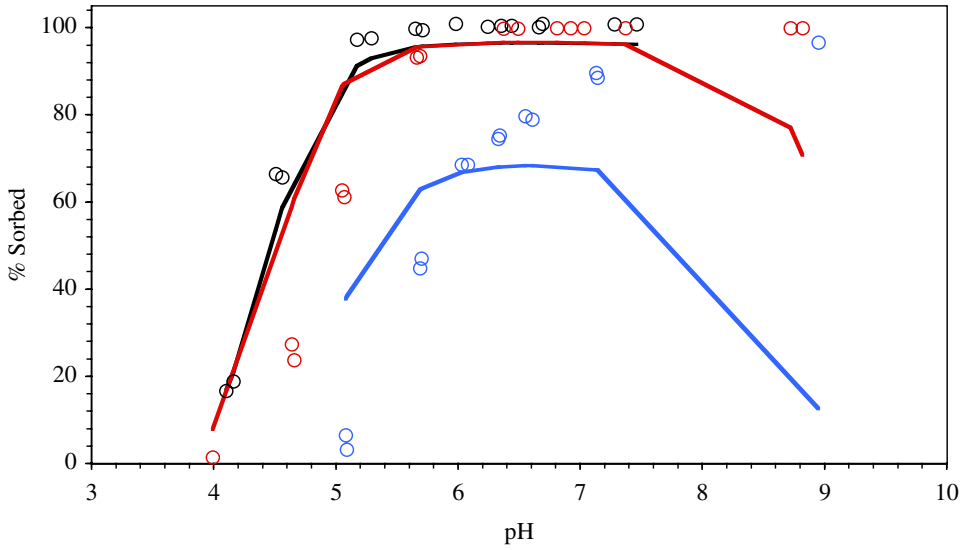

Figure 41. Sorption of 8.5×10^{-6} mol/L U(VI) on 5.59 g/L (black), 5.74 g/L (red), and 0.059 g/L (blue), $Al(OH)_3$. Solid lines represent model prediction using NEM constants from Table 2. I = 0.001, 0.1, and 0.1, respectively; 11 m^2/g $Al(OH)_3$; no CO2(g); data from Turner et al. (1996).

Pabalan et al. (1998) examined the sorption of U(VI) on α-Al_2O_3 in air at ~10% surface loads (Figure 42). Sorption decreased rapidly at high pH due to the formation of aqueous uranyl carbonate species that have much less affinity for the aluminum oxide (if any). In these experiments, the surface load was low enough such that the single surface species ($>AlOUO_2^+$) fit the data quite well. The fitted NEM constants are also in good agreement with the results of McKinley et al. (1995) and Turner et al. (1996).

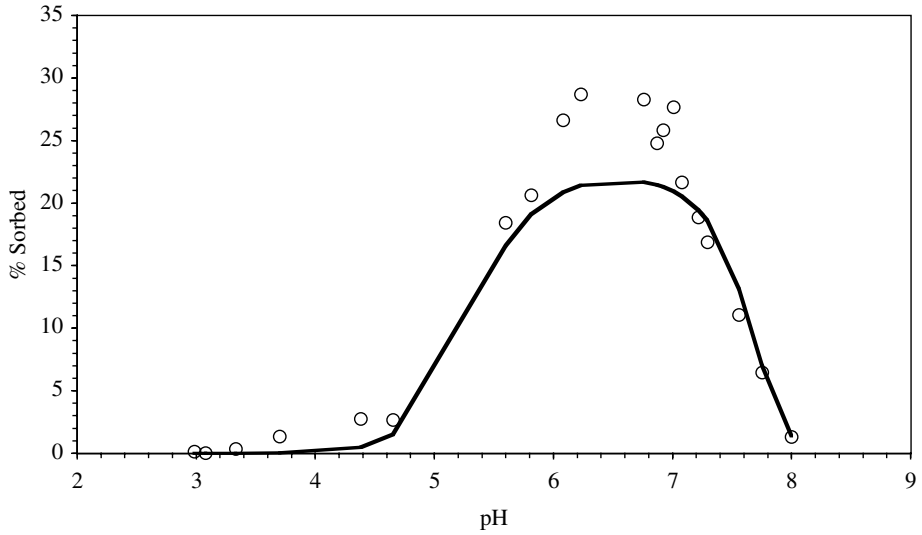

Figure 42. Sorption of 4.84×10^{-7} mol/L U(VI) on alumina. Solid lines represent model prediction using NEM constants from Table 2. I = 0.1; 2.79 g/L α-Al_2O_3; 0.23 m^2/g; open to air; data from Pabalan et al. (1998).

The fitted NEM constant for the sorption data of Allard et al. (1982) using a single surface species is good, though the NEM constant is much higher than for other data sets discussed earlier (Figure 43 and Table 1). This is consistent with all other attempts to fit the sorption data of Allard et al. (1982) and results from an underestimated surface area based on sieving data, as discussed previously. Ignoring the fitted NEM constants related to data of Allard et al. (1982), the average Log K constant for $>AlOUO_2^+$ is 3.13 ± 0.15.

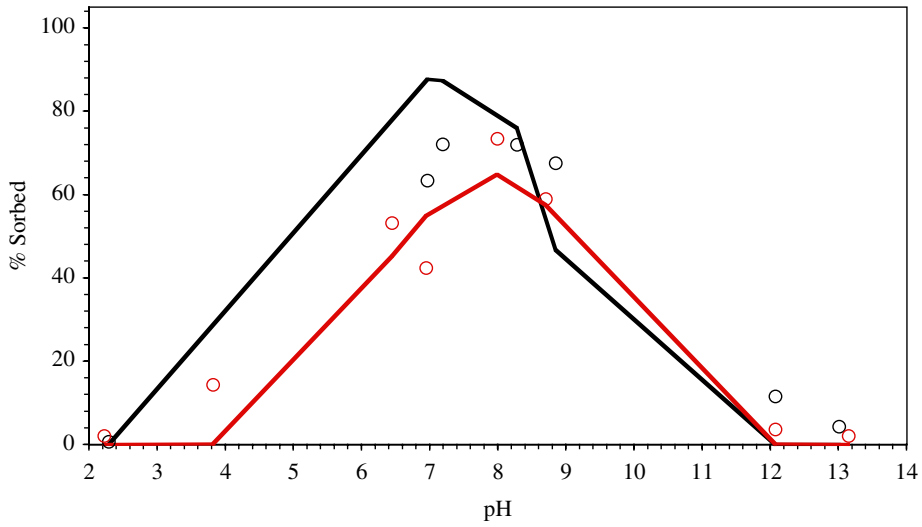

Figure 43. Sorption of 2.1×10^{-7} mol/L U(VI) on alumina (black) and silica (red). Solid lines represent data fits using best fit NEM constants. I = 0.01; 0.09 to 0.125 mm particle diameter; 0.2 g in 20 mL solution; open to air; data from Allard et al. (1982).

3.14 U(VI) on Silica

The sorption of U(VI) on SiO_2 has been studied extensively (Allard et al., 1982; Dent et al., 1992; Lieser et al., 1992; McKinley et al., 1995; Pabalan et al., 1998; Turner et al., 1996; Waite et al., 1992). Waite et al. (1992) examined U(VI) sorption at surface loads <1% (Figures 44 and 45). At high pH, the fit to the data is significantly worse than at low pH. The sorption of U(VI) at high pH under atmospheric CO_2 is extremely sensitive to the carbonate concentration in solution. Thus, if solutions are slightly undersaturated with respect to atmospheric CO_2, the sorption edge may shift to higher pH. For this reason, variability in the fitted $>SiOUO_3^-$ Log K is high (Table 1). As a conservative measure of U(VI) sorption, the NEM constant listed in Table 2 was based on the lowest fitted NEM constant in Table 1 (-12.35) instead of the average (-11.39). This results in a conservative prediction of U(VI) sorption at high pH.

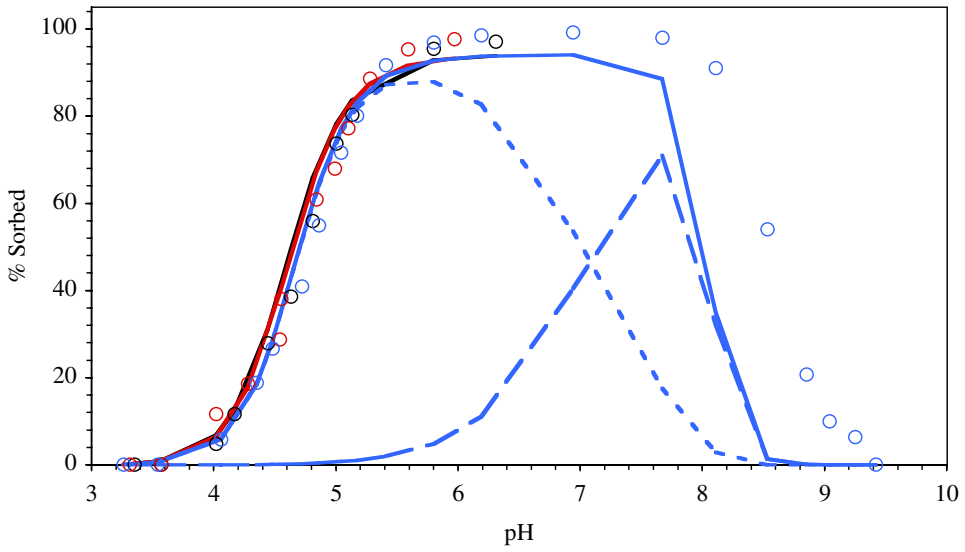

Figure 44. Sorption of 10^{-6} mol/L U(VI) on SiO_2 at I = 0.005 (black), I = 0.01 (red), and I = 0.1 (blue). Solid lines represent model prediction using NEM constants from Table 2. 100 g/L SiO_2; 0.32 m^2/g SiO_2; open to air; data from Waite et al. (1992); dashed lines indicate contribution of individual species.

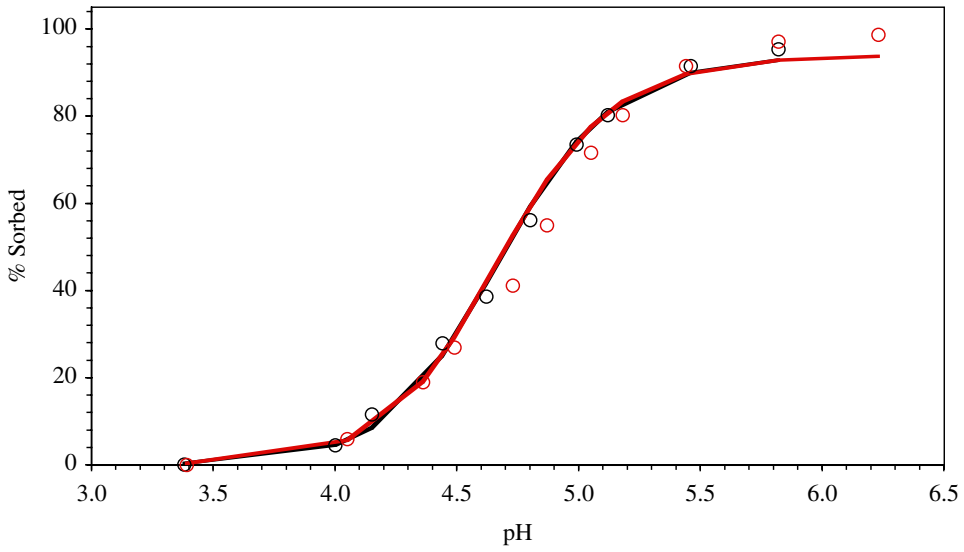

Figure 45. Sorption of 10^{-6} mol/L U(VI) on SiO_2 (black and red). Solid lines represent model prediction using NEM constants from Table 2. I = 0.1; 100 g/L SiO_2; 0.32 m^2/g SiO_2; open to air; data from Waite et al. (1992).

Lieser et al. (1992) examined the sorption of U(VI) to hydrous silica (Figure 46). The silica gel was reported to have a very high surface area (720 m^2/g). Attempts to fit the sorption data using this high surface area resulted in very low NEM constants inconsistent with the fitted values for the data of Waite et al. (1992). When the silica surface area reported by Turner (1995) was used (175 m^2/g), the NEM fit to the low CO_2(g) sorption samples was in agreement with the results of Waite et al. (1992). Nevertheless, the fit to the high CO_2(g) sorption samples was still poor. Fits using the average NEM constants are shown in Figure 46. Aside from the possible surface area effects, inconsistency between these sorption data and others may be result from poor carbonate alkalinity control. In addition, ionic strength information was not reported and had to be assumed (I ~ 0.1).

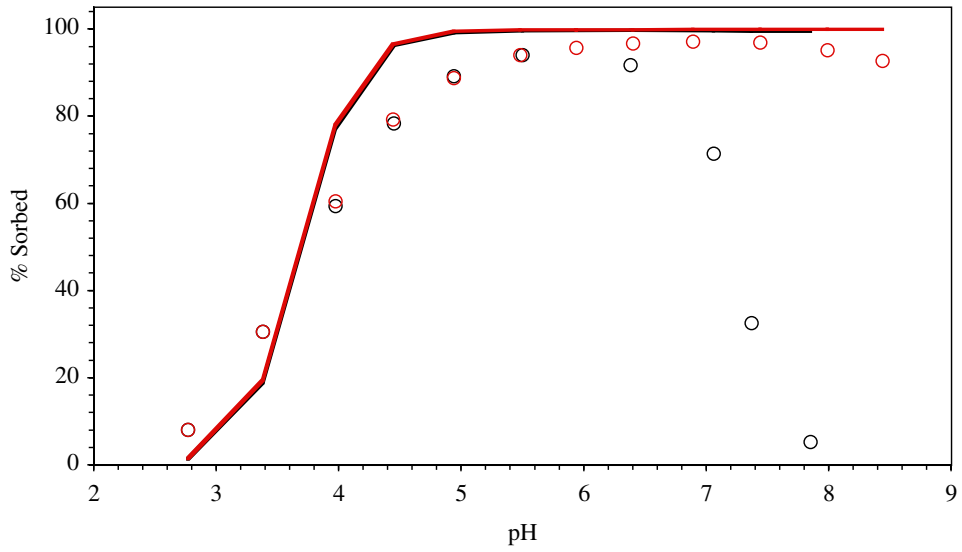

Figure 46. Sorption of 2.1×10^{-6} mol/L U(VI) on silica gel with 10^{-3} mol/L HCO_3^- (black) and no HCO_3^- (red). Solid lines represent model prediction using NEM constants from Table 2. I ~ 0.1; 10 g/L SiO_2*H_2O; 175 m^2/g SiO_2 from Turner (1995); data from Lieser et al. (1992)

Turner et al. (1996) and McKinley et al. (1995) examined U(VI) sorption to silica at 10 to 90% surface loads and in the absence of CO_2. The data fits are in good agreement with those of Waite et al. (1992). Fits using the average NEM constants are good, though the fit at high surface loads and high pH is only approximate (Figure 47). This result is similar to that of U(VI) sorption to alumina at high loads.

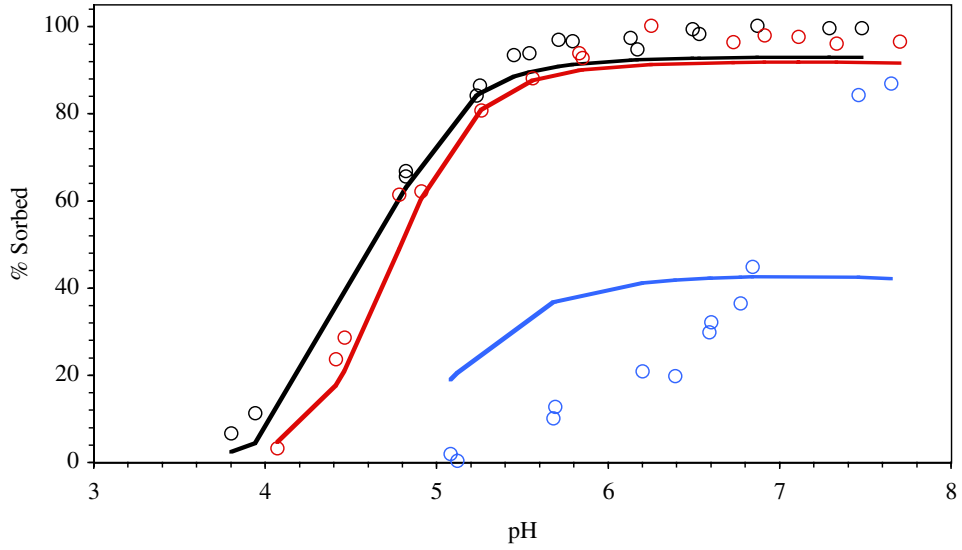

Figure 47. Sorption of 8.5×10^{-6} mol/L U(VI) on 0.15 g/L, (black), 0.13 g/L (red), and 0.013 g/L (blue) SiO_2. Solid lines represent model prediction using NEM constants from Table 2. I = 0.001, 0.1, and 0.1, respectively; 183 m^2/g SiO_2; no CO_2(g); data from Turner et al. (1996).

Dent et al. (1992) examined the sorption of U(VI) to silica colloids. X-ray absorption spectroscopic analysis of the sorption samples indicated that U(VI) sorbs directly to the silica surface, though the speciation could not be identified. The fitted constants to batch sorption experiments of Dent et al. (1992) are in approximate agreement with fitted constants for the data of Waite et al (1992) and Turner et al. (1996). The fit using average NEM constants is shown in Figure 48.

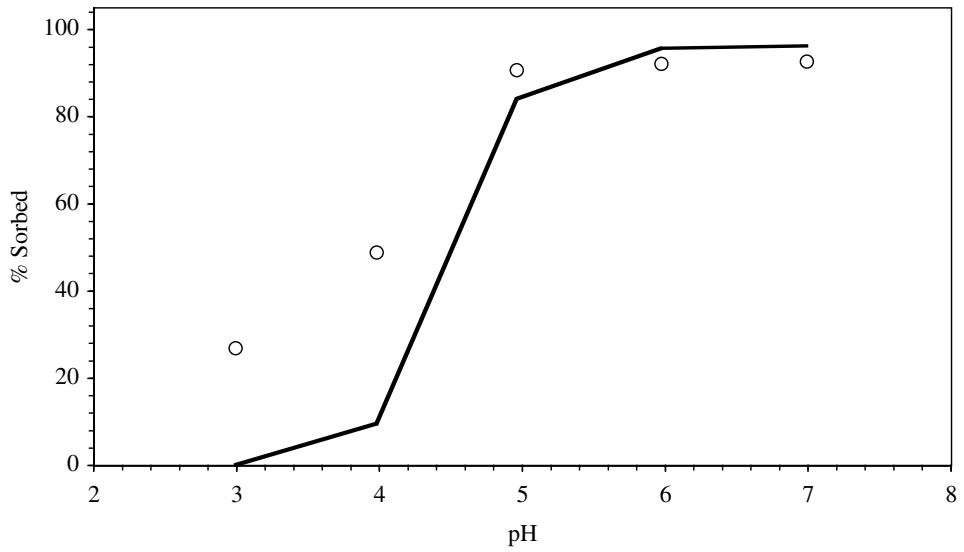

Figure 48. Sorption of 10^{-8} mol/L U(VI) on silica colloids. Solid lines represent model prediction using NEM constants from Table 2. I = not known; 1 g/L SiO_2; 50 m^2/g SiO_2; open to air; data from Dent et al. (1992).

Pabalan et al. (1998) sorbed U(VI) to silica at 1 to 40% surface loads. The model results using average NEM constants are shown in Figure 49. Fits underestimate sorption by up to 35%. The surface area of SiO_2 used in these experiments was 0.03 ± 0.01 m^2/g. Uncertainty in the surface area measurement could account entirely for the difference between the data and fits. NEM fits to the data of Allard et al. (1982) (Figure 43) yield higher Log K constants than other data fits. This is consistent with other radionuclide sorption results reported by Allard et al. and compared to other published data, as described earlier. Ignoring the results of Allard et al. (1982), the average Log K constant reported in Table 2 for $>SiOUO_3H$ is -5.18 ± 0.31. For $>SiOUO_3^-$, we chose to include the most conservative fitted Log K constant, –12.35 in Table 2. When all values are used, the Log K constants result in -5.17 ± 0.51 and -11.54 ± 0.81 for $>SiOUO_3H$ and $>SiOUO_3^-$. The former values lead to a more conservative estimate of U(VI) sorption.

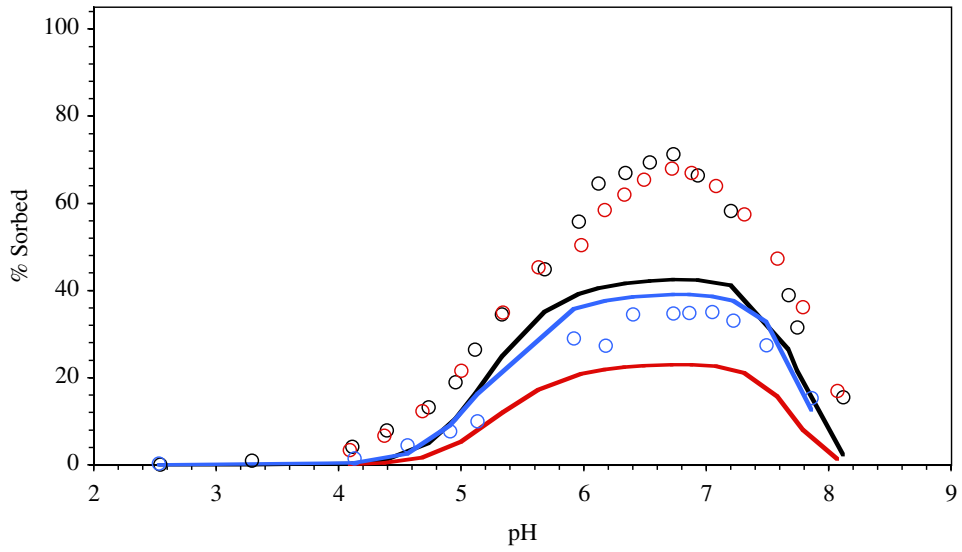

Figure 49. Sorption of 2.06×10^{-7} (black), 2×10^{-8} (red), and 2.15×10^{-6} (blue) mol/L U(VI) on silica. Solid lines represent model prediction using NEM constants from Table 2. I = 0.1; 50 g/L (black), 20 g/L (red), 50 g/L (blue); 0.03 m^2/g SiO_2; open to air; data from Pabalan et al. (1998).

3.15 U(VI) on Smectite

Several authors have examined the behavior of U(VI) in contact with the clay montmorillonite (McKinley et al., 1995; Pabalan et al., 1998; Tsunashima et al., 1981; Turner et al., 1996). Tsunashima et al. (1981) examined the ion exchange of UO_2^{2+} for Na^+, K^+, Ca^{2+}, Mg^{2+}, and Ba^{2+} at low pH. UO_2^{2+} exchange with Ca^{2+} and Mg^{2+} behaved nearly identically and the fit to the data are shown in Figure 50. The ion exchange equation used to fit the data was based on Vanselow IE. Fitting heterovalent ion exchange was not attempted using the FITEQL fitting program. Instead, the exchange constant for $UO_2^{2+} \Rightarrow 2\ Na^+$ was estimated using the fit for $UO_2^{2+} \Rightarrow Ca^{2+}$ and the $Ca^{2+} \Rightarrow 2\ Na^+$ constant determined by Fletcher and Sposito (1989). The resulting exchange constants are listed in Table 1.

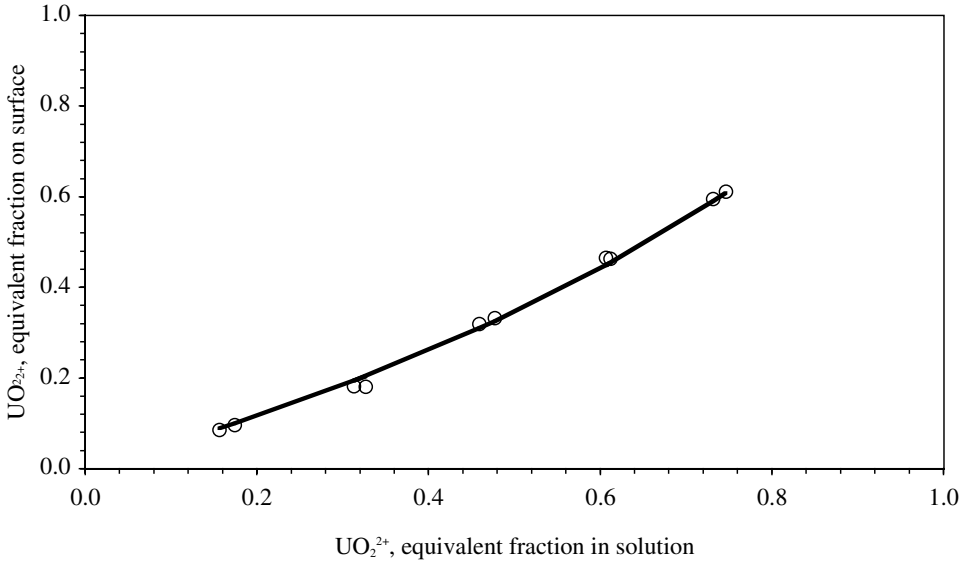

Figure 50. IE of UO_2^{2+} with Ca^{2+}/Mg^{2+} on montmorillonite. Line represents average IE constant (K=0.56). I = 0.002; 1 g/L montmorillonite; 90 meq/100g; pH 5; data from Tsunashima et al. (1981).

The model results and sorption data of Turner et al. (1996) are shown in Figures 51 and 52. In all cases, average NEM constants determined for SiO_2 and aluminum oxide (Table 2) were used. The ion exchange constant was taken from the fit to data of Tsunashima et al. (1981). The predicted sorption matched the data remarkably well. As was shown for other radionuclide-clay sorption data, ion exchange controls sorption at low pH while surface complexation dominates at pHs above ~6. Model results underestimate sorption when compared to sorption data of McKinley et al. (1995) in the region where surface complexation dominates (Figure 53). This is, most likely, the result of very high loading of the edge sites. The surface area of montmorillonite reported by McKinley et al (1995) is relatively low (31 m^2/g) and, using the generalized assumptions for edge site density described earlier, the total edge site concentration turns out to be quite low (3×10^{-6} mol/L >SiOH and >AlOH concentration). The edge site concentration calculated by McKinley et al. (1995) is significantly higher (~10^{-5} mol/L >SiOH and >AlOH concentration). The factor of 3 lower edge site concentration in these simulations results in a complete saturation of edge sites which limits sorption to a maximum of ~70%.

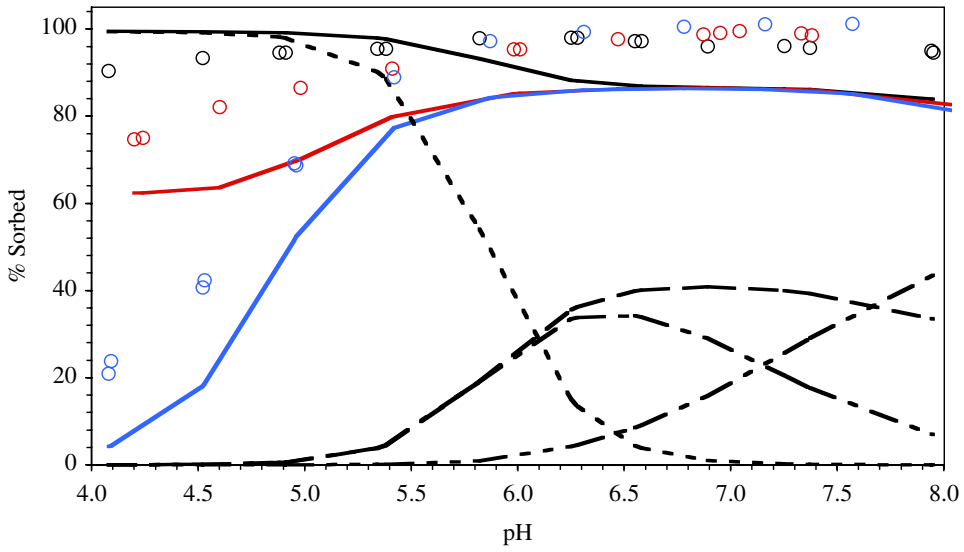

Figure 51. Sorption of 8.5×10^{-6} mol/L U(VI) on 1.5 g/L smectite at I = 0.001 (black), 0.01 (red), and 0.1 (blue). Solid lines represent model prediction using NEM constants from Table 2. Estimated edge surface area = 9.9 m^2/g (10% of BET area); 1:1 Si:Al site ratio; no CO_2; data from Turner et al. (1996).

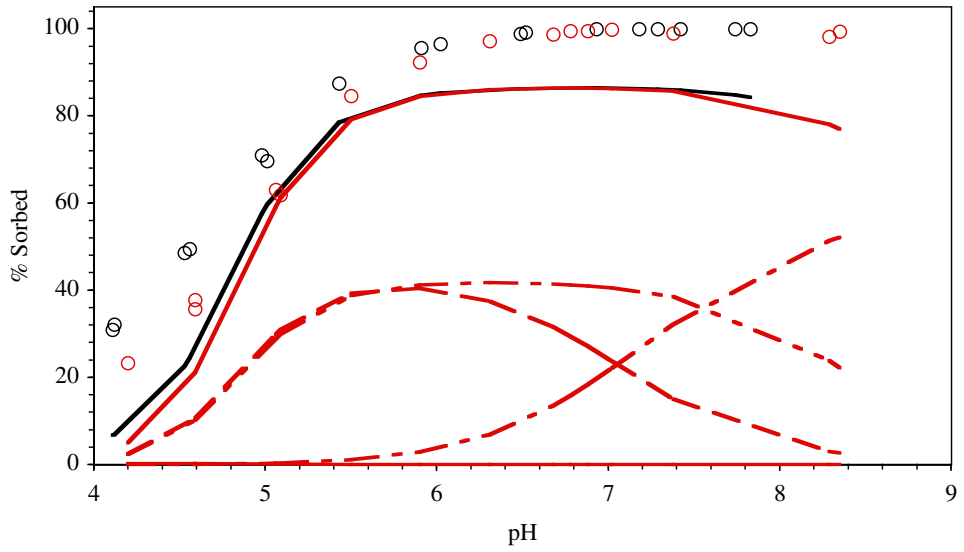

Figure 52. Sorption of 8.5×10^{-6} mol/L U(VI) on 1.5 g/L smectite in 0.0068 (black) and 0.074 (red) mol/L $Ca(ClO_4)_2$. Solid lines represent model prediction using NEM constants from Table 2. Estimated edge surface area = 9.9 m^2/g (10% of BET area); 1:1 Si:Al site ratio; no CO_2; dashed lines represent various species that affect net sorption fit; data from Turner et al. (1996).

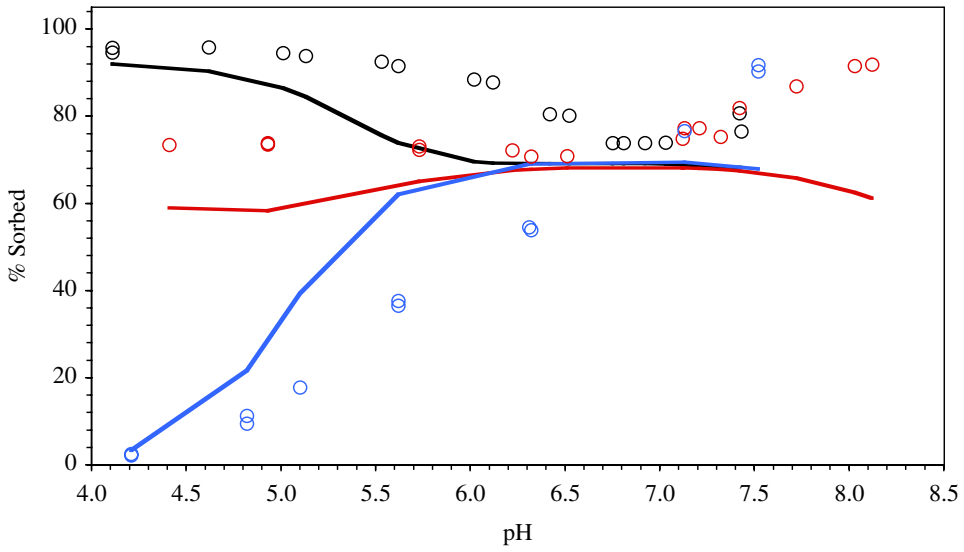

Figure 53. Sorption of 8.4×10^{-6} mol/L U(VI) on 0.5 g/L SWy-1 montmorillonite in 0.001 (black) and 0.01 (red), and (blue) 0.1 mol/L $NaClO_4$. Solid lines represent model prediction using NEM constants from Table 2. Estimated edge surface area = 3.1 m^2/g (10% of BET area); 1:1 Si:Al site ratio; no CO_2(g); data from McKinley et al. (1995).

Pabalan et al. (1998) measured the sorption of U(VI) on montmorillonite at ~1-50% surface loads. A comparison of model results to data with low surface loads is shown in Figures 54 and 55. All sorption experiments were performed at I = 0.1 to suppress ion exchange, which was effectively accomplished, as indicated by the data and ion exchange fit shown in Figures 54. At pH <5, sorption is underestimated significantly. At higher surface loads (Figure 55), sorption is underestimated at all pH. This may results from a low estimate of total reactive site concentrations or the absence of high surface load species such as $>AlO(UO_2)_3(OH)_5$ reported by McKinley et al. (1995). Turner et al. (1996) and McKinley et al. (1995) estimated much higher reactive site densities for montmorillonite which would result in higher sorption. Nevertheless, the sorption predictions shown here represent relatively conservative estimates of sorption.

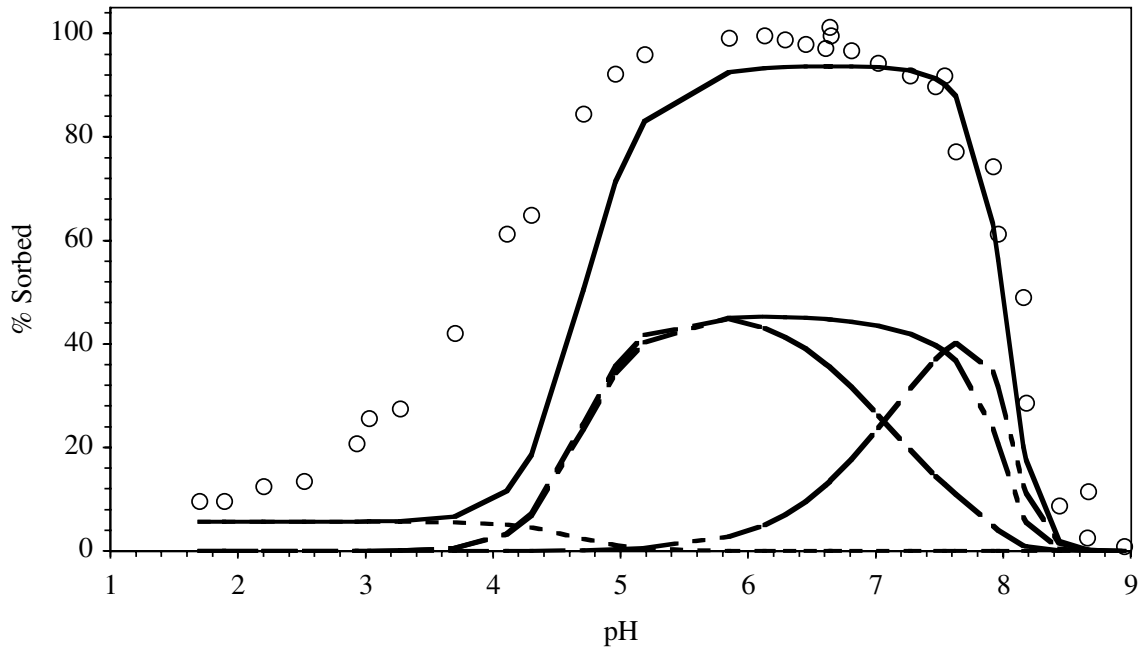

Figure 54. Sorption of 2.45×10^{-7} mol/L U(VI) on montmorillonite. Solid lines represent model prediction using NEM constants from Table 2. Dashed lines represent contribution of individual surface species. I = 0.1; 3.2 g/L montmorillonite; 97 m^2/g; 10% reactive sites; 1:1 Al:Si site ratio; open to air; data from Pabalan et al. (1998).

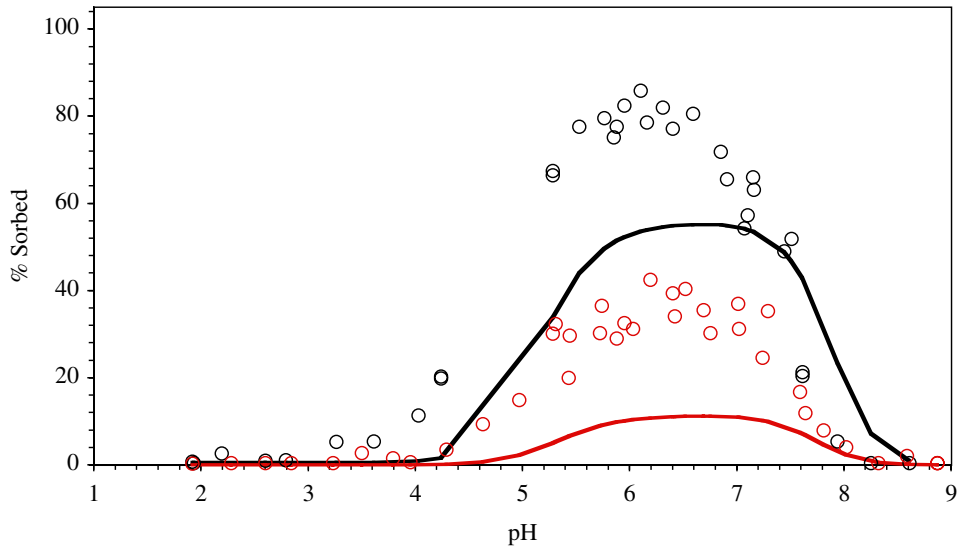

Figure 55. Sorption of 2.1×10^{-7} mol/L U(VI) on 0.27 g/L (black) and 0.028 g/L (red) montmorillonite. Solid lines represent model prediction using NEM constants from Table 2. I = 0.1; 97 m^2/g montmorillonite; 10% reactive sites; 1:1 Al:Si site ratio; open to air; data from Pabalan et al. (1998).

3.16 U(VI) on Clinoptilolite

Pabalan et al. (1992; 1998) examined the sorption of U(VI) to clinoptilolite at high ionic strength. Average Log K model results using the generalized approach equivalent to Np(V) on clinoptilolite are shown in Figures 56 to 58. At high pH, the predicted sorption edge resulting from uranium carbonate complexation is at a higher pH when compared to the data. This results in a slight overestimation of sorption at high pH. At low pH, sorption is slightly underestimated. Nevertheless, the approximate fit indicates that clinoptilolite surface sorption sites behave qualitatively similar to >SiOH and >AlOH surface groups on SiO_2 and aluminum oxide. Given the many simplifying assumption used to extrapolate the behavior of clinoptilolite, the data fit is remarkably good.

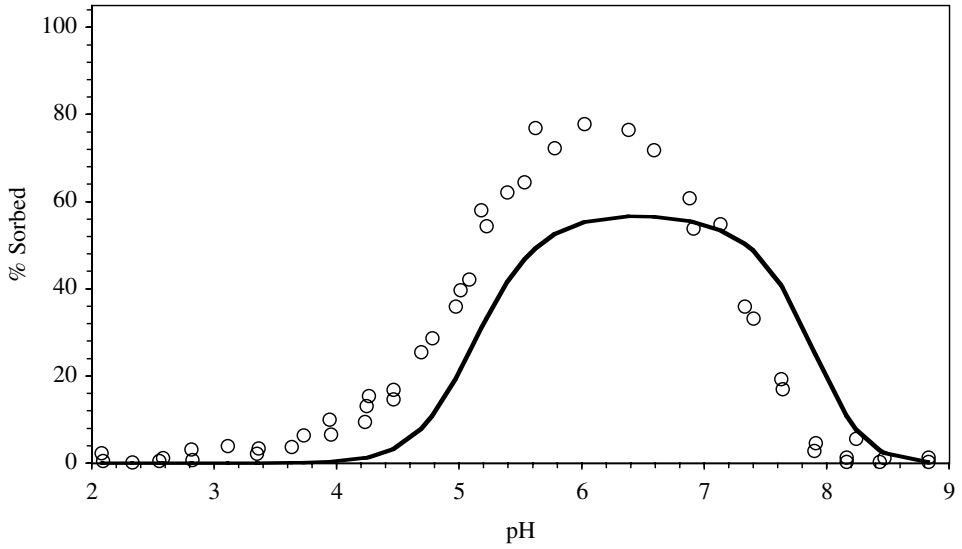

Figure 56. Sorption of 2.17×10^{-7} mol/L U(VI) on clinoptilolite. Solid lines represent model prediction using NEM constants from Table 2. I = 0.1; 2.04 g/L clinoptilolite; 10.1 m^2/g; 10% reactive sites; 15:85 Al:Si site ratio; open to air; data from Pabalan et al. (1998).

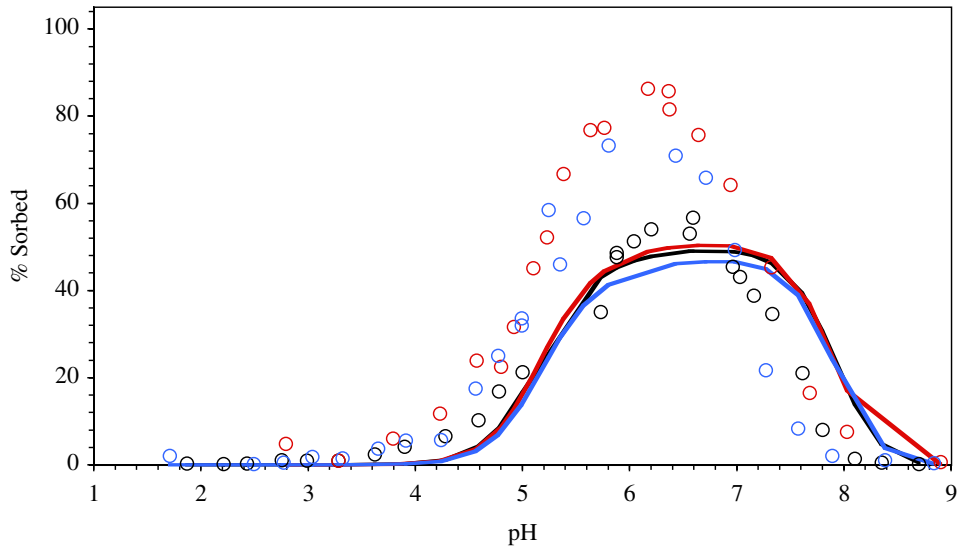

Figure 57. Sorption of 2.22×10^{-6} (I = 0.1) (black), 2.17×10^{-7} (I = 1) (blue), and 1.9×10^{-8} (I = 0.01) (red) mol/L U(VI) on clinoptilolite. Solid lines represent model prediction using NEM constants from Table 2. 2.1 g/L clinoptilolite; 10.1 m^2/g, 10% reactive sites; 15:85 Al:Si site ratio; open to air; data from Pabalan et al. (1998).

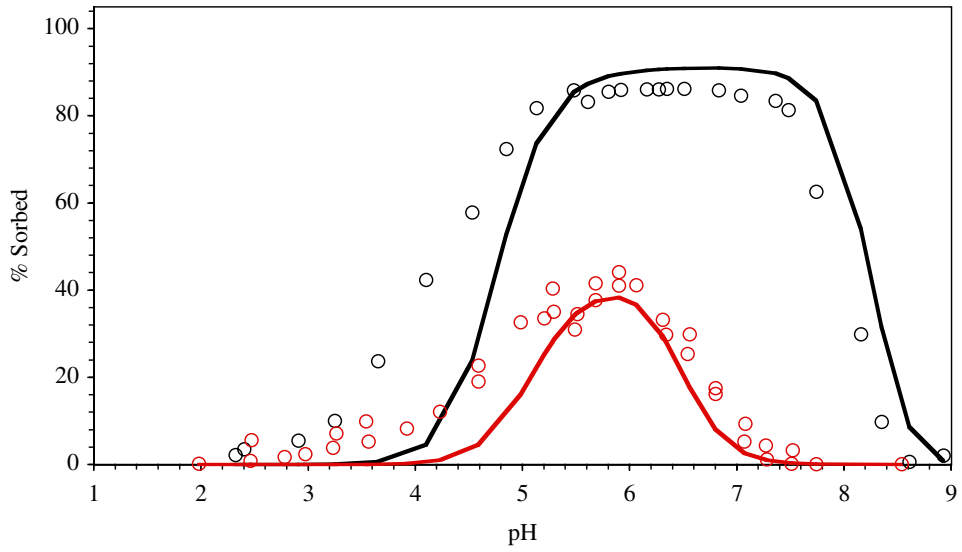

Figure 58. Sorption of 2.1×10^{-7} mol/L U(VI) on clinoptilolite. 20.28 g/L clinoptilolite and open to air (black) and 2.43 g/L clinoptilolite and 1% CO_2 (red). Solid lines represent model prediction using NEM constants from Table 2. I = 0.1; 10 m^2/g clinoptilolite; 10% reactive sites; 15:85 Al:Si site ratio; data from Pabalan et al. (1998).

4 SUMMARY OF SORPTION CONSTANTS AND COMPARISON TO EXISTING DATA

Table 2 lists the average NEM and Vanselow IE constants that comprise a database of surface complexation and ion exchange reactions on aluminosilicate minerals. The acidity constants used for >AlOH and >SiOH surface reactive sites were taken from SiO_2 and α-Al_2O_3 diffuse layer model fits reported by Turner (1995). Depending on the SC model, surface acidity Log K constants can vary drastically. If acidity constants were varied during data fitting along with radionuclide surface complexation constants, less variability in Log K constants might be achieved. However, the limited data for most radionuclide–mineral sorption reactions do not merit additional fitting parameters in our NEM model.

Table 2. Average non-electrostatic surface complexation model constants for aluminosilicates.

Reaction	# of Curves Evaluated	log K	Ref.
$>AlOH \Leftrightarrow >AlO^- + H^+$		-9.73*	
$>AlOH + H^+ \Leftrightarrow >AlOH_2^+$		8.33*	
$>SiOH \Leftrightarrow >SiO^- + H^+$		-7.20*	
$>AlOH + Am^{3+} \Leftrightarrow >AlOAm^{2+} + H^+$	11	2.49±0.26	1-5
$>SiOH + Am^{3+} \Leftrightarrow >SiOAm^{2+} + H^+$	4	0.7±0.1	2, 3, 5
$>SiOH + Am^{3+} + H_2O \Leftrightarrow >FeOAmO + 3H^+$		-14.2±0.8	
$Am^{3+} + 3NaX \Leftrightarrow AmX_3 + 3Na^+$	4	~1†	6
$>AlOH + Eu^{3+} \Leftrightarrow >AlOEu^{2+} + H^+$	5	2.29±0.45	7, 8
$>SiOH + Eu^{3+} \Leftrightarrow >SiOEu^{2+} + H^+$	4	-0.63	8-10
$>SiOH + Eu^{3+} + H_2O \Leftrightarrow >SiOEuO + 3H^+$		-14.13	
$Eu^{3+} + 3NaX \Leftrightarrow EuX_3 + 3Na^+$	4	~1‡	11
$>AlOH + NpO_2^+ \Leftrightarrow >AlONpO_2 + H^+$	9	-4.67±0.27	1-3, 12, 13††
$>AlOH + NpO_2^+ + H_2O \Leftrightarrow >AlONpO_3H^- + 2H^+$		-14.26±0.04	
$>SiOH + NpO_2^+ \Leftrightarrow >SiONpO_2 + H^+$	6	-3.72±0.15	2, 13
$>SiOH + NpO_2^+ + H_2O \Leftrightarrow >SiONpO_3H^- + 2H^+$		-12.16	
$>AlOH + Pu^{4+} + H_2O \Leftrightarrow >AlOPuO^+ + 3H^+$	4¶¶	5.95±0.47	2, 3, 15
$>AlOH + Pu^{4+} + 2H_2O \Leftrightarrow >AlOPuO_2^- + 5H^+$		-11.93	
$>SiOH + Pu^{4+} + H_2O \Leftrightarrow >SiOPuO^+ + H^+$		2.32±0.89	
$>AlOH + PuO_2^+ \Leftrightarrow >AlOPuO_2$	2§§	-3.09	15
$>SiOH + PuO_2^+ \Leftrightarrow >SiOPuO_2$	2	-6.43	15
$>SiOH + PuO_2^+ + H_2O \Leftrightarrow >SiOPuO_3H^- + 2H^+$		-14.80	
$>AlOH + UO_2^{2+} \Leftrightarrow >AlOUO_2^+ + H^+$	5	3.13±0.15	3, 16, 17‡‡
$>SiOH + UO_2^{2+} + H_2O \Leftrightarrow >SiOUO_3H + 2H^+$	15	-5.18±0.31	3, 16-20
$>SiOH + UO_2^{2+} + H_2O \Leftrightarrow >SiOUO_3^- + 3H^+$		-12.35	
$UO_2^{2+} + CaX_2 \Leftrightarrow UO_2X_2 + Ca^{2+}$	1	-0.25¶	21
$UO_2^{2+} + 2NaX \Leftrightarrow UO_2X_2 + 2Na^+$		-0.08§	22

* Surface acidity constants taken from Turner (1995) SiO_2 and α-Al_2O_3 diffuse layer surface complexation model data.
† mixed layer smectite/kaolinite clay, fit is only approximate due to small data set.
‡ illite, fit is only approximate due to small data set.
¶ smectite
§ extrapolated from data of Fletcher and Sposito (1989) in conjunction with UO_2^{2+} ➔ Ca^{2+} IE determined here.
†† 2 montmorillonite curves and 4 clinoptilolite curves fit using average aluminol/silanol sites (refs. 13 and 14).
¶¶ Fitted to montmorillonite sorption data and correlated with aluminum oxide sorption data.
§§ Fitted to montmorillonite sorption data with silanol sorption constants from silica sorption data.
‡‡ 11 montmorillonite curves and 6 clinoptilolite curves fit using average aluminol/silanol sites (refs. 23, 17, and 16).
REFERENCES: 1. (Righetto et al., 1988); 2. (Righetto et al., 1991); 3. (Allard et al., 1982); 4. (Allard et al., 1989); 5. (Moulin et al., 1992); 6. (Stammose and Dolo, 1990); 7. (Shiao et al., 1981); 8. (Norden et al., 1994); 9. (Ledin et al., 1994); 10. (Fairhurst et al., 1995); 11. (Wang et al., 1998); 12. (Nakayama and Sakamoto, 1991); 13. (Bertetti et al., 1998); 14. (Turner et al., 1998); 15. (Sanchez, 1983); 16. (Turner et al., 1996); 17. (Pabalan et al., 1998); 18. (Waite et al., 1992); 19. (Lieser et al., 1992); 20. (Dent et al., 1992); 21. (Tsunashima et al., 1981); 22. (Fletcher and Sposito, 1989); 23. (McKinley et al., 1995).

The NEM constants in Table 2 are valid only when they are used in conjunction with the listed acidity constants. In addition, all NEM constants are dependent on the aqueous speciation constants used to model the data. This is particularly important for actinides and lanthanides for which aqueous speciation can be very complex. Aqueous complexation constants were based on the GEMBOCHS thermodynamic data base version data.com.V8.R6 (Johnson and Lundeen, 1997) with revisions as noted in Pawloski et al. (2001). These aqueous complexation constants are listed in Appendix A.

Based on the average NEM constants calculated in this report and the companion report (Zavarin and Bruton, 2004), Table 3 lists estimated distribution coefficients for radionuclides on calcite, iron oxide, and aluminosilicate minerals under aqueous conditions similar to those found in the Frenchman Flat region of the Nevada Test Site. For Cs(I) and Sr(II), sorption to illite, smectite, and clinoptilolite aluminosilicate minerals was described by ion exchange (Vanselow ion exchange constants listed in Table 4). The GIMRT code (Steefel and Yabusaki, 1995) was used to calculate radionuclide sorption to minerals using the average NEM and ion exchange constants. The groundwater composition used to predict distribution coefficients was based on Tompson et al. (1999). The composite Frenchman Flat mineralogy was also based on Tompson et al. (1999) and is identical to the alluvium composition used in reactive transport simulations reported in Zavarin and Bruton (2004). Three columns of data are listed. **In the first column**, the retardation ratio (R) is reported. We define the retardation ratio as the ratio of mol sorbed to mol aqueous.[5] This value can be used to compare the relative contribution of each mineral to the total retardation ratio for the composite Frenchman Flat alluvium (e.g. $R_{calc} + R_{iron} + R_{alumino} = R_{tot}$). **The second column** contains distribution coefficients in units of mL/g. These values can be compared to published K_ds for single minerals as well as Frenchman Flat alluvium (typically reported as mL/g). The NEM constants used to determine distribution coefficients for calcite and iron oxide minerals were described in a companion report (Zavarin and Bruton, 2004). To determine the retardation ratios and distribution coefficients for radionuclides on aluminosilicate minerals, it was assumed that all radionuclides (except Cs(I) and Sr(II)) sorb via surface complexation to a smectite with 100 m^2/g surface area and with reactive site densities as described earlier. **In the third column**, a variety of published K_d data (mL/g) are listed. These data were gathered largely from Yucca Mountain Project publications. The water chemistry at Frenchman Flat is similar to that found at Yucca Mountain, which allows for a comparison of our predicted single mineral K_d data to data from Yucca Mountain. The composite Frenchman Flat mineralogy predicted K_d data can be compared to measured K_d data for sediments from Frenchman Flat (Wolfsberg, 1978).

[5] The R reported here is not the same as the retardation factor typically used in transport models. Here, R is defined as the ratio of sorbed to aqueous mol. The retardation factor is defined as one plus the ratio of sorbed to aqueous mol.

Table 3. Predicted K_ds under conditions of Frenchman Flat, NTS, groundwater and sediment composition.[1]

	Log R $(mol_{ads}/L_{aq})/(mol_{aq}/L_{aq})$	Log K_d $(mol_{ads}/g_{min})/(mol_{aq}/mL_{aq})$	Log K_d[2] mL/g
	Calcite[3]		
Am	4.6	5.7	
Cs			-0.5 - 0.1[b, calc]
Eu	4.4	5.5	
Np	1.9	3.0	2 - 3[a, calc], 1.1 - 2.8[b, calc]
Pu[6]	0.95 (1.9)	2.1 (3.0)	1.5 - 3.5[a, calc]
Sm	4.9	6.1	
Sr	-1.2	-0.1	-0.4 - 0.8[b, calc]
U	-1.8	-0.7	
	Iron Oxide Minerals[4]		
Am	4.6	5.4	(3 - 3.7)[a]
Cs			-1.4 - 0.5[b, goe]
Eu	4.7	5.6	
Np	3.0	3.8	2.4 - 3.0[d, hem] 3.5 - 5.3[b, hem/goe] (2.7 - 3)[a]
Pu[6]	2.4 (3.4)	3.3 (4.2)	3.5 - 5.3[e, hem] (3 - 3.5)[a]
Sm	4.9[7]	5.7[7]	
Sr	1.1	1.9	1.4 - 3.1[b, goe] (<1.5)[a]
U	3.7	4.5	(2 - 3)[a]
	Aluminosilicate Minerals[5]		
Am	4.8	5.2	3.6 - 3.8[c, clin]
Cs	3.6[ill], 0.9[smec], 3.0[clin]	4.7[ill], 2.0[smec], 4.2[clin]	3.1[b, smec]
Eu	4.1	4.5	
Np	1.3	1.7	1.7 - 1.8[b, smec], 1.4[d, smec]
Pu[6]	0.9 (1.9)	1.3 (2.2)	3.6 - 4.4[a, smec]
Sm	4.3[7]	4.7[7]	
Sr	1.1[ill], 1.8[smec], 3.0[clin]	1.2[ill], 1.9[smec], 3.2[clin]	3.1[b, smec]
U	1.3	1.7	
	Composite Frenchman Flat Mineralogy		
Am	5.1	4.4	
Cs	3.7	3.0	3.8
Eu	5.0	4.3	>4.3
Np	3.0	2.3	
Pu[6]	2.5 (3.4)	1.8 (2.7)	
Sm	5.3	4.6	
Sr	3.0	2.3	2.3
U	3.7	3.0	1.5

[1] Groundwater and mineral composition taken from Tompson et al. (1999). Trace quantities of sorbing radionuclides were added to determine K_d; pH ~ 8, 35% porosity, 1% calcite, 1% iron oxide, 1% illite, 5% smectite, and 5% clinoptilolite (by volume).

[2] K_ds as reported in Wolfsberg (1978) (Frenchman Flat composite) and [a]Triay et al. (1997) (performance assessment recommendation in parentheses) [b]Triay et al. (1991) [c]Triay et al. (1989) [d]Triay et al. (1993) [e]Triay et al. (1996) (single mineral; mineral type listed in superscript).

[3] 2.2 m^2/g, 8.31×10^{-6} mol sites/m^2 calcite in simulation.

[4] 50 m^2/g, 3.8×10^{-6} mol sites/m^2 iron oxide in simulation.

[5] 100 m^2/g smectite, 10% of surface area accounts for SC edge sites, 1:1 Si:Al site ratio, 3.8×10^{-6} mol sites/m^2 smectite EXCEPT Cs and Sr described by IE with illite, smectite, and clinoptilolite. See Zavarin and Bruton (2000) for details on Cs and Sr.

[6] Predicted Pu distribution coefficients calculated at $O_2(g)$ fugacity of 0.2 bars. Values in parentheses calculated at 10^{-7} bars.

[7] Based on surface complexation constants of Eu(III).

Table 4. Ion exchange reactions used to prediction Sr(II) and Cs(I) sorption to smectite, illite/mica, and clinoptilolite. Data taken from Viani and Bruton (1992; 1996).

Exchange Reaction	log K	Site Type
---------- SMECTITE † ----------		
Na^+ --> 0.5 Ca^{2+}, 0.5 Mg^{2+}, 0.5 Sr^{2+}	0.085	
Na^+ --> K^+	0.255	
Na^+ --> Cs^+	0.792	
---------- ILLITE/MICA ‡ ----------		
Na^+ --> 0.5 Ca^{2+}, 0.5 Mg^{2+}, 0.5 Sr^{2+}	-1.026	I
	-0.147	II
	0.000	III
Na^+ --> K^+	1.613	I
	1.686	II
	0.894	III
Na^+ --> Cs^+	5.718	I
	3.079	II
	1.539	III
---------- CLINOPTILOLITE ¶ ----------		
Na^+ --> K^+	1.100	
Na^+ --> Cs^+	1.708	
Na^+ --> 0.5 Ca^{2+}	-0.037	
Na^+ --> 0.5 Sr^{2+}	0.037	

† 0.85 meq/g smectite
‡ 0.2 meq/g illite/mica total, 0.005 = I, 0.03 = II, 0.965 = III
¶ 2.12 meq/g clinoptilolite

4.1 Am(III) Sorption

The contribution of calcite, iron oxide, and smectite minerals to Am(III) sorption to the simulated Frenchman Flat mineralogy is nearly equivalent (Table 3, column 1). Smectite may, therefore, contribute to Am(III) retardation to an equivalent extent as calcite and iron oxide minerals. While there is no data to evaluate the predicted Frenchman Flat alluvium K_d, the K_d reported by Wolfsberg (1978) for Eu(III) on Frenchman Flat alluvium (Log K_d >4.3) is similar to our predicted K_d for Am(III) (Log K_d = 4.4). Since Eu(III) and Am(III) are expected to behave similarly, the data suggest that our predicted K_d is consistent with measured data.

Some comparison between predicted and measured K_ds for Am(III) on individual minerals is possible. The K_d for Am(III) on hematite estimated for YMP performance assessment (Triay et al., 1997) ranged from Log K_d = 3 to 3.7. Our predicted distribution coefficient for Am(III) on iron oxide (Log K_d = 6.1) is significantly higher. The K_d range of Triay et al. (1997) was based on sorption data on hematite, typically a low surface area iron oxide. The iron oxide surface area used in our simulation was 50 m^2/g, more typical of higher surface area (goethite) iron oxide. Thus, the difference in Kd is predominantly a result of mineral surface area.

Triay et al. (1989) reported a Log K_d range of 3.6 to 3.8 for Am(III) on clinoptilolite in J-13 waters. This Log K_d is significantly less than our predicted K_d for Am(III) on smectite but cannot be compared due to the difference in aluminosilicate mineralogy. Triay et al. (1989) reported an Am(III) Log K_d of ~4 for tuff containing feldspar and cristobalite with trace (~1%) smectite. If smectite were the *principal* sorbing mineral, the resulting single mineral smectite Log K_d would be ~6. This is in approximately agreement with our predicted smectite K_d (Table 3, Log K_d = 5.2).

4.2 Cs(I) Sorption

Cs(I) sorption data collected for YMP site characterization indicates that sorption to aluminosilicates with significant ion exchange capacity (smectite, in this case) will be much more significant than sorption to iron oxides and calcite (Table 3, column 3). Based on this and other published data, Cs(I) sorption to iron oxide and calcite was not evaluated in Zavarin and Bruton (2004). However, ion exchange to three aluminosilicate minerals (illite, smectite, and clinoptilolite) was reported for Cs(I). Predicted distribution coefficients are presented in Table 3. Illite is predicted to be the dominant sorber in the composite Frenchman Flat alluvium (Table 3, column 1). The predicted K_d based on the composite Frenchman Flat alluvium is also in good agreement with the value reported by Wolfsberg (1978) (Log K_d (mL/g) = 3.0 and 3.8, respectively). The predicted and measured K_ds are not expected to be identical since the alluvium mineralogy of Wolfsberg (1978) is not known while the alluvium mineralogy used to predict K_d was based on alluvium mineralogy data from near the Cambric site of Frenchman Flat.

Triay et al. (1991) reported that the Log K_d of Cs(I) on smectite in J-13 waters is 3.1. This is significantly higher than our predicted value (2.0). The reaction constant used to predict Cs-Na exchange on smectite was based on the standard free energies reported in Gast (1972) for Wyoming bentonite. However, reaction constants determined in Gast (1972) for two smectites over a range of cesium concentrations revealed that the cesium affinity for smectite is non-linear (see Table 3 of Gast, 1972), increasing at low Cs(I) loads. The Cs(I) concentration in batch sorption experiments of Triay et al. (1991) was low ($<10^{-6}$ mol/L) and, thus, Cs(I) may have accessed high affinity sites preferentially. Our model did not account for high affinity sites, resulting in a more conservative K_d.

4.3 Eu(III) Sorption

The contribution of calcite, iron oxide, and smectite minerals to Eu(III) sorption to the simulated composite Frenchman Flat mineralogy follows the order iron oxide > calcite > smectite (Table 3, column 1). However, all three minerals are predicted to sorb Eu(III) quite strongly. This results in a very high K_d for the composite Frenchman Flat alluvium (Log K_d = 4.3), consistent with the measured value of Wolfsberg (1978) (Log K_d > 4.3).

YMP distribution coefficient data for Eu(III) sorption to single minerals were not found. However, it is interesting to note that the predicted single mineral K_ds for Eu(III) and Am(III) are quite similar (column 2), as might be expected given their similar speciation behavior in solution and similar electron configuration.

4.4 Np(V) Sorption

With respect to the composite Frenchman Flat mineralogy, smectite is predicted to contribute the least to Np(V) sorption (Table 3, Column 1). Nevertheless, smectite may be an important Np(V) sorber in zones of high smectite and low iron oxide and calcite. The predicted K_ds for calcite, iron oxide, and smectite minerals are consistent with the K_ds reported by Triay et al. (1991; 1993; 1997).

4.5 Pu(IV) and Pu(V) Sorption

Plutonium distribution coefficients were predicted at two O_2(g) fugacities: 0.2 and 10^{-7} bars. At 0.2 bars, Pu(VI) dominates in the aqueous phase. At 10^{-7} bars, Pu(V) dominates the aqueous phase. The decrease in O_2(g) fugacity results in an order of magnitude increase in K_d for all minerals. Since both Pu(IV) and Pu(V) (but not Pu(VI)) are allowed to sorb to mineral surfaces and Pu(IV) sorbs much more strongly than Pu(V), predicted Pu sorption will tend to increase with decreasing O_2(g) fugacity. This was reported in Zavarin and Bruton (2004). The results presented here illustrate the need to better understand the redox behavior of Pu in NTS waters.

While there is significant evidence to suggest that Pu(V) is the dominant Pu oxidation state in the aqueous phase in NTS type waters (Nitsche et al., 1993; Nitsche et al., 1994), the redox behavior of Pu in contact with mineral surfaces has been shown to be quite complex (Keeney-Kennicutt and Morse, 1985; Sanchez, 1983). Notwithstanding the complex redox behavior of Pu, its sorption behavior is, in general, similar to that of Np(V). At an O_2(g) fugacity of 0.2 bars, Pu has overall less affinity for the mineral surfaces compared to Np(V). However, at an O_2(g) fugacity of 10^{-7} bars (where Pu(V) dominates the aqueous phase), the behavior of Pu approaches that of Np(V). This is consistent with the similar aqueous speciation behavior of Pu(V) and Np(V).

While predicted K_ds for Pu on calcite and iron oxide are in reasonable agreement with single mineral YMP data (Table 3, Column 3), the predicted K_d for Pu on smectite (at 0.2 and 10^{-7} bar O_2(g) fugacities) is significantly lower. The results may suggest that Pu sorption prediction should be based on lower O_2(g) fugacities. However, in light of the scarce sorption data from which the Pu surface complexation model is based, it is as likely that surface complexation constants are underestimating the affinity of Pu for smectite surfaces. Additional single mineral sorption data and redox transformation data would be required to better predict the sorptive behavior of Pu.

4.6 Sm(III) Sorption

Predicted Sm(III) distribution coefficients for iron oxide and smectite were based on surface complexation reaction constants of Eu(III). Sm(III) and Eu(III) sorption chemistry is expected to be similar (Koeppenkastrop and Decarlo, 1992; Zhong and Mucci, 1995). However, published batch sorption data were not available to evaluate predicted distribution coefficients. Recently, the transport behavior of Sm(III) based on the sorption constants listed in Table 2 was evaluated (Zavarin et al., 2001). These data suggest that Sm(III) surface complexation to iron oxide and smectite based on the constants derived from Eu(III) data are in agreement with flow-through and batch sorption experiments.

4.7 Sr(II) Sorption

Based on the composite Frenchman Flat mineralogy, the predicted affinity of Sr(II) for aluminosilicates with large ion exchange capacities (smectite and clinoptilolite) are significantly larger than for iron oxide and much larger than for calcite. Sr sorption to illite, smectite and clinoptilolite was simulated by accounting for ion exchange while ignoring surface complexation. Because Sr^{2+} is the dominant aqueous species in solution at the simulated pH (8.0) (unlike actinide and lanthanide aqueous speciation which is domination by carbonate or hydroxide species), ion exchange is likely to remain the principle mechanism for Sr(II) sorption to aluminosilicates with significant cation exchange capacities. The resulting predicted K_d based on the composite Frenchman Flat alluvium is in good agreement with the batch sorption results of Wolfsberg (1978).

The predicted single mineral K_d results for Sr(II) are in good agreement with YMP data (Triay et al., 1997; Triay et al., 1991). However, Sr(II) sorption to smectite is underpredicted. The underpredicted distribution coefficient may result from several factors including uncertainty in the ion exchange constants and dissimilarity between solution chemistry of model and batch sorption experiments.

4.8 U(VI) Sorption

In the case of U(VI), smectite contributes very little to the predicted distribution coefficient of the composite Frenchman Flat mineralogy; the composite K_d is controlled by iron oxide. The contribution of calcite to the composite Frenchman Flat mineralogy K_d is still smaller than smectite. Thus, in areas where smectite is abundant and iron oxide is lacking, surface complexation to smectite will control U(VI) retardation. Furthermore, the predicted composite Frenchman Flat mineralogy K_d is in poor agreement with data of Wolfsberg (1978). This suggests that the role of iron oxide may be overstated in our model; recent flow-through experiments (Zavarin et al., 2001) suggest that the abundance and reactive surface area of iron oxides in Frenchman Flat alluvium may be significantly lower than iron oxide abundance and surface areas used in Tompson et al. (1999). Thus, the role of smectite may be more significant than predicted by the simulations presented here. The effect of reactive surface area on predicted distribution coefficients is also observed when comparing iron oxide single mineral K_ds for iron oxide; the K_d range reported in Triay et al. (1997) based of U(VI) sorption to hematite (low surface area) is significantly lower that predicted by our model (based on goethite, which typically has a much higher surface area).

5 CONCLUSIONS

Sorption of radionuclides (Am(III), Eu(III), Np(V), Pu(IV), Pu(V), and U(VI)) to aluminum oxide, silica, and aluminosilicate minerals using a generalized NEM approach, in combination with Vanselow IE, results in a consistent set of NEM reactions. Results indicate that generalized >SiOH and >AlOH reactive sites can be used to describe sorption on a variety of minerals. Although this generalized approach may result in greater uncertainty in mineral sorption constants (when compared to a mineral-dependent model), the number of equations necessary to describe sorption is minimized. This approach also minimizes the number of fitting parameters while retaining the principal pH, ionic strength, and surface loading effects.

The sorption fitting results indicate that surface complexation will dominate over ion exchange at pH>7 for rare earth and actinide ions examined here. Ion exchange is effectively suppressed due to aqueous speciation which results in neutral or negatively charged carbonate or hydroxide species less likely to undergo ion exchange. Cs and Sr sorption to aluminosilicates was modeled by ion exchange only; these ions have significantly less tendency to form hydroxide or carbonate species in solution and, thus, ion exchange is not suppressed at high pH. The predicted K_ds based on average NEM and Vanselow IE constants (including those reported in Zavarin and Bruton, 2004) compare well with published Yucca Mountain Project K_d data. Predicted single mineral K_ds are largely consistent with experimental data. In some cases, differences could be explained by surface area, mineralogy, or redox state uncertainties. A limited comparison of predicted K_ds with measured K_ds reported by Wolfsberg (1978) for alluvium from Frenchman Flat, indicates that the constants developed here would provide a good estimate for radionuclide reactive transport. However, the iron oxide abundance and/or reactive surface area used to predict sorption (1 % by volume and 50 m^2/g) appears to be significantly too high. This is in agreement with recent flow-through experiments (Zavarin et al., 2001).

The NEM and Vanselow IE constants described here (and in the companion report, Zavarin and Bruton, 2004) are an attempt to arrive at a consistent simplified database of sorption constants that can be used in reactive transport simulations in chemically and mineralogically heterogeneous environments. The accuracy of the resulting equations is limited by the quality and quantity of available sorption data and the limitations of the generalized NEM approach used. The reactivity of natural minerals is complicated and cannot be assumed to behave ideally. Thus, the validity of the NEM and Vanselow IE constants must always be evaluated with respect to the particular sediment and sediment mineralogy of interest. For example, Triay et al. (1997) suggested that the weak sorption of Np(V) on tuff containing small amounts of hematite may indicate the iron oxide mineral is passivated. It, therefore, may not be appropriate to include surface complexation to iron oxide in reactive transport simulations in all instances.

6 ACKNOWLEDGEMENTS

This work was conducted under the auspices of the U. S. Department of Energy by Lawrence Livermore National Laboratory under contract W-7405-Eng-48. This work was funded by the Underground Test Area Project, U. S. Department of Energy, National Nuclear Security Administration, Nevada Site Office.

7 REFERENCES

Aksoyoglu, S., Burkart, W. and Goerlich, W., 1991. Sorption of neptunium on clays. Journal of Radioanalytical Nuclear Chemistry, 149(1): 119-122.

Allard, B., Moulin, V., Basso, L., Tran, M.T. and Stammose, D., 1989. Americium adsorption on alumina in the presence of humic materials. Geoderma, 44: 181-187.

Allard, B., Olofsson, U., Torstenfelt, B., Kipatsi, H. and Andersson, K., 1982. Sorption of actinides in well-defined oxidation states on geologic media. In: W. Lutze (Editor), Scientific basis for radioactive waste management - V. Elsevier Science Pub. Co., pp. 775-782.

Bertetti, F.P., Pabalan, R.T. and Almendarez, M.G., 1998. Studies on neptunium(V) sorption on quartz, clinoptilolite, montmorillonite, and a-alumina. In: E.A. Jenne (Editor), Adsorption of metals by geomedia. Academic Press, San Diego, pp. 131-148.

Bertetti, F.P., Pabalan, R.T., Turner, D.R. and Almendarez, M.G., 1995. Neptunium(V) sorption behavior on clinoptilolite, quartz, and montmorillonite. In: W.M. Murphy and D.A. Knecht (Editors), Materials Research Society Symposium Proceedings. Materials Research Society, Boston, MA, pp. 631-638.

Bethke, C.M., 1996. Geochemical Reaction Modeling. Oxford University Press, New York, NY, 397 pp.

Bradbury, M.H. and Baeyens, B., 1997. A mechanistic description of Ni and Zn sorption on Na- montmorillonite .2. Modelling. Journal of Contaminant Hydrology, 27(3-4): 223-248.

Davis, J.A., Coston, J.A., Kent, D.B. and Fuller, C.C., 1998. Application of the surface complexation concept to complex mineral assemblages. Environmental Science & Technology, 32(19): 2820-2828.

Dent, A.J., Ramsay, J.D.F. and Swanton, S.W., 1992. An EXAFS study of uranyl ion in solution and sorbed onto silica and montmorillonite clay colloids. Journal of Colloid and Interface Science, 150(1): 45-60.

Fairhurst, A.J., Warwick, P. and Richardson, S., 1995. The effect of pH on europium-mineral interactions in the presence of humic acid. Radiochimica Acta, 69: 103-111.

Fletcher, P. and Sposito, G., 1989. The chemical modelling of clay/electrolyte interactions for montmorillonite. Clay Minerals, 24: 375-391.

Gast, R.G., 1972. Alkali metal cation exchange on Chambers montmorillonite. Soil Science Society of America Proceedings, 36: 14-19.

Helgeson, H.C., 1969. Thermodyncamics of hydrothermal systems at elevated temperatures and pressures. American J. Science, 267: 729-804.

Herbelin, A.L. and Westall, J.C., 1994. FITEQL, A computer program for determination of chemical equilibrium constants from experimental data. Department of Chemistry, Oregon State University.

Huysen, K. and van der Laan, J., 1992. DataTheif. National Institute for Nuclear Physics and High Energy Physics, Amsterdam.

Johnson, J.W. and Lundeen, S.R., 1997. GEMBOCHS thermodynamic datafiles for use with the EQ3/6 modeling package, Lawrence Livermore National Laboratory, Livermore.

Keeney-Kennicutt, W.L. and Morse, J.W., 1985. The redox chemistry of $Pu(V)O_2^+$ interaction with common mineral surfaces in dilute solutions and seawater. Geochimica et Cosmochimica Acta, 49(12): 2577-2588.

Koeppenkastrop, D. and Decarlo, E.H., 1992. Sorption of Rare-Earth Elements From Seawater Onto Synthetic Mineral Particles - an Experimental Approach. Chemical Geology, 95(3-4): 251-263.

Kornilovich, B.Y., Mas'ko, A.N., Pshinko, G.N. and Spasenkova, L.N., 1997. Influence of fulvic acids on Eu(III) adsorption by mineral constituents of soil. Radiochimia, 39(4): 370-374.

Kurbatov, M.H., Wood, G.B. and Kurbatov, J.D., 1951. Isothermal adsorption of cobalt from dilute solutions. Journal of Physical Chemistry, 55: 1170-1182.

Ledin, A., Karlsson, S., Duker, A. and Allard, B., 1994. The adsorption of europium to colloidal iron oxyhydroxides and quartz - The impact of pH and an aquatic fulvic acid. Radiochimica Acta, 66-7: 213-220.

Lemire, R. J., Fuger, J., Spahiu, K., Nitsche, H., Ullman, W. J., Potter, P., Vitorge, P., Rand, M. H., Wanner, H., and Rydberg, J. (2001) *Chemical Thermodynamics of Neptunium and Plutoniu*m, Vol. 4, Elsevier, New York.Lieser, K.H., Aqandt-Klend, S. and Thybusch, B., 1992. Sorption of uranyl ions on hydrous silicon dioxide. Radiochimica Acta, 57: 45-50.

McKinley, J.P., Zachara, J.M., Smith, S.C. and Turner, G.D., 1995. The influence of uranyl-hydrolysis and multiple site-binding reaction on adsorption of U(VI) to montmorillonite. Clays and Clay Minerals, 45(5): 586-598.

Moulin, V., Stammose, D. and Ouzounian, G., 1992. Actinide sorption at oxide-water interfaces: Application to alpha-alumina and amorphous silica. Applied Geochemistry(Supplemental Issue #1): 163-166.

Nakayama, S. and Sakamoto, Y., 1991. Sorption of neptunium on naturally-occurring iron-containing minerals. Radiochimica Acta, 52-3(P1): 153-157.

Newton, T.W., Hobart, D.E. and Palmer, P.D., 1986. The formation of Pu(IV)-colloid by the alpha-reduction of Pu(V) or Pu(VI) in aqueous solutions. Radiochimica Acta, 39: 139-147.

Nitsche, H., Gatti, R.C., Standifer, E.M., Lee, S.C., Muller, A., Prussin, T., Deinhammer, R.S., Maurer, H., Becraft, K., Leung, S. and Carpenter, S.A., 1993. Measured solubilities and speciations of neptunium, plutonium, and americium in a typical groundwater (J-13) from Yucca Mountain region. LA-12562-MS, Los Alamos National Laboratory, Los Alamos.

Nitsche, H., Roberts, K., Prussin, T., Muller, A., Becraft, K., Keeney, D., Carpenter, S.A. and Gatti, R.C., 1994. Measured solubilities and speciations from oversaturated experiments on neptunium, plutonium, and americium in UE-25p #1 well water from the Yucca Mountain region. LA-12563-MS, Los Alamos National Laboratory, Los Alamos.

Norden, M., Ephraim, J.H. and Allard, B., 1994. The influence of a fulvic acid on the adsorption of europium and strontium by alumina and quartz: Effects of pH and ionic strength. Radiochimica Acta, 65: 265-270.

Pabalan, R.T., 1994. Thermodynamics of ion-exchange between clinoptilolite and aqueous solutions of Na+/K+ and Na+/Ca2+. Geochimica et Cosmochimica Acta, 58: 4573-4590.

Pabalan, R.T., Prikryl, J.D., Muller, P.M. and Dietrich, T.B., 1992. Experimental study of uranium(6+) sorption on the zeolite mineral clinoptilolite. In: C.G. Interrante and R.T. Pabalan (Editors), Matericals Research Society Symposium. Scientific Basis for Nuclear Waste Management XVI. MRS, Boston, MA, pp. 177-182.

Pabalan, R.T., Turner, D.R., Bertetti, F.P. and Prikryl, J.D., 1998. UraniumVI sorption onto selected mineral surfaces: Key geochemical parameters. In: E.A. Jenne (Editor), Adsorption of metals by geomedia. Academic Press, San Diego, pp. 99-130.

Pawloski, G.A., Tompson, A.F.B. and Carle, S.F., eds., 2001. Evaluation of the Hydrologic Source Term for Underground Nuclear Tests on Pahute Mesa and the Nevada Test Site: The Cheshire Test, Contributors: W.L. Bourcier, C.J. Bruton, S.F. Carle, J.I. Daniels, R.M. Maxwell, G.A. Pawloski, D.E. Shumaker, D.K. Smith, A.F.B. Tompson, and M. Zavarin., UCRL-ID-147023, Lawrence Livermore National Laboratory, Livermore, California.

Rai, D., Hess, N.J., Felmy, A.R., Moore, D.A., Yui, M. and Vitorge, P., 1999. A thermodynamic model for the solubility of PuO2(am) in the aqueous K^+-HCO_3^--CO_3^{2-}-OH^--H_2O system. Radiochimica Acta, 86(3-4): 89-99.

Righetto, L., Bidoglio, G., Azimonti, G. and Bellebono, I.R., 1991. Competitive actinide interaction in colloidal humic acid-mineral oxide systems. Environmental Science and Technology, 25(1): 1913-1919.

Righetto, L., Bidoglio, G., Marcandalli, B. and Bellobono, I.R., 1988. Surface interactions of actinites with alumina colloids. Radiochimica Acta, 44/45: 73-75.

Sanchez, A.L., 1983. Chemical speciation and adsorption behavior of plutonium in natural waters, University of Washington, Seattle, 191 pp.

Sanchez, A.L., Murray, J.W. and Sibley, T.H., 1985. The adsorption of plutonium IV and V on goethite. Geochimica et Cosmochimica Acta, 49(11): 2297-2307.

Shiao, S., Egozy, Y. and Meyer, R.E., 1981. Adsorption of Cs(I), Eu(III), Co(II), and Cd(II) by Al2O3. Journal of Inorganic and Nuclear Chemistry, 43(12): 3309-3315.

Stammose, D. and Dolo, J., 1990. Sorption of americium at trace level on a clay mineral. Radiochimica Acta, 51: 189-193.

Steefel, C.I. and Yabusaki, S.B., 1995. OS3D/GIMRT, Software for modeling multicomponent-multidimensional reactive transport, User manual and programmer's guide. Pacific Northwest National Laboratory, Richland, WA.

Tompson, A.F.B., Bruton, C.J. and Pawloski, G.A., 1999. Evaluation of the hydrologic source term from the underground nuclear tests in Frenchman Flat and the Nevada Test Site: The CAMBRIC test. UCRL-ID-132300, Lawrence Livermore National Laboratory, Livermore.

Triay, I.R., Cotter, C.R., Kraus, S.M., Huddleston, M.H., Chipera, S.J. and Bish, D.L., 1996. Radionuclide sorption in Yucca Mountain tuffs with J-13 well water: neptunium, uranium, and plutonium. LA-12956-MS, Los Alamos National Laboratory, Los Alamos.

Triay, I.R., Meijer, A., Ciscneros, M.R., Miller, G.G., Mitchell, A.J., Ott, M.A., Hobart, D.E., Palmer, P.D., Perrin, R.E. and Aguilar, R.D., 1989. Sorption of americium in tuff and pure minerals using synthetic and natural groundwaters. LA-UR-89-3733, Los Alamos National Laboratory, Los Alamos.

Triay, I.R., Meijer, A., Conca, J.L., Kung, K.S., Rundberg, R.S., Streitelmeier, b.A., Tait, C.D., Clark, D.L., Neu, M.P. and Hobart, D.E., 1997. Summary and synthesis report on radionuclide retardation for the yucca montain site characterization project. LA-13262-MS, Los Alamos National Laboratory, Los Alamos.

Triay, I.R., Mitchell, A.J. and Ott, M.A., 1991. Radionuclide migration as a function of mineralogy. LA-UR-91-113, Los Alamos National Laboratory, Los Alamos.

Triay, I.R., Robinson, B.A., Lopez, R.M., Mitchell, A.J. and Overly, C.M., 1993. Neptunium retardation with tuffs and groundwaters from Yucca Mountain. LA-UR-93-436, Los Alaamos National Laboratory, Los Alamos.

Tsunashima, A., Brindley, G.W. and Bastovanova, M., 1981. Adsorption of uranium from solution by montmorillonite: composition and properties of uranyl montmorillonites. Clays and Clay Minerals, 29(1): 10-16.

Turner, D.R., 1995. A uniform approach to surface complexation modeling of radionuclide sorption. cnwra 95-001, Center for Nuclear Waste Regulatory Analyses, San Antonio.

Turner, D.R., Pabalan, R.T. and Bertetti, F.P., 1998. Neptunium(V) sorption on montmorillonite: An experimental and surface complexation modeling study. Clays and Clay Minerals, 46(3): 256-269.

Turner, G.D., Zachara, J.M., McKinley, J.P. and Smith, S.C., 1996. Surface charge properties and UO22+ adsorption of a subsurface smectite. Geochimica et Cosmochimica Acta, 60(18): 3399-3414.

Viani, B.E. and Bruton, C.J., 1992. Modeling fluid-rock interaction at Yucca Mountain, Nevada: A progress report. UCRL-ID-109921, Lawrence Livermore National Laboratory, Livermore, CA.

Viani, B.E. and Bruton, C.J., 1996. Assessing the role of cation exchange in controlling groundwater chemistry during fluid mixing in fractured granite at Aspo, Sweden. UCRL-JC-121527, Lawrence Livermore National Laboratory, Livermore, CA.

Waite, T.D., Payne, T.E., Davis, J.A. and Sekine, K., 1992. Alligator Rivers Analogue Project, Final Report, Volume 13: Uranium sorption. Volume 13, Australian Nuclear Science and Technology Organisation, Menai.

Wang, L., Maes, A., de Canniere, P. and van der Lee, J., 1998. Sorption of europium on illite (Silver Hill, Montana). Radiochimica Acta, 82: 233-237.

Wanner, H., Albinsson, Y., Karnl, O., Wieland, I., Wersin, P. and Charlet, L., 1994. The acid/base chemistry of montmorillonite. Radiochimica Acta, 66/67: 733-738.

Wolfsberg, K., 1978. Sorption-desorption studies of Nevada Test Site alluvium and leaching studies of nuclear test debris. LA-7216-MS, Los Alamos National Laboratory, Los Alamos.

Zachara, J.M., Resch, C.T. and Smith, S.C., 1994. Influence of humic substances on Co2+ sorption by a subsurface mineral separate and its mineralogic components. Geochimica et Cosmochimica Acta, 58(2): 553-566.

Zavarin, M. and Bruton, C.J., 2004. A Non-Electrostatic Surface Complexation Approach to Modeling Radionuclide Migration at the Nevada Test Site: Iron Oxides and Calcite. UCRL-ID-141841, Lawrence Livermore National Laboratory, Livermore.

Zavarin, M., Roberts, S.K., Rose, T.P. and Phinney, D.L., 2001. Validating Mechanistic Sorption Model Parameters and Processes for Reactive Transport in Alluvium, UCRL-ID-149728, Lawrence Livermore National Laboratory, Livermore, California.

Zhong, S.J. and Mucci, A., 1995. Partitioning of rare earth elements (REEs) between calcite and seawater solutions at 25-degrees-C and 1 atm, and high dissolved REE concentrations. Geochimica et Cosmochimica Acta, 59(3): 443-453.

APPENDIX A. AQUEOUS SPECIATION DATA USED IN DATA FITTING ROUTINES

Thermodynamic data for aqueous species were taken from version com.V8.R6 of the GEMBOCHS thermodynamic database (Johnson and Lundeen, 1997) with revised and updated thermodynamic data as given in Pawloski et al. (2001) and noted below. Pu speciation data were taken, in part, from a recent compilation of Pu data (Lemire, 2001). The extended Debye-Hückel formulation (also known as the B-DOT model) was used to calculate activity coefficients of aqueous species (Bethke, 1996; Helgeson, 1969) in GIMRT simulations. Values of the ion size parameter (Bethke, 1996; Helgeson, 1969) for aqueous species added to the database were estimated by analogy to aqueous species of similar valence and ligand. Parameters used in the Debye-Hückel activity coefficient model are listed in Tables A.1 and A.2. The Davies equations was used to calculate activity coefficients in the FITEQL data fitting routine. The Davies equation requires only one constant (C) which was set to 0.3 (Table A.2).

Table A.1 Basis species used in thermodynamic database

	Ion size Å†	Mol. Wt. g/mol
H_2O	3	18.0
Al^{3+}	9	27.0
Am^{3+}	5	243.0
Ca^{2+}	6	40.1
Cl^-	3	35.5
Cs^+	2.5	132.9
Eu^{3+}	5	152.0
Fe^{2+}	6	55.8
H^+	9	1.0
HCO_3^-	4	61.0
K^+	3	39.1
Mg^{2+}	8	24.3
Na^+	4	23.0
Np^{4+}	5.5	237.0
Pu^{4+}	5.5	244.0
SO_4^{2-}	4	96.1
$SiO_2(aq)$	3	60.1
Sm^{3+}	9	150.4
Sr^{2+}	5	87.6
UO_2^{2+}	4.5	270.0
$O_2(aq)$	3	32.0

† Ion size parameter used in Debye-Huckel activity coefficient model.

Table A.2 Parameters in extended Debye-Huckel activity coefficient model and Davies activity coefficient models.

Constants	25 ˚C
A	0.5114
B	0.3288
$B^{\bullet}$	0.041
C	0.3

Table A.3 Logarithm of equilibrium constants (K) of aqueous reactions at 25 ˚C.

Reaction	log K	Ion size† Å
$H_2O = OH^- + H^+$	14.0	3.5
$Al^{3+} + 2\ H_2O = AlO_2^- + 4\ H^+$	22.2	4
$HCO_3^- = CO_3^{2-} + H^+$	10.3	4.5
$HCO_3^- + H^+ = CO_2(aq) + H_2O$	-6.345	4.5
$HCO_3^- + H^+ = CO_2(g) + H_2O$	7.814	-
$Fe^{2+} + 0.25\ O_2(g) + H^+ = Fe^{3+} + 0.5\ H_2O$	-7.8	9
$Fe^{3+} + 2\ H_2O = FeO_2^- + 4\ H^+$	21.6	4
$Fe^{3+} + 2\ H_2O = HFeO_2^0 + 3\ H^+$	12.0	3
$SiO_2(aq) + H_2O = HSiO_3^- + H^+$	9.6	4
$Ca^{2+} + HCO_3^- = CaCO_3^0 + H^+$	7.0	3
$O_2(aq) = O_2(g)$	2.898	-
$Sr^{2+} + H_2O = SrOH^+ + H^+$	13.3	3
$Sr^{2+} + HCO_3^- = SrCO_3^0 + H^+$	7.46	3
$Sr^{2+} + HCO_3^- = SrHCO_3^+$	-1.18	3
$Eu^{3+} + H_2O = EuOH^{2+} + H^+$	9.20	4
$Eu^{3+} + 2\ H_2O = Eu(OH)_2^+ + 2\ H^+$	14.86	4
$Eu^{3+} + 3\ H_2O = Eu(OH)_3^0 + 3\ H^+$	24.13	4
$Eu^{3+} + HCO_3^- = EuCO_3^+ + H^+$	2.41	4
$Eu^{3+} + 2\ HCO_3^- = Eu(CO_3)_2^- + 2\ H^+$	7.67	4
$Eu^{3+} + 3\ HCO_3^- = Eu(CO_3)_3^{3-} + 3\ H^+$	18.32	4
$Sm^{3+} + HCO_3^- = SmCO_3^+ + H^+$	2.5	4
$Sm^{3+} + 2\ HCO_3^- = Sm(CO_3)_2^- + 2\ H^+$	7.9	4
$Am^{3+} + H_2O = AmOH^{2+} + H^+$	6.41	4.5
$Am^{3+} + 2\ H_2O = Am(OH)_2^+ + 2\ H^+$	14.11	4
$Am^{3+} + 3\ H_2O = Am(OH)_3^0 + 3\ H^+$	25.72	4
$Am^{3+} + HCO_3^- = AmCO_3^+ + H^+$	2.54	4
$Am^{3+} + 2\ HCO_3^- = Am(CO_3)_2^- + 2\ H^+$	8.38	4
$Am^{3+} + 3\ HCO_3^- = Am(CO_3)_3^{3-} + 3\ H^+$	15.82	4

TABLE A.3 (continued)

Reaction	log K	Ion size† Å
$UO_2^{2+} + H_2O = UO_2OH^+ + H^+$	5.22	3
$UO_2^{2+} + 2\ H_2O = UO_2(OH)_2^0 + 2\ H^+$	10.31	3
$UO_2^{2+} + 3\ H_2O = UO_2(OH)_3^- + 3\ H^+$	19.25	3
$UO_2^{2+} + HCO_3^- = UO_2CO_3^0 + H^+$	0.67	4
$UO_2^{2+} + 2\ HCO_3^- = UO_2(CO_3)_2^{2-} + 2\ H^+$	3.76	4
$UO_2^{2+} + 3\ HCO_3^- = UO_2(CO_3)_3^{4-} + 3\ H^+$	9.44	4
$Np^{4+} + 0.25\ O_2(g) + 1.5\ H_2O = NpO_2^+ + 3\ H^+$	9.9	4
$NpO_2^+ + H_2O = NpO_2OH^0 + H^+$	8.90	3
$NpO_2^+ + HCO_3^- = NpO_2CO_3^- + H^+$	5.73	4
$NpO_2^+ + 2\ HCO_3^- = NpO_2(CO_3)_2^{3-} + 2\ H^+$	13.66	4
$NpO_2^+ + 3\ HCO_3^- = NpO_2(CO_3)_3^{5-} + 3\ H^+$	22.49	4
$Pu^{4+} + H_2O = PuOH^{3+} + H^+$	0.5	3
$Pu^{4+} + 2\ H_2O = Pu(OH)_2^{2+} + 2\ H^+$	1.66	3
$Pu^{4+} + 3\ H_2O = Pu(OH)_3^+ + 3\ H^+$	4.62	3
$Pu^{4+} + 4\ H_2O = Pu(OH)_4^0 + 4\ H^+$	8.85	3
$Pu^{4+} + 2\ HCO_3^- + 2\ H_2O = Pu(OH)_2(CO_3)_2^{2-} + 4\ H^+$	2.76§	3
$Pu^{4+} + 5\ HCO_3^- = Pu(CO_3)_5^{6-} + 5\ H^+$	16.31	4
$PuO_2^+ + H_2O = PuO_2OH^0 + H^+$	9.73	3
$PuO_2^+ + HCO_3^- = PuO_2CO_3^- + H^+$	5.21	4
$PuO_2^+ + 2\ HCO_3^- = PuO_2(CO_3)_2^{3-} + 2\ H^+$	13.66[a]	4
$PuO_2^+ + 3\ HCO_3^- = PuO_2(CO_3)_3^{5-} + 3\ H^+$	26.00	4

† Ion size parameter, used in Debye-Huckel activity coefficient model, for the aqueous complex formed by the basis species.

§ Speciation constant derived from Rai et al. (1999).

[a] Estimated from reaction constant for $NpO_2(CO_3)_2^{3-}$.

University of California
Lawrence Livermore National Laboratory
Technical Information Department
Livermore, CA 94551